Politecnico di Torino

ScuDo
Scuola di Dottorato ~ Doctoral School
WHAT YOU ARE, TAKES YOU FAR

Doctoral Dissertation
Doctoral Program in Electrical, Electronics and Communications Engineering
(37^{th}cycle)

Methodologies for Modeling, Assessment, and Optimization of Integrated Community Energy Systems

By

Gianmarco Lorenti

******

Supervisor(s):
Prof. Maurizio Repetto, Supervisor
Dr. Paolo Lazzeroni, Co-Supervisor

Doctoral Examination Committee:
Prof. Marco Raugi, Referee, Università di Pisa
Prof. Francesco Grimaccia, Referee, Politecnico di Milano
Prof. Bruno Sareni, Université de Toulouse
Prof. Aldo Canova, Politecnico di Torino
Prof. Fabio Freschi, Politecnico di Torino

Politecnico di Torino
2025

Declaration

I hereby declare that the contents and organization of this dissertation constitute my own original work and do not compromise in any way the rights of third parties, including those relating to the security of personal data.

Gianmarco Lorenti
2025

* This dissertation is presented in partial fulfillment of the requirements for **Ph.D. degree** in the Graduate School of Politecnico di Torino (ScuDo).

I dedicate this thesis to its readers, with the hope that they find inspiration and intrigue within its pages

Acknowledgements

I would like to acknowledge several people who, directly or indirectly, knowingly or unknowingly, have influenced the past three years of my life. I may have been imperfect in determining who made it onto this list, so please forgive any oversights; I trust that anyone who should have been mentioned but isn't will still know the place they hold in my journey.

In no particular order[1]... Serena –ministro Plaffof-, Daouda, Nicola P., Olga, Giuxy, Nicolò P., Mario e Rina, Rob, Angela, Abdul, Concetta e Ignazio, Mathis, Daniele, Alessio e Matteo –los Zirillos–, Andrea T., Rocio L., Alessandro S., Adamo, Michele T., Ornella C., Lorenzo B., Evelise, Lucien, Chris, Pietro R. M., Alice, Anna Fra, Cola, Silvana –mia madre–, Sara, WD 40, Elena, Josef, Giuliana e Leonardo, Soukry, Mariangela e Franco, Maxime, Jhonny, Chiara, Youssef, Ale T., Lucas, Luca, Alessandro S. F., Angelo T., Denise, Andrea, Ele, Mike, Enzo, e la signora, Cosimo –mio padre–, Stefania, Simone, Edoardo F., Ivan G., Romain, Claudia D.V., Assunta e Gianfranco, Nadia, Leo, Stefano e Vera, Francesco –il Demiurgo–, Irene, Mattia F., Mariolino, Cristina, Ally, Fabrizio M., Matte e Serena, Consuelo, Song, Francesco Moraglio, Maedeh, Uma, Dov, Paul, Luigi, Antonio, Lorenzo, Antonietta, Irene d'A., Paul S., Madison?, Marcello F., Franco e Patrizia, Lucio –mio fratello–, Michele, Andrea, Paolo, Sire, Lilla, Aldo, Ragusa, Pietro, Georgios, Corentin, Maurizio, Alberto, Bharath, Bruno, Faabiu, Miriam, Michele M., Emanuel G., Mimmo e Maria, Leez, Saba, Edoardo P., Fabio, Marco, Claudia B., Noe, Massimo D. C., Sofia, Luc, Maria, martinas, Stefano e Cate, Danilo, matteo, Diego, Arnau, Ryan, Federico e gli altri, Aleandro, Adelaide, Ro, Vincenzo, Igor, Federico R., Bastien, Chab, Alicia, Matteo, Michela.

[1] Truly, I used Python.

Abstract

The transition to sustainable energy systems is driven by decarbonization and decentralization of energy production, necessitating community-level integration of renewables for optimal use. Integrated Community Energy Systems (ICES) and Renewable Energy Communities (RECs) have emerged as key paradigms in this context. ICES offer a framework for managing multi-energy systems across communities, while RECs provide a practical means to implement these models within existing regulatory and market landscapes.

This thesis advances ICES and REC modeling, optimization, and assessment by developing methodologies to address key challenges in their design and operation. A multi-node, multi-energy model is formalized to capture the complexities of community energy systems, incorporating sector coupling and storage. Key Performance Indicators (KPIs) are introduced to evaluate ICES from energy, environmental, and economic perspectives. Three key areas are explored: optimal energy management, energy consumption prediction, and many-objective design.

First, a Mixed-Integer Linear Programming (MILP) framework is developed to optimize operational energy flows in complex ICES, enabling assessment of energy, environmental, and economic performance. Results show the benefits of coordinated optimization strategies and detailed multi-node modeling for accurate economic evaluations. However, scalability analysis highlights that trade-offs between model accuracy and computational complexity are required, suggesting that data-driven approximations could enhance scalability.

Second, a data-driven methodology is proposed to predict hourly electricity consumption profiles from minimal data, such as time-of-use bills. This is often necessary due to the lack of measurements, while other data (e.g., renewable generation or prices) can be derived from historical records or consolidated methods. A regression approach is shown to outperform traditional benchmarks, particularly for non-residential end users. This method is validated for ICES optimization, offering solutions in data-limited scenarios. Future work could refine this ap-

proach by incorporating category-specific models and accounting for seasonal variability.

Finally, the thesis explores many-objective design optimization of ICES, focusing on scalarization approaches to identify compromises between conflicting objectives. Game-theory concepts are used to treat objectives as players in a cooperative game, identifying equilibria. A preliminary study samples the design space, highlighting the increasing complexity of Pareto-dominance relationships as objectives increase. Scalarization metrics offer insights into many-objective optimization strategies, though further research is needed to validate these findings in real-world scenarios.

Overall, key contributions and innovations to the current state-of-the-art include:

- Formalization of a multi-node modeling and optimization framework for assessing physical and virtual energy flows within ICES.
- Integration of sector coupling, storage, and multi-energy modeling in ICES for integrated assessment.
- Comparison of individual node and overall ICES perspectives through optimization and KPI assessment.
- Testing the scalability of MILP-based optimization in relation to an increasing ICES size.
- Data-driven approach for predicting hourly load profiles to improve ICES assessment in data-limited contexts.
- Preliminary exploration of game theory-inspired strategies for multi and many-objective optimization in ICES design.

These contributions advance the understanding and capabilities of ICES and RECs, laying a foundation for their broader adoption and the transition to sustainable energy systems. While offering impactful methodologies and insights, this work highlights the need for further research in areas not covered, including sensitivity analysis and optimization under uncertainty, real-time resource management, and scalable data-driven methods.

Contents

List of Figures

List of Tables

Nomenclature

Acronyms, Abbreviations

ARERA Italian Regulatory Authority for Energy, Networks, and Environment ("*Autorità di Regolazione per Energia Reti e Ambiente*")

BTA Non-domestic end user ("*Bassa Tensione Altri usi*")

DER Distributed Energy Resource

DOM Household end user ("*DOMestico*")

EU European Union

GSE Italian Energy Services Manager ("*Gestore Servizi Energetici*")

HDD Heating Degree Day

ICES Integrated Community Energy System

JRC Joint Research Center

KPI Key Performance Indicator

LCA Life Cycle Assessment

PUN Italian national average market price ("*Prezzo Unico Nazionale*")

PVGIS PhotoVoltaic Geographical Information System

REC Renewable Energy Community

RES Renewable Energoy Source

SM Smart Meter

SOC State of Charge

SOH State of Health

ToU Time-of-Use

Components

BESS Battery Energy Storage System

BOIL Gas-fired boiler

HP Heat pump

HTS Heat Thermal Storage

PV PhotoVoltaic generator

UE Electric load ("*Utenza Elettrica*")

UT Thermal load ("*Utenza Termica*")

Quantities

δ Binary variable

ϵ Emission factor

η Efficiency

κ Conversion factor

C Cost

E Energy

P Power

S Component size

t Time

n Lifetime

r Discount factor

Key Performance Indicators

CR (Total actualized) Cost Reduction

EM Equivalent CO_2 EMissions

ER Emissions Reduction

IRR Internal rate of return

NPV Net Present Value

PBT Pay-Back Time

SC Self-Consumption rate

SS Self-sufficiency rate

TAC Total Actualized Costs

Subscripts, Superscripts

cons Consumption

h Time-step

inj Network injection

in Input quantity

i Component

j Energy node

local Local self-consumption

out Output quantity

prod Production

self – cons Individual self-consumption

shared Virtual energy sharing

stor Stored quantity

t Year

v Energy vector

with Network withdrawal

Main power quantities

P^{cons} Energy consumption (for energy vector)

$P^{\text{inj,sh}}$ Incentivizable injection into the grid

P^{inj} Injection into the grid

P^{prod} Energy generation (for energy vector)

P^{PV} Photovoltaic generation

$P^{\text{self-cons}}$ Self-consumption within a single node

P^{shared} Sharing within the ICES

P^{UE} Electricity demand

P^{UT} Thermal demand

P^{with} Withdrawal from the grid

Introduction

The formal recognition of Renewable Energy Communities (RECs) by the European Union (EU) through the EU 2018/2001 Directive (REDII) [1] marked a turning point in shaping the future energy landscape. By establishing a clear legal framework for energy communities, REDII empowered citizens to *take energy matters into their own hands* [2], highlights the active role of end users in achieving the EU's ambitious targets for climate neutrality in 2050 [3].

RECs represent a new energy paradigm where local energy producers, prosumers, and end users own and collectively manage distributed energy resources (DERs) and other assets to increase renewables penetration and energy self-sufficiency [4]. A defining feature of RECs is *energy sharing*, enabling the local consumption of self-produced renewable energy, and addressing traditional barriers which enables local consumption of self-produced renewable energy and overcomes traditional barriers associated with individual self-generation and self-consumption [5, 6]. Typically, RECs prioritize energy and environmental targets over profits and focus strongly on social impacts, such as addressing energy poverty and promoting energy democracy [5, 7].

While RECs are defined within specific regulatory boundaries, Integrated Community Energy Systems (ICES) represent a broader and more comprehensive concept. ICES encompasses multifaceted energy systems designed to meet local community needs across multiple energy vectors. They provide a holistic framework for managing energy generation, consumption, and sharing by leveraging advanced technologies, such as renewable energy systems and energy storage, and the integration of multiple energy vectors through sector coupling [8]. Moreover, ICES integrates infrastructure and information and communication technologies to enable optimal management of DERs [7]. In this context, ICES serve as the theoretical and methodological foundation for designing and optimizing energy

communities, while RECs put in effect the principles of ICES within the existing regulatory landscape.

Background

Community-energy projects have a long history, particularly in Europe, where local initiatives laid the groundwork for energy democratization and renewable energy adoption [2]. However, the formal recognition of these initiatives under REDII has established a structured framework that incentivizes their spread and development. This recognition has stimulated renewed interest across regulatory, business, social, and research spheres [9].

Over the past few decades, research has advanced significantly in distributed and multi-energy systems. These efforts have introduced diverse concepts, spanning infrastructure (e.g., microgrids, smart grids), business models (e.g., peer-to-peer energy trading, virtual power plants), and technological solutions (e.g., energy hubs) [7].

ICES integrates many of these concepts and therefore faces similar challenges. In particular, several studies highlight the challenges inherent in modeling and optimizing distributed and community energy systems. Key issues include:

- Integrating DERs, managing demand, and incorporating storage solutions to enhance flexibility and mitigate variability in renewable energy generation [9, 10].
- Addressing sector coupling to optimize the interaction between electricity, heating, and cooling systems [11].
- Addressing data challenges, such as ensuring high-resolution spatial and temporal data while maintaining confidentiality.
- Balancing multiple and conflicting energy, environmental, economic, and social goals.
- Developing regulatory and business models that support energy sharing and collective self-consumption [6, 12].

Motivation and objectives

The emergence of RECs as a means of implementing ICES principles underscores the need to formalize their modeling and assessment. One critical question is whether existing methodologies are adequate to address the specific needs of RECs. These needs include managing the complexities of configurations with multiple energy production and consumption locations, integrating storage technologies, and coupling different energy carriers. Additionally, they involve facilitating energy sharing and aligning with socio-environmental objectives

ICES appear as complex multi-energy systems, and the objective of this thesis is to address these challenges by:

1. Developing a comprehensive framework for modeling ICES as multi-node, multi-energy systems, incorporating sector coupling and storage solutions.
2. Establishing performance evaluation metrics across energy, environmental, and economic dimensions.
3. Formalizing and testing optimization models for ICES energy management, including regulatory and technical constraints.
4. Investigating multi and many-objective approaches to system design, addressing trade-offs between conflicting objectives.
5. Leveraging data-driven methods to predict energy consumption when information is scarce or unavailable.

Contribution

This thesis advances the state of the art in the modeling, optimization, and assessment of ICES and RECs by addressing three critical areas: modeling and assessment, optimal energy management, and many-objective design.

The thesis contributes to the field by formalizing a multi-energy, multi-node framework that captures the complexities of energy systems within communities. Building on existing optimization methodologies, it tests their applicability and scalability with growing ICES size.

Data-driven methodologies are integrated to predict consumption profiles, which are essential for optimizing real-world systems where high-resolution data

is often scarce. In contrast, data such as energy prices or renewable generation or can be derived from historical records or consolidated methods (e.g., weather-based models).

Additionally, game theory-inspired optimization methods are explored to address the multi-objective nature of community energy systems. These approaches allow for the analysis of both the individual perspective within the community and the community as a whole, laying the foundation for more comprehensive and scalable solutions.

The following paragraphs detail the specific contributions.

Modeling and assessment The first contribution lies in formalizing a comprehensive framework for analyzing ICES, integrating key concepts such as energy nodes, multi-energy flows, and virtual energy-sharing mechanisms. The model represents a multi-node energy system, where each node corresponds to a distinct energy entity within the community (with its own physical energy flows), though interacting through virtual energy sharing. The framework offers a structured approach to understanding the operational complexities of energy communities. Additionally, performance metrics are proposed based on energy, environmental, and economic key performance indicators (KPIs), providing a quantitative basis for evaluating REC performance.

Optimal energy management A Mixed-Integer Linear Programming (MILP) framework is developed to optimize the operational energy flows in ICES, addressing technical and regulatory constraints. The adopted optimization framework is tested across multiple scenarios to assess the impact of key modeling choices, such as coordinated optimization strategies and detailed multi-node modeling. Scalability problems are analyzed with increasing number of nodes to be collectively optimized.

Data-driven load prediction The third key contribution addresses the issue of limited energy consumption data, which often lacks detailed measurements. A k-nearest neighbors (k-NN) regression model is proposed to predict energy load profiles from time-of-use (ToU) bills, accommodating a range of end users. The model's predictions are validated for use in system optimization and design, demonstrating its practical applicability in real-world scenarios.

Many-objective design optimization Lastly, the thesis explores the design optimization of ICES as a many-objective problem. A preliminary analysis investigates the growing complexity of Pareto-dominance relationships with increasing objectives and effective scalarization approaches to manage trade-offs among conflicting goals. In particular, an approach based on game theory is explored, that treats objectives as players in a cooperative game.

Structure of the Thesis

The thesis is organized into chapters as shown in Fig. 1. This diagram illustrates the interrelations between the chapters, showing how each section builds upon other ones to provide a comprehensive approach to ICES and RECs modeling, optimization, and assessment.

The following paragraphs describe the content of each chapter in more detail.

Chapter 1 provides the foundational framework for ICES, offering a taxonomy of local energy systems and highlighting their synergies with RECs. It explores key concepts such as multi-node and multi-energy modeling, energy sharing mechanisms, and relevant regulatory frameworks. The chapter also introduces the performance evaluation framework using energy, environmental, and economic Key Performance Indicators (KPIs), which will be used in subsequent analyses.

Chapter 2 focuses on the data sources used in subsequent analyses of the modeling and optimization frameworks. It describes the collection and preparation procedures of key data, including electricity demand, photovoltaic generation, heating loads, and energy prices. Finally, this chapter establishes a preliminary baseline assessment of an ICES scenario.

Chapter 3 formalizes the operational optimization framework for ICES, a key step for assessing these complex systems performance. The chapter adopts Mixed-Integer Linear Programming to optimize their performance. Test cases are evaluated to benchmark the effects of key modeling choices –collective optimization, multi-node modeling, and storage modeling– on energy, environmental, and economic KPIs, and on computational complexity.

Chapter 4 addresses the challenge of predicting hourly electricity consumption profiles using limited input data as an alternative source when historical data are unavailable. In fact, the optimization models requires these data as input, but they are seldom available, particularly in heterogeneous end-user settings

(while other data like renewable generation already have consolidated methodologies). A data-driven approach based on k-nearest neighbors (k-NN) regression is introduced and benchmarked against standard load profiles and other data-driven methods. The applicability of the predicted load profiles is validated for operational optimization and design tasks.

Building on the operation optimization, Chapter 5 shifts focus to the design optimization of ICES, exploring the mani-objective nature of this problem. Considering a simplified layout of REC in a multifamily building with sectors-coupling, the chapter examines trade-offs among conflicting objectives, such as energy self-sufficiency, emission reduction, and cost minimization. Scalarization metrics inspired by game theory are evaluated to identify balanced compromise solutions, paving the way for future studies on many-objective optimization.

Finally, Conclusion summarizes the key findings of the thesis, outlining potential directions for advancing the modeling, optimization, and assessment of ICES and RECs.

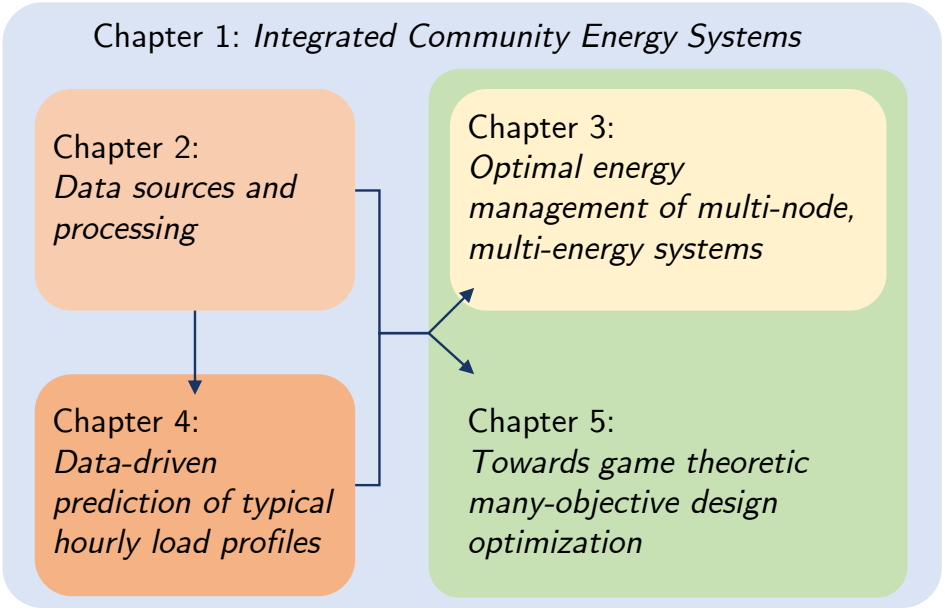

Fig. 1 Outline of the thesis structure and relations between chapters.

Published papers

This thesis is partially based on the following papers published in scientific journals or international conference proceedings, which were foundational to the development and testing of the methodologies proposed here.

- G. Lorenti, P. Lazzeroni, and M. Repetto, "A Data-Driven Approach to Predict Hourly Load Profiles From Time-of-Use Electricity Bills," in *IEEE Access*, vol. 11, pp. 60501–60515, 2023 [13].
- A. Canova, P. Lazzeroni, G. Lorenti, F. Moraglio, A. Porcelli, and M. Repetto, "Decarbonizing Residential Energy Consumption Under the Italian Collective Self-Consumption Regulation," in *Sustainable Cities and Society*, vol. 87, 2022 [11].
- F. Gullì, P. Lazzeroni, G. Lorenti, I. Mariuzzo, F. Moraglio, and M. Repetto, "Recoupled: A Simulation Tool for Renewable Energy Communities Coupling Electric and Thermal Energies," in *Economics and Policy of Energy and the Environment*, vol. 2, 2022 [14].
- G. Lorenti, P. Lazzeroni, and M. Repetto, "A Game Theory Approach to the Multi-Objective Design of Renewable Energy Communities," 2024 International Conference on Smart Energy Systems and Technologies (SEST), Torino, Italy, 2024, pp. 1–6 [15].
- P. Lazzeroni, G. Lorenti, F. Moraglio, and M. Repetto, "Modeling of Renewable Energy Communities: The RECoupled Approach," 2022 IEEE 46th Annual Computers, Software, and Applications Conference (COMPSAC), Los Alamitos, CA, USA, 2022, pp. 1349–1354 [16].
- P. Lazzeroni, G. Lorenti, F. Moraglio, and M. Repetto, "A MILP Approach for Demand Management in Renewable Energy Communities With Residential End-Users," 36th International Conference on Efficiency, Cost, Optimization, Simulation, and Environmental Impact of Energy Systems (ECOS 2023), 2023 [17].

In particular, the foundational modeling and assessment of multi-energy RECs discussed in Chapter 1 are developed in [11, 14, 16]. The methodologies employed in Chapter 2 concerning data sources and processing also draw from [11].

Chapter 3 expands on the modeling and optimization framework introduced in [16], offering a thorough analysis of energy sharing and multi-node configurations. Chapter 4 builds upon [13], reporting the core ideas and results while extending the application of data-driven methodologies to ICES assessment and design. Finally, Chapter 5 incorporates results from [14, 15], presenting a new exploratory analysis of the many-objective optimization problem for ICES design.

Other papers The following works, while focusing on other fields of application (mainly the design of electromagnetic devices), also involve and integrate optimization techniques (both deterministic and stochastic, such as metaheuristics) and data-driven modeling.

- G. Lorenti, C.S. Ragusa, M. Repetto, and L. Solimene, "Data-Driven Constraint Handling in Multi-Objective Inductor Design," in *Electronics*, vol. 12, pp. 781, 2023 [18].
- G. Lorenti, I. Mariuzzo, F. Moraglio, and M. Repetto, "Heuristic Optimization Applied to ANN Training for Predicting Renewable Energy Sources Production," in *COMPEL: The International Journal for Computation and Mathematics in Electrical and Electronic Engineering*, vol. ahead-of-print, 2022 [19].
- M. Repetto, F. Moraglio, and G. Lorenti, "Understanding Reinforcement Learning Control in Cyber-Physical Energy Systems," 2022 10th Workshop on Modeling and Simulation of Cyber-Physical Energy Systems (MSCPES), Milan, Italy, 2022, pp. 1–6 [20].
- L. Solimene et al., "Data-Driven Approaches for Electromagnetic Analysis of Traction Electrical Motors: A Proposal for a Benchmark Problem," 2024 International Conference on Electrical Machines (ICEM), Torino, Italy, 2024, pp. 1–7 [21].
- G. Lorenti, C.S. Ragusa, M. Repetto, and L. Solimene, "Support Vector Classifier for Constraints Handling in the Design of Inductors for DC-DC Converters," 2023 24th International Conference on the Computation of Electromagnetic Fields (COMPUMAG), Kyoto, Japan, 2023, pp. 1–4 [22].

Chapter 1

Integrated Community Energy Systems

Summary

This chapter introduces the key concepts of Integrated Community Energy Systems (ICES), providing a foundational framework for the thesis. It frames ICES within the broader landscape of local energy systems, focusing on their community-level and multi-energy integration. Synergies with Renewable Energy Communities (RECs) are highlighted, positioning them as practical ways to put ICES in effect under current regulatory frameworks. Additionally, the chapter establishes the modeling and multi-criteria assessment frameworks adopted throughout the thesis, laying the ground for the methodological developments in subsequent chapters (Chapters 3, 4, and 5).

Key objectives

- Establishing a taxonomy of local and community energy systems, positioning ICES as a holistic framework for optimizing energy use at the community level.
- Highlighting synergies between the concepts of ICES and RECs and exploring the regulatory frameworks in Europe and Italy.

- Formalizing a modeling framework for ICES, covering their multi-node and multi-energy nature, and their performance evaluation, including energy, environmental, and economic objectives.

The chapter is organized as follows. Section 1.1 introduces key concepts in local energy systems, including microgrids, smart grids, energy hubs, and energy communities, positioning ICES as a comprehensive framework to manage multi-energy systems, and discussing their relationship with RECs as practical implementation tools. Section 1.2 presents European and Italian regulatory frameworks for RECs, focusing on virtual energy-sharing mechanisms in Italy. Then, the modeling of ICES as multi-node and multi-energy systems is detailed in Section 1.3, framing the energy-sharing mechanism as a foundational element. Finally, the performance evaluation framework for ICES is outlined in Section 1.4, focusing on energy, environmental, and economic key performance indicators (KPIs).

1.1 Taxonomy

The evolving energy landscape has given rise to varied concepts in the context of local energy systems, each addressing different aspects of decentralization, resource optimization, and community participation. This section provides a taxonomy of key concepts and definitions essential for understanding integrated community energy systems. These definitions not only clarify the distinctions between various system types but also highlight their complementary roles in advancing sustainable energy systems.

1.1.1 Key definitions and concepts

Microgrid A localized, self-contained electricity network capable of operating independently (off-grid) or in conjunction with the centralized grid. Microgrids integrate distributed energy resources (DERs), such as solar photovoltaics and battery storage, to supply electricity within defined boundaries [8], and are often considered a foundational infrastructural element for broader energy systems concepts. They span different sizes depending on the context and application, ranging from the hundreds of kW to tenths of MW [23].

Smart Grid An electricity network enhanced by information and communication technologies (ICT) to enable real-time monitoring, automation, and integration of renewable energy sources. Smart grids are designed to improve reliability, efficiency, and resilience in energy distribution [7].

Sector Coupling The integration of multiple energy sectors –such as electricity, heating, cooling, and transportation– to improve overall system efficiency and flexibility, facilitating decarbonization and the large-scale integration of renewable energy [24].

Energy Hub A local system that manages the flow and conversion of multiple energy carriers (electricity, heat, gas) to optimize local energy systems. Energy hubs are equipped with storage, conversion, and distribution technologies, enabling multi-carrier optimization [8].

Virtual Power Plant (VPP) An aggregation of DERs (generation, storage, and flexible loads) managed to act as a single power plant [8]. VPPs can be either technical (location-specific) or commercial (location-agnostic), enabling DERs to participate in energy markets and grid services.

Prosumer An individual or entity that, differently from traditional "passive" consumers, both produces and consumes energy, typically from RES, their own needs, or within a community setting [25].

Peer-to-Peer (P2P) Energy Trading Direct energy transactions between prosumers within a community, enabled by smart grid technologies, supporting decentralized energy exchanges.

Energy Community Collaborative groups of producers, consumers, and prosumers who generate, share, and consume energy locally. These communities may focus on optimizing self-consumption, reducing energy costs, or meeting sustainability goals. Some are geographically bound (place-based), while others operate across wider regions without physical boundaries [7].

Renewable Energy Community A regulatory concept under the EU RED-II directive, promoting local renewable energy generation and consumption. RECs prioritize social and environmental goals over profit, emphasizing inclusivity, community engagement, and local governance [7].

Integrated Community Energy System A multifaceted energy system aimed at providing a comprehensive approach to managing local energy systems. ICESs integrate multiple energy carriers (e.g., electricity, heat, gas) and optimize distributed energy resources to fulfill the needs of local communities. They incorporate advanced technologies, promote energy autonomy, and emphasize community-scale integration, enabling collective decision-making and resource sharing, thus merging technological and social dimensions [7, 8].

The taxonomy reveals overlaps and distinctions between these concepts, all of which fall under the broader category of local energy systems but address different dimensions. Some concepts focus on infrastructure (e.g., microgrids, smart grids), others on energy management (e.g., energy hubs, VPPs), on the economic organization or business model (e.g., P2P energy trading, VPPs), or on regulatory frameworks and governance structures (e.g., energy communities, RECs). Despite their differences, these concepts are not mutually exclusive; they are largely complementary and collectively contribute to the transition toward decentralized and sustainable energy systems.

Among these concepts, ICES stands out as a more comprehensive and general framework, synthesizing technological, economic, and social dimensions into a unified system. ICES integrates elements of smart grids (e.g., optimized operation), energy hubs (for multi-carrier management), and energy communities (for collective action and decision-making). While microgrids are technologically sophisticated, they do not necessarily encompass the broader multi-carrier scope of ICES. Energy hubs, incorporating multiple energy carriers, do not inherently address the community-scale integration that ICES demands or ensure the inclusion of all relevant stakeholders. VPPs and P2P energy trading lack the social structures that ICES embodies, focusing primarily on economic structure and without addressing the full spectrum of technological integration and community collaboration.

1.1.2 Synergies between ICES and RECs

RECs are conceptually aligned with ICES, focusing on renewable energy generation, energy self-sufficiency, local scale, and sector coupling (i.e., integration of multi-energy carriers). Both emphasize energy efficiency, environmental sustainability, and economic viability. However, ICES is a broader concept encompassing multi-energy systems at the local level, while RECs represent a regulatory framework specifically designed to facilitate the implementation of such systems under existing governance structures. In the future, these schemes can extend their role to other energy markets thanks to their community-scale organization and the collective management of distributed energy resources, enabling them to contribute to grid stability through ancillary services, such as balancing supply and demand or supporting voltage regulation, further enhancing their value to the wider energy system.

In this sense, ICES can be viewed as a paradigm for comprehensive local energy systems, integrating technical, economic, and social dimensions, whereas RECs serve as a practical structure to implement these systems within the current regulatory landscape. However, RECs are constrained by specific national regulations (see Section 1.2), limiting their range of applicability. In contrast, ICESs provide a more flexible and forward-looking framework, enabling advanced multi-carrier optimization and integration of diverse energy sources.

The next section, therefore, provides an overview of REC definitions and regulations, with a particular focus on the Italian context and the mechanisms of virtual energy sharing. This discussion highlights the practical implementation of REC principles and their potential to serve as a foundation for the broader adoption of ICES.

1.2 Renewable Energy Communities

In recent years, RECs have emerged as a viable paradigm for citizens, local authorities, and SMEs, to collectively own and manage renewable generation assets and energy storage systems. A key feature of RECs is the possibility of sharing energy among local producers, prosumers, and consumers, facilitated through virtual energy-sharing mechanisms. Before RECs, self-consumers could install RES generation systems only for their consumption; a practice referred to as "behind-the-meter" or individual self-consumption. In contrast, energy sharing

within RECs allows members to collectively consume self-produced renewable energy through the public distribution grid.

Energy sharing increases local self-consumption due to the potential for serving multiple consumers and leveraging diversity in production and consumption profiles. Moreover, utilizing the public grid for these virtual exchanges makes energy sharing accessible without needing private infrastructure.

1.2.1 European and Italian regulatory frameworks

Although energy communities have a long history in Europe, RECs have been formally defined and legally recognized only recently. The *Clean Energy for All Europeans* package [3], aimed at empowering energy consumers and promoting the adoption of renewable energy, provides the primary regulatory basis for RECs. Specifically, Directive (EU) 2018/2001 on the promotion of the use of energy from renewable sources (RED II) [1] offers the foundational legal definitions and framework. This directive introduced the concept of the renewable self-consumer as a final customer capable of producing and consuming their energy from RES (a "one-to-one" paradigm[1]), therefore engaging in individual self-consumption. It then expanded this concept to:

- Jointly-acting renewable self-consumers, renewable self-consumers located within the same building or building block who can consume and share energy from a collective renewable plant ("one-to-many").
- Renewable energy communities, groups of multiple producers, consumers, and prosumers located in proximity to community-managed RES generation plants, enabling energy sharing among members ("many-to-many").

Fig. 1.1 provides a qualitative representation of the different levels of end user aggregation defined by the directive.

The directive outlined the rights of individuals and entities to establish RECs, allowing them to collectively produce, consume, store, and sell renewable energy while preserving their rights as end users. However, the directive left some aspects, such as the specific geographic perimeter of RECs and the detailed economic regulations, open for interpretation by individual member states. Additionally,

[1] Only one producer and one consumer, as opposed to "one-to-many" (i.e., one producer but multiple consumers) and "many-to-many".

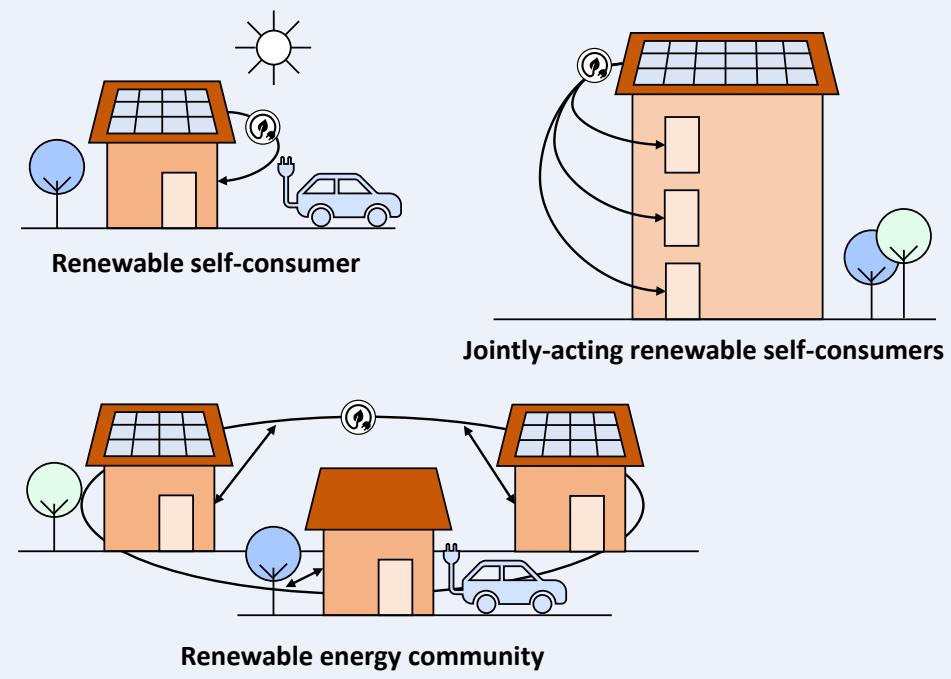

Fig. 1.1 Different levels of end user aggregation according to the directive RED II. (Adapted from https://ibmix.de/en/blog/energy-communities).

the directive allowed flexibility regarding whether RECs could own and manage private distribution grids and participate in ancillary services. Notably, the directive emphasizes that RECs should prioritize environmental and social objectives rather than economic benefits for their members, promoting sustainability and community engagement.

In Italy, the legislative journey towards the European directive transposition began in 2020 with the Decree-Law *Milleproroghe* [26], which introduced definitions aligned with those in RED II. According to this decree, RECs can consist of various end-user types, including citizens, local governments, and SMEs, utilizing renewable energy sources to produce, consume, and share electricity through the same public distribution grid. Initially, the regulatory framework limited REC participation to plants with capacities up to 200 kW, and all members had to be connected to the same low-voltage distribution grid, corresponding to the same secondary substation. This preliminary framework was complemented by regulations from the Italian Regulatory Authority for Energy, Networks, and Environment (ARERA) [27], decrees from the Ministry of Economic Development [28], and technical guidelines from the Energy Services Manager (GSE) [29].

The regulatory landscape progressed with the full transposition of the EU directive through Legislative Decree 199/2021 [30], which broadened the scope of energy-sharing configurations to include general collective self-consumption schemes. Additionally, the regulatory updates raised the allowable renewable plant capacity to 1 MW and extended the REC perimeter to encompass all members connected to the same medium-voltage distribution grid (primary substation). The full transposition process was finalized between 2022 and 2024 with the introduction of new regulations by ARERA [31], the revised incentive framework [32], and updated technical guidelines [33].

1.2.2 Virtual energy sharing

A significant feature of RECs is the concept of virtual energy sharing, as defined and regulated in Italy (and other European countries). Unlike individual self-consumption, which pertains to a single end user, energy sharing enables collective self-consumption among REC members. In the transposition of EU directives, RECs were restricted from operating private distribution grids, making the public grid essential for energy sharing. In this model, end users and renewable generation plants exchange electricity with the public grid through their connection points. Energy is considered shared when injected by some REC members and withdrawn by others in the same time frame.

Individual self-consumption occurs behind the meter and is measurable (hence called "physical"), as the difference between what is produced and what is injected into the grid. Energy sharing through the grid is instead a virtual mechanism, relying on measurements at each REC member's POD without tracing physical energy flows. The shared energy is calculated hourly as the minimum value between total injections and withdrawals by REC members.

While primarily an accounting method, regulatory frameworks treat shared energy similarly to physical self-consumption, as general "local self-consumption" –although some differences arise in the economic regulation, as detailed later. Given the geographic proximity of REC members to generation plants, it is reasonable to assume that most shared energy is consumed locally.

Tab. 1.1 summarizes this comparison between physical self-consumption and virtual energy sharing. An indirect difference between the two is the energy vectors that can be involved, aside from electricity. Physical self-consumption can theoretically involve any energy vector –unless specific regulations. In contrast,

Table 1.1 Comparison between physical self-consumption and virtual energy sharing.

Physical self-consumption	**Virtual energy sharing**
Through a direct –private– connection	Through the public grid
Individual (one-to-one)	Collective (one-to-many, many-to-many)
Measurable	Calculated
Instantaneous	Hour by hour
Any energy vector [1]	Depending on the existing infrastructure[2]
Economic savings	Incentivized[3]
Local self-consumption	

[1] In theory; in practice specific regulations apply; [2] Under the current regulations, only electricity; [3] Details are provided later on.

virtual energy sharing depends on existing public infrastructure and is currently limited to electricity under the regulatory framework. Furthermore, accurate implementation of virtual energy sharing requires precise measurement of energy flows for each REC member. This necessitates the use of advanced metering infrastructure, such as 2G smart meters, which can provide the granularity and reliability of data required to calculate shared energy accurately.

Despite energy sharing currently being limited to electricity, RECs enable a more integrated approach to energy self-consumption through sector coupling. For instance, electric vehicle charging stations could be part of a REC, allowing for a potentially more flexible energy load. Coupling multiple energy carriers is also possible—for example, converting surplus electricity generated within the community to meet other needs, such as heating through heat pumps—adding flexibility and enhancing overall self-consumption.

1.2.3 Economic regulation

Under the virtual scheme implemented in Italy, all electricity injected into the grid (i.e., all RES generation not consumed on-site) is eligible for the dedicated withdrawal service ("*ritiro dedicato*"). This service remunerates injected electricity at the hourly zonal market price, which is generally lower than the retail price.

Conversely, electricity withdrawn from the grid is still purchased by users at the retail rate from their energy suppliers.

The economic viability of RECs in Italy is supported by specific financial incentives designed to promote energy sharing:

- REC members receive a 20-year incentive for shared energy, established by the Ministry of Energy (MASE) [32]. While specific calculations are detailed in Section 2.4, a reference value of 130 €/MWh can be considered.
- Shared energy is regarded as locally consumed, exempting it from variable transmission and distribution charges, worth roughly 10 €/MWh as of 2024.

Overall, the economic value of shared energy in RECs is estimated at approximately 140 €/MWh. By comparison, market and retail electricity prices in 2024 were roughly 110 and 310 €/MWh, respectively [34, 35].

The significant gap between market and retail prices arises from various additional costs included in the retail rate: retail marketing (i.e., revenue for electricity suppliers), metering and transportation fees, system charges, and taxes. These costs typically consist of a variable component, proportional to energy consumption, and a fixed component based on the contracted power level of each end user, making the effective retail price higher for end users with low consumption.

As shared energy is reimbursed for transportation fees, the incentive can be interpreted as an additional compensation to offset the other costs for shared energy. System charges are intentionally applied to shared energy since RECs remain integrated into the broader energy system [26]. Considering that each unit of shared energy is injected (by some members) and withdrawn (by others), the incentive narrows but does not fully bridge the gap between retail and market prices. As a result, shared energy is less economically attractive than physical self-consumption, although it is generally easier to achieve.

Tab. 1.2 summarizes the economic regulations for RECs (in Italy), which however can differ across countries. For instance, in France, shared electricity is directly deducted from the end users' bills without remuneration to the producers, while a network fee is applied to account for the use of the public grid [36].

1.3 Multi-node and multi-energy modeling

The insights about RECs presented in Section 1.2 highlight their role as a bridge between theoretical energy community concepts and practical energy-sharing ap-

plications. RECs provide an effective approach for implementing an ICES within current regulatory frameworks, particularly in Italy. This is largely due to their capacity for virtual energy-sharing mechanisms, which facilitate the distribution of renewable energy among multiple members using the public grid. Understanding these mechanisms helps frame the ICES modeling presented in the following, where multiple interconnected energy nodes can coordinate the local energy production and consumption.

ICES is modeled as an ensemble of "energy nodes", interconnected through one or more energy networks. Each energy node is characterized by its point(s) of connection to the energy network(s), which enables energy withdrawal and/or injection: active nodes can inject energy (e.g., producers and prosumers), while passive nodes can only withdraw energy (pure consumers).

Fig. 1.2 shows a simple example of an ICES that complies with the definition of a REC: a set of electricity consumers, prosumers, and producers, all connected to the same (public) electricity distribution grid.

Within an energy node, it is possible to meet the demand of different energy carriers using a combination of local generators, and conversion and storage technologies ("components"), thus creating an individual multi-energy system. Since they are interconnected, any energy surplus generated by one node and injected into the network can be utilized by others. In such cases, energy is shared among nodes, and consumed within the ICES boundaries. Conversely, any locally produced energy vector without an interconnecting network must be consumed internally, i.e., within the boundaries of a single node.

Based on these considerations, two spatial scales are considered in the model: the individual energy nodes and the overall ICES. Regarding temporal resolution,

Table 1.2 Summary of the economic regulation for RECs in Italy.

Flow of energy	**Economic value**	**Reference value (€/MWh)**
Withdrawn	Retail price[4]	330
Injected	Market price[5]	110
Shared	Incentive	130
	Network fee	10

[4] Cost for REC members; [5] Revenue for REC members.

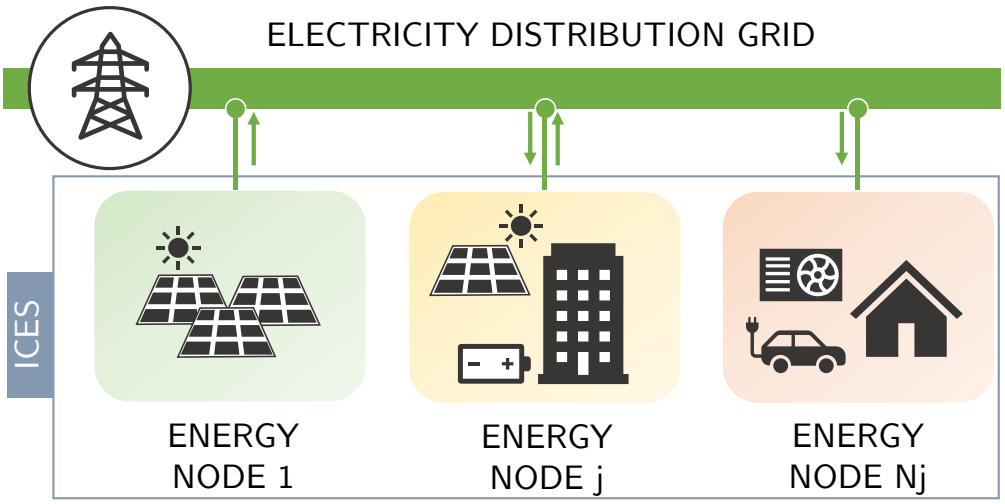

Fig. 1.2 Simple example of ICES as a group of electricity consumers, prosumers, and producers. (Adapted from [16]).

instantaneous power balances are ideally considered. However, a discrete-time approach is adopted due to computational constraints and the unavailability of high-resolution data, typically using hourly time steps, as detailed later on. This aligns with regulatory requirements for RECs, where shared energy is evaluated hourly.

Despite the discrete-time approach the term 'power' is still used, indicating the uniform average value corresponding to the same energy during each time step. The term 'energy' is used instead for quantities with coarser granularity (e.g., daily or monthly). Each variable is assigned a name along with a set of subscripts and superscripts, which uniquely identify it by its associated energy node, component, type (e.g., input or output power), energy vector, and specific time step, as depicted in Fig. 1.3. However, subscripts and superscripts are omitted wherever they are not strictly necessary, to lighten the notation.

1.3.1 Energy nodes

Energy nodes integrate multiple components –i.e., technologies for energy production, conversion, and storage– to fulfill local energy demands. Loads –electricity, heating, etc.– are also considered components, functioning as energy sinks. Detailed models for these components are provided in Section 3.2, while this section focuses on the general equations governing energy nodes and their interactions with the networks.

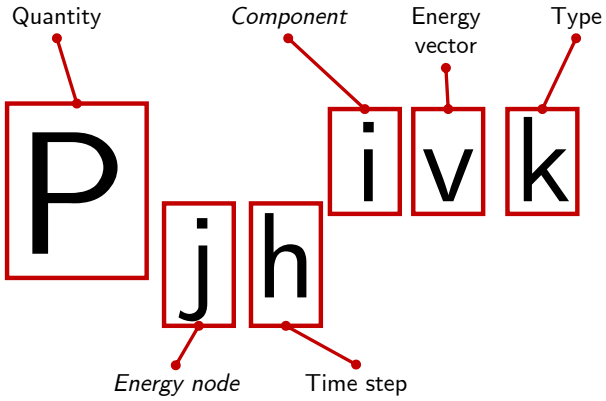

Quantity	Power, energy, cost, etc.
Component	Generator (e.g., photovoltaic), load (e.g., electric), storage (e.g., battery)
Energy vector	Electricity, heat, etc.
Type	Input, output, etc

Fig. 1.3 Notation adopted in the ICES model equations.

All nodes in an ICES are connected to one or more energy networks. Certain networks –e.g., the gas distribution network– only allow energy withdrawal, while others –such as the electric grid– support withdrawal and injection, enabling energy sharing with other nodes. Fig. 1.4 presents a detailed, though not exhaustive, example of a "multi-energy" node.

Nodes within an ICES must maintain individual balances between the energy they consume, produce, and exchange with the networks, ensuring the demand for each energy vector is met at all time steps. This power balance is expressed mathematically for each node j as follows:

$$\sum_{i \in I_{\mathrm{j}}^{\mathrm{in}}} P^{\mathrm{i,in}} + P^{\mathrm{inj}} = \sum_{i \in I_{\mathrm{j}}^{\mathrm{out}}} P^{\mathrm{i,out}} + P^{\mathrm{with}}, \tag{1.1}$$

where $P^{\mathrm{i,in}}$ and $P^{\mathrm{i,out}}$ represent the inflows and outflows of power to/from component i in node j, while P^{inj} and P^{with} are the exchanges with the network (injection and withdrawal, respectively). Sets $I_{\mathrm{j}}^{\mathrm{in}}$ and $I_{\mathrm{j}}^{\mathrm{out}}$ include the components for which the vector v (whose superscript is omitted) is an inflow and an outflow, respectively. The balance holds at each time step, for each energy node.

Network exchanges in (1.1) may not always be present, for instance for an energy carrier that is only internal to the node. When network injections are not feasible –due to infrastructure constraints or regulatory limitations– the balance states that any self-generation must be consumed locally.

According to (1.1), all components involving a specific energy carrier –as an inflow or outflow– contribute to this balance equation. Additional energy vectors

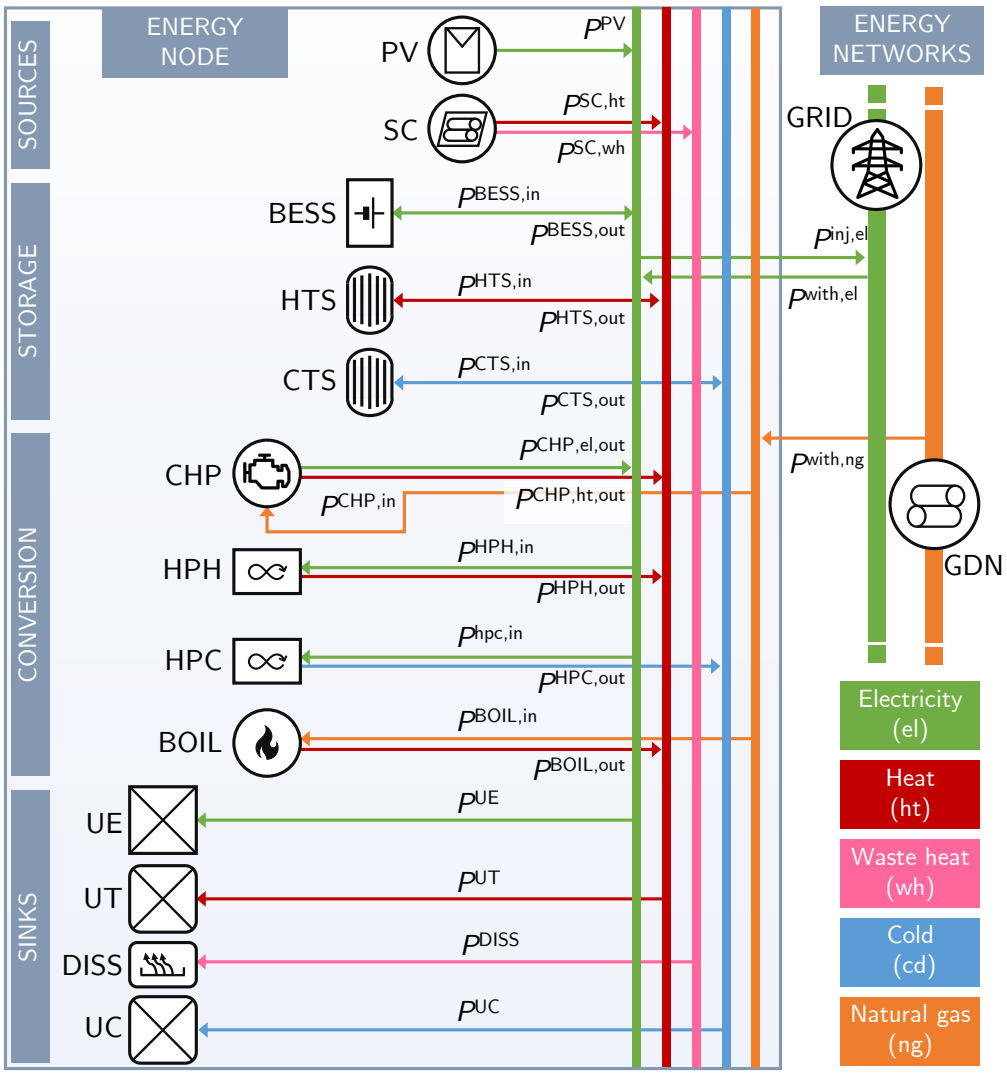

BESS	Battery Energy Storage System	BOIL	Gas-fired boiler
CHP	Micro-cogeneration unit	CTS	Cold Thermal Storage
DISS	Heat dissipation unit	GDN	Natural Gas Distribution Network
GRID	Electricity distribution grid	HPC	Heat Pump for Cooling
HPH	Heat Pump for Heating	HTS	Heat Thermal Storage
PV	PhotoVoltaic generator	SC	Solar Collectors system
UC	Cooling load	UE	Electric load
UT	Thermal load		

Fig. 1.4 Example of an energy node as a multi-energy system. (Adapted from [16] and [37]).

can then be incorporated into the model to represent particular situations and adapt to specific needs. For example, waste heat is included in the node depicted in Fig. 1.4, to avoid unrealistic scenarios. However, only the solar collectors can dissipate heat, and a distinct vector is introduced to represent this process.

1.3.2 ICES

Fig. 1.5 shows a general representation of an ICES as an ensemble of energy nodes of different types (active, passive) involving different energy vectors, interconnected by multiple energy networks.

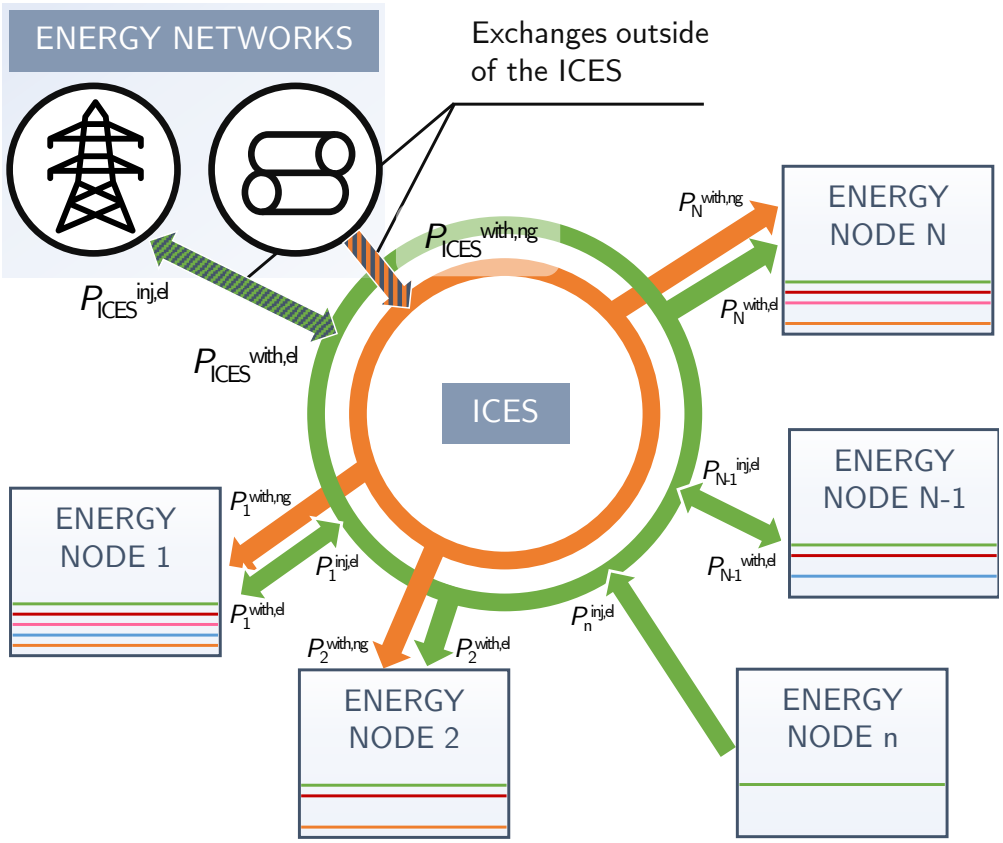

Fig. 1.5 Example of an ICES as an ensemble of energy nodes interconnected by some energy networks. The exchanges outside of the ICES are highlighted.

The nodes in an ICES exchange energy with each other through the available networks. As mentioned earlier, energy is shared when it is simultaneously injected by some nodes and withdrawn by others. Thus, it is calculated as the

minimum between the total injections and withdrawals from the nodes, as follows:

$$P^{\text{shared}} = \min\left(\sum_{j\in J} P_{\text{j}}^{\text{inj}}; \sum_{j\in J} P_{\text{j}}^{\text{with}}\right), \tag{1.2}$$

where J is the set of nodes in the ICES. This equation is written for each vector and each time step.

Shared energy is assumed to be produced and consumed within the ICES boundaries, reducing the energy flows to and from external networks. In fact, the global energy balance on each network is given by:

$$P_{\text{ICES}}^{\text{inj}} - P_{\text{ICES}}^{\text{with}} = \sum_{j\in J} P_{\text{j}}^{\text{inj}} - \sum_{j\in J} P_{\text{j}}^{\text{with}}, \tag{1.3}$$

where $P_{\text{ICES}}^{\text{inj}}$ and $P_{\text{ICES}}^{\text{with}}$ represent the powers exchanged by the ICES beyond its boundaries (injections and withdrawals, respectively). As before, subscripts for the energy vector v and time step h have been omitted.

By combining (1.2) and (1.3), and noting that power injections and withdrawals from the ICES cannot occur simultaneously (i.e., they are mutually exclusive in each time step), the following equations are derived:

$$P_{\text{ICES}}^{\text{inj}} = \sum_{j\in J} P_{\text{j}}^{\text{inj}} - P^{\text{shared}}, \tag{1.4}$$

$$P_{\text{ICES}}^{\text{with}} = \sum_{j\in J} P_{\text{j}}^{\text{with}} - P^{\text{shared}}. \tag{1.5}$$

These equations explicitly show how shared energy reduces the exchanges outside the ICES compared to what would occur if only individual nodes were considered.

1.3.3 Time discretization

As mentioned earlier, time step length and overall time horizon are crucial aspects of ICES modeling. A finer time resolution and an extended time horizon provide a more accurate representation of variability in input quantities, improving model fidelity. In real applications, a sufficiently long time horizon should be considered to capture key aspects such as the lifespan of system components and, where relevant, the duration of policy incentives (e.g., 20 years for REC support schemes).

However, enhancing time quality comes at the cost of computational complexity, particularly when optimization is involved (see Chapter 3). Furthermore, data availability usually plays a significant role in determining the level of detail that can be incorporated into the model. A resolution finer than one hour may not always be achievable, especially considering energy consumption data, limiting the granularity of the time discretization. Likewise, data covering periods longer than one year are seldom available, restricting the time horizon that can be considered.

To maintain generality, the ICES modeling equations presented earlier and the performance assessment in the following section are formulated for a general, sufficiently long time horizon.

However, in the practical evaluations conducted in this thesis, a one-year time horizon with an hourly time step is adopted for ICES operation, balancing data availability (see Chapter 2) with computational burden (see Chapter 3). For long-term performance evaluations, such as for economic and environmental assessment (e.g., 20 years), this one-year horizon serves as a reference period, assumed to repeat over time.

This choice balances computational feasibility and model accuracy, allowing seasonal variations in renewable generation and energy consumption to be captured.

1.4 Multi-criteria evaluation

ICES are assessed from different perspectives to capture their multiple (and often conflicting) objectives, including environmental, social, and economic aspects. Key Performance Indicators (KPIs) provide an easy-to-grasp yet comprehensive method for evaluating these systems. They are valuable for assessing efficiency, sustainability, and economic viability, and enabling comparisons between different configurations thus supporting decision-making during the design phase.

A key aspect of ICES evaluation is the dual perspective of individual nodes versus the entire community. Energy balances are first performed at the node level and then aggregated for the whole ICES, as described in the previous sections. Consequently, energy-related quantities -such as production, consumption, and self-consumption– can be assessed at both scales. Accordingly, KPIs can be defined for both individual nodes and the entire system, although in this thesis, they are primarily reported at the community level.

As briefly introduced in Chapter 2 and further detailed in Chapter 5, KPIs often conflict with each other (e.g., economic vs. environmental objectives). This complexity is further amplified at the individual node scale, where additional layers of conflict may emerge, not only in economics but also in energy and environmental performance. Moreover, as the number of individual KPIs grows, so does the complexity of multi-criteria decision-making. Methods to address this increased complexity and facilitate decision-making are analyzed in Chapter 5.

1.4.1 Individual energy node

The calculation of KPIs begins with assessing relevant energy quantities within the ICES. For each energy node j and energy vector ν (whose superscript is omitted in the notation), two quantities can be calculated, by integrating over the considered time horizon (or summing over discrete time steps):

- The energy produced ($E_{\mathrm{j}}^{\mathrm{prod}}$) is the sum of the output across generators.
- The energy consumed ($E_{\mathrm{j}}^{\mathrm{cons}}$) is the sum of the input across loads.

Energy exchanges with the network, such as injections ($E_{\mathrm{j}}^{\mathrm{inj}}$) and withdrawals ($E_{\mathrm{j}}^{\mathrm{with}}$), are similarly assessed by integrating the respective power flows over time.

Individual self-consumption, representing the portion of local generation used directly within the node, is calculated by subtracting network injections from the total production, as follows:

$$E_{\mathrm{j}}^{\mathrm{self-cons}} = E_{\mathrm{j}}^{\mathrm{prod}} - E_{\mathrm{j}}^{\mathrm{inj}}. \tag{1.6}$$

Based on the energy balance at each node from (1.1), and under the assumption that network injections and withdrawals cannot occur simultaneously, individual self-consumption can alternatively be expressed as:

$$E_{\mathrm{j}}^{\mathrm{self-cons}} = E_{\mathrm{j}}^{\mathrm{cons}} - E_{\mathrm{j}}^{\mathrm{with}}. \tag{1.7}$$

When components, such as heat pumps or storage systems, modify the energy consumption of a node beyond its direct loads, the definitions of $E_{\mathrm{j}}^{\mathrm{prod}}$ and $E_{\mathrm{j}}^{\mathrm{cons}}$ must be carefully reconsidered. The decision to evaluate node consumption and production based on only direct loads or to include all components can

significantly impact metrics such as self-consumption and self-sufficiency rates (described in the following) [38].

In this thesis, all components involving energy storage or conversion are included in this calculation, ensuring consistency between the energy balances and the definition of quantities like $E_{\mathrm{j}}^{\mathrm{self-cons}}$ at the node level. For instance, in the case of a heat pump, its output power is included as heat production (treated as if it were a generator in this vector), while its input power is classified as electricity consumption (treated as if it were a load).

1.4.2 ICES-level

ICES-level quantities for these relevant energy quantities can be obtained by summing the respective values across all nodes, as follows:

$$\begin{aligned} E^{\mathrm{prod}} &= \sum_j E_{\mathrm{j}}^{\mathrm{prod}}, \\ E^{\mathrm{cons}} &= \sum_j E_{\mathrm{j}}^{\mathrm{cons}}, \\ E^{\mathrm{inj}} &= \sum_j E_{\mathrm{j}}^{\mathrm{inj}}, \\ E^{\mathrm{with}} &= \sum_j E_{\mathrm{j}}^{\mathrm{with}}, \\ E^{\mathrm{self-cons}} &= \sum_j E_{\mathrm{j}}^{\mathrm{self-cons}}. \end{aligned} \tag{1.8}$$

The total energy consumed locally within the ICES, encompassing both individual self-consumption and shared energy, is given by:

$$E^{\mathrm{local}} = E^{\mathrm{self-cons}} + E^{\mathrm{shared}}. \tag{1.9}$$

Using the energy balance equations for individual nodes and the overall ICES:

$$\begin{aligned} E^{\mathrm{local}} &= E^{\mathrm{self-cons}} + E^{\mathrm{shared}} \\ &= \left(E^{\mathrm{prod}} - \sum_j \cancel{E_{\mathrm{j}}^{\mathrm{inj}}} \right) + \left(\sum_j \cancel{E_{\mathrm{j}}^{\mathrm{inj}}} - E_{\mathrm{ICES}}^{\mathrm{inj}} \right) \\ &= E^{\mathrm{prod}} - E_{\mathrm{ICES}}^{\mathrm{inj}}. \end{aligned}$$

Similarly, it can be shown that $E^{\mathrm{local}} = E^{\mathrm{cons}} - E_{\mathrm{ICES}}^{\mathrm{with}}$.

1.4.3 Energy KPIs

Two fundamental indicators for assessing the performance of an ICES are the self-consumption (SC) and self-sufficiency (SS) rates [4]. Self-consumption represents the proportion of locally produced renewable energy consumed within the ICES, while self-sufficiency measures the extent to which the energy demand in the ICES is met by local generation.

Physical self-consumption and self-sufficiency consider only individual self-consumption, at the level of each energy node, or across the entire ICES as follows:

$$\mathrm{SC}_{\mathrm{phy}} = \frac{E^{\mathrm{self-cons}}}{E^{\mathrm{prod}}} = 1 - \frac{\sum_j E_{\mathrm{j}}^{\mathrm{inj}}}{E^{\mathrm{prod}}}, \tag{1.10}$$

$$\mathrm{SS}_{\mathrm{phy}} = \frac{E^{\mathrm{self-cons}}}{E^{\mathrm{cons}}} = 1 - \frac{\sum_j E_{\mathrm{j}}^{\mathrm{with}}}{E^{\mathrm{cons}}}. \tag{1.11}$$

Here, the alternative expressions for each KPI utilize the definitions of self-consumption from (1.6) and (1.7), respectively.

Virtual self-consumption and self-sufficiency represent the proportion of shared energy relative to total injections and withdrawals and are calculated as follows:

$$\mathrm{SC}_{\mathrm{vir}} = \frac{E^{\mathrm{shared}}}{\sum_j E_{\mathrm{j}}^{\mathrm{inj}}} = 1 - \frac{E_{\mathrm{ICES}}^{\mathrm{inj}}}{\sum_j E_{\mathrm{j}}^{\mathrm{inj}}}, \tag{1.12}$$

$$\mathrm{SS}_{\mathrm{vir}} = \frac{E^{\mathrm{shared}}}{\sum_j E_{\mathrm{j}}^{\mathrm{with}}} = 1 - \frac{E_{\mathrm{ICES}}^{\mathrm{with}}}{\sum_j E_{\mathrm{j}}^{\mathrm{with}}}, \tag{1.13}$$

where the alternative expressions on the right leverage the relations from (1.4) and (1.5).

Unique KPIs encompassing physical self-consumption and virtual energy sharing can be derived by considering the local self-consumption defined in (1.9).

Based on these definitions, the global self-consumption and self-sufficiency rates are calculated as follows:

$$\mathrm{SC} = \frac{E^{\mathrm{local}}}{E^{\mathrm{prod}}} = 1 - \frac{E_{\mathrm{ICES}}^{\mathrm{inj}}}{E^{\mathrm{prod}}}, \tag{1.14}$$

$$\mathrm{SS} = \frac{E^{\mathrm{local}}}{E^{\mathrm{cons}}} = 1 - \frac{E_{\mathrm{ICES}}^{\mathrm{with}}}{E^{\mathrm{cons}}}. \tag{1.15}$$

Production and consumption are used as denominators in (1.14) and (1.15) (instead of injection and withdrawal) to ensure that the KPIs range between 0 and 1, maintaining consistency with other metrics.

1.4.4 Environmental KPIs

The environmental performance is assessed by evaluating the equivalent CO_2 emissions in the ICES configuration, denoted as $\mathrm{EM}_{\mathrm{CO_2}}$. These emissions depend on the ICES operations. Specifically, individual self-consumption and virtual energy sharing from renewable sources reduce the need for energy withdrawals from external grids, which typically have associated emission factors (ϵ). The operative emissions at the ICES level are calculated as follows:

$$\mathrm{EM}^{\mathrm{oper}}_{\mathrm{CO_2}} = \sum_{\mathrm{v}} \left(\epsilon^{\mathrm{with,v}} E^{\mathrm{with,v}}_{\mathrm{ICES}} - \cancel{\epsilon^{\mathrm{inj,v}} E^{\mathrm{inj,v}}_{\mathrm{ICES}}} \right) = \sum_{\mathrm{v}} \epsilon^{\mathrm{with,v}} E^{\mathrm{with,v}}_{\mathrm{ICES}}. \tag{1.16}$$

where the emissions are summed over all energy vectors v.

The term $\epsilon^{\mathrm{inj,v}} E^{\mathrm{inj,v}}_{\mathrm{ICES}}$, which could represent avoided emissions due to renewable energy produced by the ICES but not consumed locally, is excluded to maintain the local focus of the ICES.

Renewable generators, coupling technologies, and energy storage systems typically have emissions associated with their production, maintenance, and dismantling cycles. These "life-cycle" emissions are incorporated into the overall assessment. They are generally proportional to the size of the technologies and are determined using specific emission factors. If the lifetime of a technology is shorter than the chosen time horizon, these emissions are scaled to account for multiple replacements over the analysis period.

Considering the component i, its life-cycle emissions, denoted as $\mathrm{EM}^{\mathrm{LCA,i}}_{\mathrm{CO_2}}$, are calculated as follows:

$$\begin{aligned} \mathrm{EM}^{\mathrm{LCA,i}}_{\mathrm{CO_2}} &= q^{\mathrm{i}} \epsilon^{\mathrm{i}} S^{\mathrm{i}}, \\ \text{where } q^{\mathrm{i}} &= \left\lceil \frac{n}{n^{\mathrm{i}}} \right\rceil. \end{aligned} \tag{1.17}$$

Here, n represents the analysis time horizon, n^{i}, ϵ^{i} and S^{i} are the useful life, size, and life-cycle emission factor of the component, respectively. The operator $\lceil \cdot \rceil$ denotes the ceiling function, and q^{i} indicates the number of times the component needs to be replaced within the time horizon –including the first purchase.

For example, a photovoltaic generator typically has a useful life of 25–30 years [39], meaning that over a 20-year horizon, only one purchase would be required. Electrochemical batteries, on the other hand, generally have a shorter lifespan due to degradation [40]. For instance, assuming a 10-year useful life (see Section 2.5 for details), a 20-year analysis horizon would require two purchases, effectively doubling the associated LCA emissions.

The total CO_2 emissions for the ICES are expressed as:

$$\mathrm{EM}_{\mathrm{CO}_2} = n\mathrm{EM}^{\mathrm{oper}}_{\mathrm{CO}_2} + \mathrm{EM}^{\mathrm{LCA}}_{\mathrm{CO}_2}, \tag{1.18}$$

where the annual operative emissions are adjusted according to the time horizon of the ICES operation, and the life-cycle emissions $\mathrm{EM}^{\mathrm{LCA}}_{\mathrm{CO}_2}$ are obtained by summing across all components in the ICES.

A KPI for the environmental performance of the ICES can be calculated by comparing its emissions against a baseline scenario. In this thesis, the baseline assumes that all energy demands of the nodes are met exclusively using existing energy networks without any local generation. The emissions for this base case are calculated as follows:

$$\mathrm{EM}^{(0)}_{\mathrm{CO}_2} = \mathrm{EM}^{\mathrm{oper}(0)}_{\mathrm{CO}_2} = n\sum_{v} \epsilon^{\mathrm{with,v}} E^{\mathrm{with(0),v}}_{\mathrm{ICES}} = n\sum_{v} \epsilon^{\mathrm{with,v}} E^{\mathrm{cons,v}}. \tag{1.19}$$

Here, $E^{\mathrm{with(0),v}}_{\mathrm{ICES}}$ represents the network withdrawals of the ICES in the base case and is equal to $E^{\mathrm{cons,v}}$, the total energy consumption by loads requiring an input of energy vector v.

Finally, an emissions reduction coefficient (ER) can be evaluated to quantify the environmental improvement provided by the ICES compared to the baseline:

$$\mathrm{ER} = \frac{\mathrm{EM}^{(0)}_{\mathrm{CO}_2} - \mathrm{EM}_{\mathrm{CO}_2}}{\mathrm{EM}^{(0)}_{\mathrm{CO}_2}}. \tag{1.20}$$

Since the avoided emissions from network injections outside the ICES are excluded from (1.16), the total ICES emissions will always be greater than zero. As a result, the ER value cannot exceed 1. However, unlike self-consumption and self-sufficiency, ER could, in principle, be negative. This scenario could occur if the lifecycle emissions of the ICES components are significantly higher than

the baseline emissions. Numerical considerations regarding the choices for ICES emissions calculation are discussed in Section 2.6.

1.4.5 Economic KPIs

The economic performance of an ICES is assessed by evaluating the total costs over its operational period, including both initial investments (CAPEX) and operational expenditures (OPEX). The total actualized cost (TAC) is used to capture the combined financial burden of capital and operational costs:

$$\mathrm{TAC} = C^{\mathrm{capex}} + \sum_{t=1}^{n} \frac{C_{\mathrm{t}}^{\mathrm{opex}} + C_{\mathrm{t}}^{\mathrm{energy}}}{(1+r)^t} - \frac{C^{\mathrm{residual}}}{(1+r)^n}. \tag{1.21}$$

Here, C^{capex} represents the initial capital expenditure for purchasing and installing components, and C^{residual} denotes the residual value of the assets at the end of the analysis period, properly actualized. $C_{\mathrm{t}}^{\mathrm{opex}}$ includes annual operational costs –e.g., maintenance, insurance, taxes– while $C_{\mathrm{t}}^{\mathrm{energy}}$ encompasses yearly energy expenses and incomes. Finally, n and r refer to the project lifetime and the discount rate, respectively.

Similarly to LCA emissions, calculating costs accounts for the possibility of multiple purchases for a given component. These purchases are determined based on the component's replacement cycle, occurring at intervals equal to its useful life. Each expenditure is discounted to its present value at the initial (0-th). For each component i, the capital expenditure $C^{\mathrm{capex,i}}$ is calculated by summing up the costs of all purchases required over the considered time horizon, as follows:

$$\begin{aligned} C^{\mathrm{capex,i}} &= \sum_{\mathrm{t}=0}^{\mathrm{n}} \frac{C_{\mathrm{t}}^{\mathrm{capex,i}}}{(1+r)^t}, \\ \text{where } C_{\mathrm{t}}^{\mathrm{capex,i}} &= \begin{cases} c^{\mathrm{i}} S^{\mathrm{i}}, & \text{if } t = \lfloor n^{\mathrm{i}} k \rfloor, \text{ for } k = 0, \ldots, q^{\mathrm{i}} - 1, \\ 0, & \text{otherwise.} \end{cases} \end{aligned} \tag{1.22}$$

Here, c^{i} is the unit purchase cost of component i, S^{i} is its size, and n^{i} its useful life. The term q^{i} represents the total number of replacements required within the considered time horizon n –including the initial purchase– and is calculated as in (1.17). The operator $\lfloor \cdot \rfloor$ is the "floor" function, which returns the first useful year at which the component must be replaced.

Consequently, the residual value of each component i at the end of the time horizon is computed as:

$$C^{\text{residual,i}} = \frac{n - q^{\text{i}} n^{\text{i}}}{n^{\text{i}}} c^{\text{i}} S^{\text{i}}, \tag{1.23}$$

which represents the remaining lifetime of the most recently purchased component at the end of the horizon, expressed as a fraction of its useful life, multiplied by the purchase cost. As described in (1.21), this residual value is discounted to its present value at the end of the time horizon.

Fig. 1.6 illustrates three examples of the calculation (and discounting) of capital expenditure and residual value for components with different life spans over a conventional 20-year time horizon. Components with a life span longer than the time horizon (A) do not require replacement and retain a residual value at the end of the period. Components with a shorter life span require replacement upon reaching the end of their useful life, and the new expenditure is discounted based on the year in which it occurs. Then, if the time horizon is an exact multiple of their lifetime, they will not have a residual value (B); otherwise, they will (C).

Yearly operative costs, which primarily include maintenance and insurance expenses for the components are proportional to the size of each component and are evaluated based on unit cost rates.

The calculation of yearly energy costs depends on the specific regulations governing the ICES. These typically include expenditures for energy withdrawn from the network(s) and revenues from energy injected into the network. When shared energy is allowed, incentives like those described in Section 1.2.3 for RECs can also be considered. Energy costs are further discussed in Section 3.3.2.

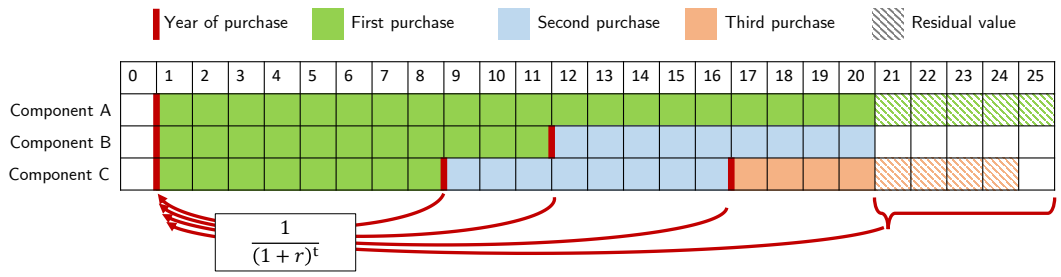

Fig. 1.6 Examples of capital expenditure and residual value calculation (and discounting) for three components with different life spans over a conventional 20-year time horizon: components A, B, and C have a useful life of, respectively, 25, 10, and 8 years.

A baseline scenario provides a benchmark for economic evaluation. Similar to the environmental performance, this cost ($\mathrm{TAC}^{(0)}$) considers the energy costs incurred when all demands are met using only existing energy networks, without local generation:

$$\mathrm{TAC}^{(0)} = \sum_{t=1}^{n} \frac{C_{\mathrm{t}}^{\mathrm{energy}(0)}}{(1+r)^t}. \tag{1.24}$$

The cost reduction (CR) KPI quantifies the financial savings achieved by implementing the ICES:

$$\mathrm{CR} = \frac{\mathrm{TAC}^{(0)} - \mathrm{TAC}}{\mathrm{TAC}^{(0)}}. \tag{1.25}$$

In addition to CR, other financial metrics, such as Net Present Value (NPV), Internal Rate of Return (IRR), and Payback Time (PBT), are used to assess the economic performance.

The NPV is calculated by considering ICES costs and revenues, while the costs in the baseline scenario are treated as additional revenues, i.e., savings:

$$\mathrm{NPV} = -C^{\mathrm{capex}} - \sum_{t=1}^{n} \frac{C_{\mathrm{t}}^{\mathrm{opex}} + C_{\mathrm{t}}^{\mathrm{energy}} - C_{\mathrm{t}}^{\mathrm{energy}(0)}}{(1+r)^t} + \frac{C^{\mathrm{residual}}}{(1+r)^n}. \tag{1.26}$$

The IRR is defined as the discount rate (r) that makes the NPV equal to 0 in (1.26). PBT is the earliest year (t) at which the NPV becomes positive, provided such a year exists within the considered time horizon.

As mentioned earlier in this section, these KPIs can be calculated either for the entire ICES or at the level of individual nodes. The latter approach introduces an additional layer of complexity, as it requires defining internal transactions and allocating costs and benefits. For example, in the context of a REC, the incentive for shared energy must be distributed among members according to criteria set by the REC itself. These criteria could be based on fair-sharing mechanisms [41], among other possible allocation strategies.

Chapter 2

Data sources and processing

Summary

This chapter presents the data used throughout the thesis, providing the foundation for assessing the modeling, evaluation, and optimization frameworks developed in subsequent chapters. Without a real-world case study, these data were collected from multiple sources to construct a comprehensive dataset. The chapter emphasizes the processing and preparation of these data to ensure consistency and applicability to the proposed methodologies.

Key objectives

- Detailing the sources and processing methods of the data used in the thesis.
- Constructing a consistent and representative dataset to support the proposed analyses.
- Establishing a preliminary baseline assessment of the ICES under consideration.

The chapter is organized as follows. Hourly electricity consumption data collected from about one hundred end users in a small city near Turin (Northern Italy) are presented in Section 2.1. Section 2.2 describes photovoltaic generation data sourced from the Photovoltaic Geographical Information System (PVGIS). Section 2.3 outlines the modeling approach for estimating the heating demand based on a typical multi-family residential building using meteorological data. Electricity price data, including market values, incentives, and retail tariffs, and

their processing is described in Section 2.4, while Section 2.5 complements with data about the technologies considered in the different cases. Finally, a preliminary baseline assessment is performed in Section 2.6, evaluating an ICES scenario with varying photovoltaic capacities and establishing trends in energy, environmental, and economic KPIs.

2.1 Electric Load

The electric load data used in this thesis are derived from a dataset of hourly electricity consumption spanning April 2021 to the end of March 2022. The dataset, provided by a local multi-utility, contains measurements of 114 end-users from a small city near Turin, in Piedmont (Northern Italy). As the first filtering, users with extremely high consumption were identified from the histograms of the annual energy consumption and removed from the dataset, leaving 103 end-users.

The remaining end-users are categorized into households (DOM) and non-domestic users (BTA – *bassa tensione altri usi*). They can be further divided based on the rated power level at the point of delivery (POD), as detailed in Tab. 2.1, or by specific end-user category. Fig. 2.1 illustrates the composition of the dataset according to these classifications, where the class DOM1, having just one sample, was merged into DOM2 to form a new category, DOM1-2.

Household (DOM) end-users typically exhibit distinct consumption patterns compared to non-domestic (BTA) users, who are more influence by specific energy uses. For instance, a bakery may consume more energy at night, whereas an office usually has peak consumption during daytime hours. Additionally, household users generally have lower energy consumption, as shown in Fig. 2.2.

Therefore, the annual consumption profiles are presented separately for households and non-domestic users to enhance clarity. Fig. 2.3 shows the hourly profile of household energy consumption over the entire year (top), along with the cor-

Table 2.1 Codes assigned to end-user classes according to type (DOM and BTA) and level of contractual power at their POD (in kW), as defined by ARERA.

	1	2	3	4	5	6
DOM	≤1.5	1.5–3	>3	∀[6]	n.a.	n.a.
BTA	≤1.5	1.5–3	3–6	6–10	10–16.5	>16.5

[6] Non-resident.

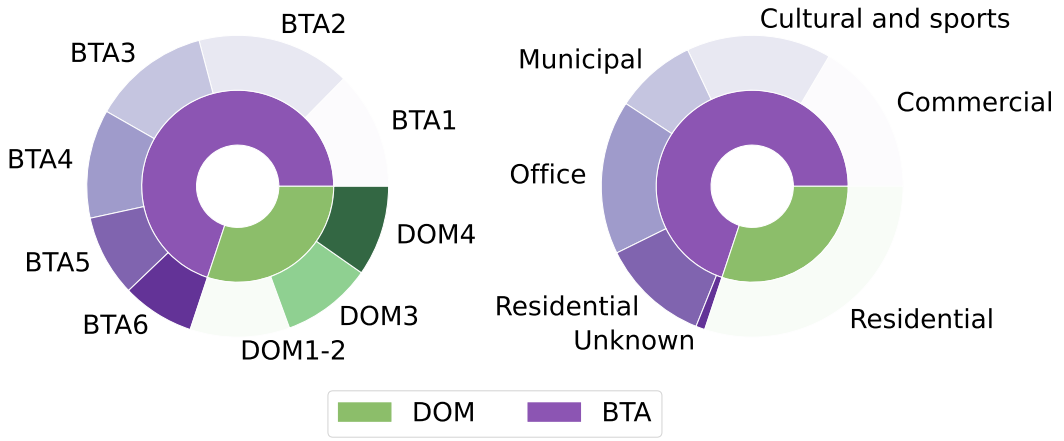

Fig. 2.1 Composition of the dataset based on user types (household, DOM, and non-domestic, BTA). The left plot represents the distribution according to the level of contractual power, while the right plot shows the distribution by end-user category.

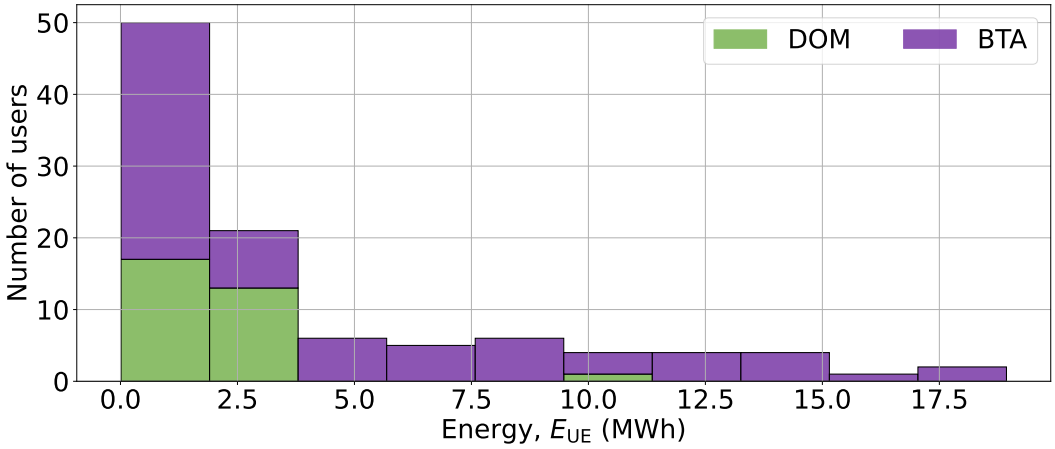

Fig. 2.2 Histogram of the yearly energy consumption across end-users, divided by type (households, DOM, and non-domestic, BTA).

responding monthly energy usage (bottom). Similarly, Fig. 2.4 displays the same data for non-domestic end-users.

Fig. 2.5 highlights the daily consumption patterns for two end-users randomly selected from the dataset: one household (left) and one non-domestic (right). The figure illustrates the distinct consumption behaviors depending on the type of end-user. Household profiles typically feature two peaks, one around noon and

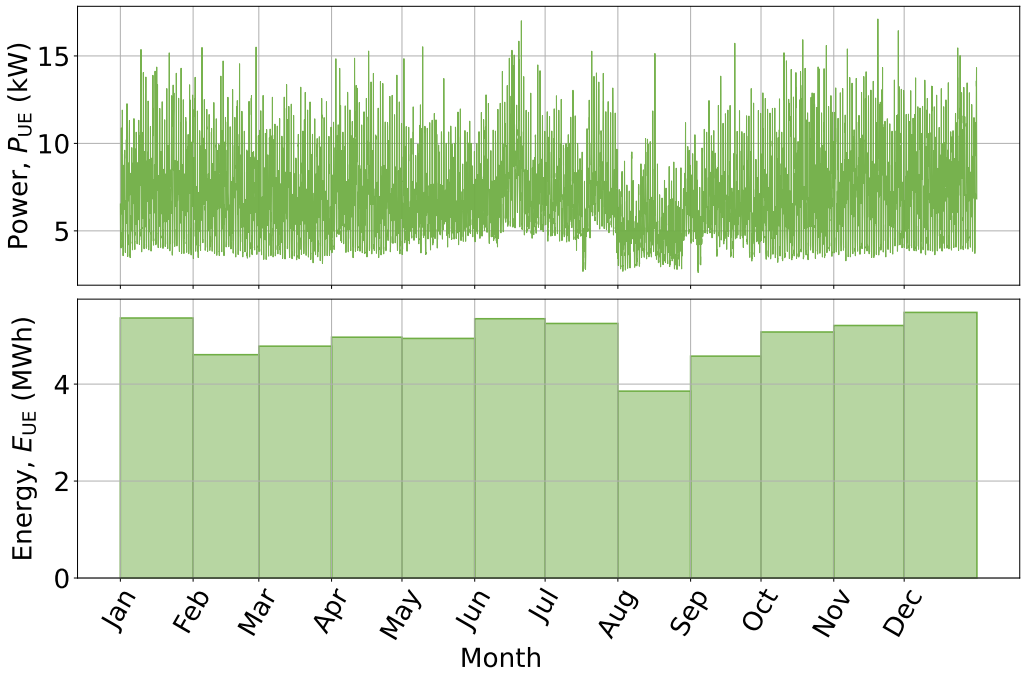

Fig. 2.3 Electricity consumption profile the household end-users. The top subplot depicts the hourly electricity demand profile throughout the year. The bottom subplot shows the corresponding monthly energy consumption as a bar plot.

another in the evening, whereas the non-domestic user –commercial activity– shows peak consumption during the central hours of the day.

The total yearly electricity consumption of the dataset's end-users amounts to **345.0 MWh** for non-household end-users and **59.46 MWh** for households, resulting in a combined total of **404.5 MWh**. Among the 31 households in the dataset, the average yearly consumption is roughly 1.92 MWh, lower than the Italian residential average of 2.5 MWh in 2022 [42]. This discrepancy is likely due to the presence of households with very low consumption (around 0.5 MWh/year), potentially reflecting non-resident household end users.

2.2 Photovoltaic generation

In the absence of an existing PV plant, photovoltaic generation data were obtained at the geographical coordinates of Turin, using the PVGIS (Photovoltaic Geographical Information System) [43] developed by the European Commission's Joint Research Centre (JRC). This tool provides detailed estimates for specific geographical locations, employing high-resolution solar irradiance and temperature data

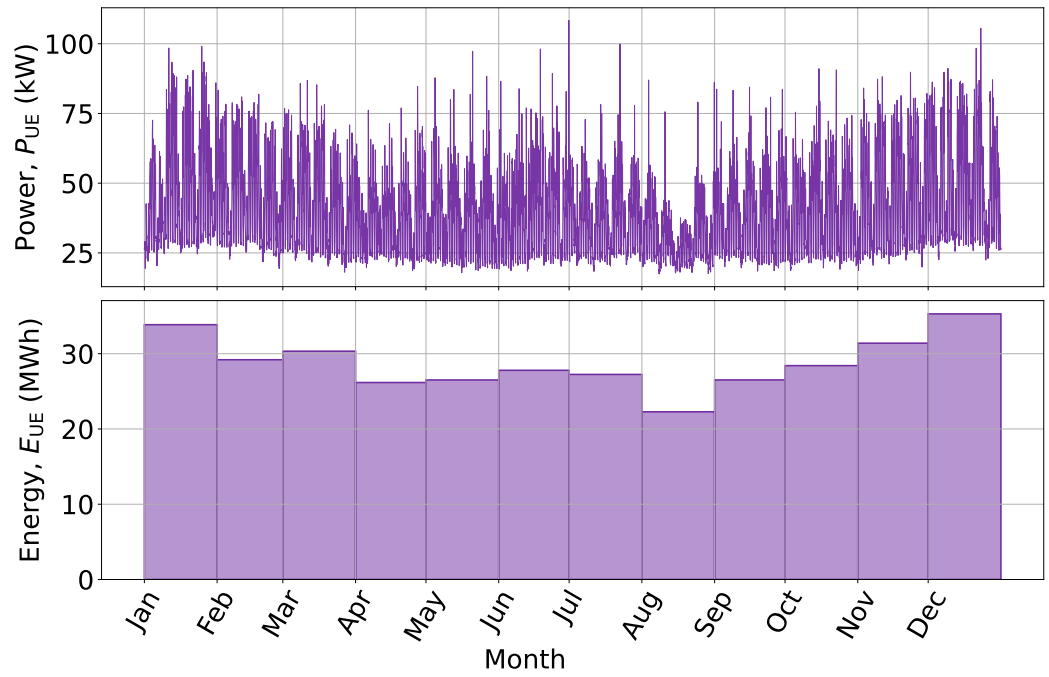

Fig. 2.4 Electricity consumption profile the non-domestic end-users. The top subplot depicts the hourly electricity demand profile throughout the year. The bottom subplot shows the corresponding monthly energy consumption as a bar plot.

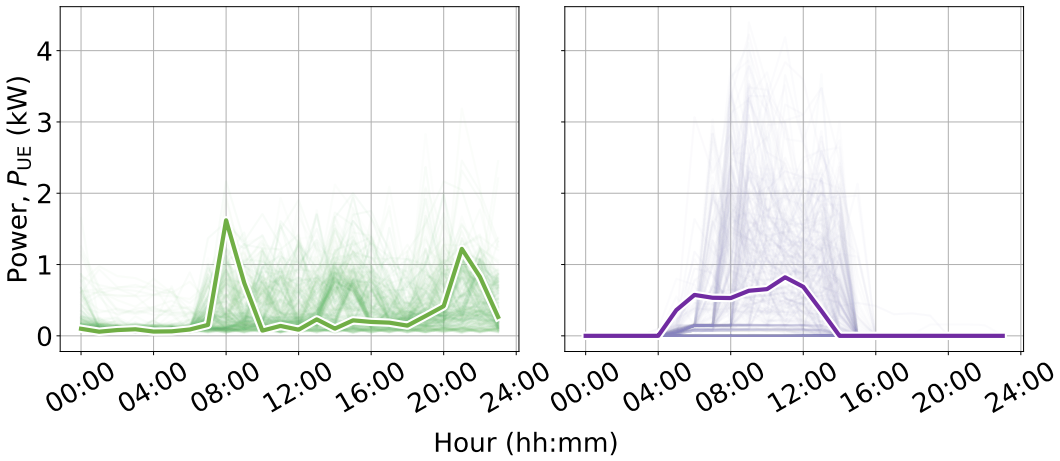

Fig. 2.5 Daily electricity consumption profiles for a household (left) and a non-domestic end-user (right). The background in each subplot displays all daily profiles throughout the year, with the highlighted line representing the profile closest to the median daily consumption.

–in this case, sourced from the PVGIS-ERA5 weather database. PVGIS calculates the hourly photovoltaic generation by considering the installation plane azimuth (orientation) and tilt (elevation). Default total system losses of 14% account for factors such as dusting of panels and inverter inefficiencies. The generation data were normalized by setting the peak power to 1 kW, yielding power generation values per unit of installed power and facilitating subsequent analyses.

Fig. 2.6 provides an overview of the photovoltaic output throughout the year, including the hourly generation profile and a bar plot of the corresponding monthly energy values. Fig. 2.7 focuses on typical daily variations in photovoltaic generation: the left subplot shows a day with lower photovoltaic output, while the right subplot presents a day with higher generation. The estimated annual photovoltaic generation per unit of installed power for Turin was **1.353 MWh/kW$_\mathrm{p}$** according to PVGIS.

Advanced software such as PV*SOL premium [44] can be utilized for more detailed and site-specific modeling. This tool allows 3D models of building rooftops, accounting for shadowing, barriers to PV placement, and panel string layouts. Such advanced modeling is beneficial for precise energy yield predictions and is more suited for detailed planning phases or specific project assessments.

2.3 Heating load

The heating load is estimated considering a 40-apartment multi-family residential building, typical of the Italian residential stock [11], employing a simplified steady-state approach based on [45]. This approach calculates thermal losses through the building's external walls, roof, ground, internal walls, windows, and ventilation. These losses are influenced by the temperature difference between the internal environment (T_int) and the external air ($T_\mathrm{a,h}$), as well as building-specific characteristics such as thermal transmittance and surface areas.

The hourly heating load P_h^UT (in W) at each time step h is calculated as:

$$\begin{aligned} P_\mathrm{h}^\mathrm{UT} &= \frac{Q_\mathrm{ext,h} + Q_\mathrm{r,h} + Q_\mathrm{g,h} + Q_\mathrm{i,h} + Q_\mathrm{w,h} + Q_\mathrm{v,h}}{\eta_\mathrm{d}} \\ &= \frac{U_\mathrm{ext} S_\mathrm{ext} + U_\mathrm{r} S_\mathrm{r} + U_\mathrm{g} S_\mathrm{g} + U_\mathrm{i} S_\mathrm{i} b + U_\mathrm{w} S_\mathrm{w} + \rho_\mathrm{air} C_\mathrm{p,air} n V_\mathrm{net}}{\eta_\mathrm{d}} \left(T_\mathrm{int} - T_\mathrm{a,h}\right), \end{aligned} \tag{2.1}$$

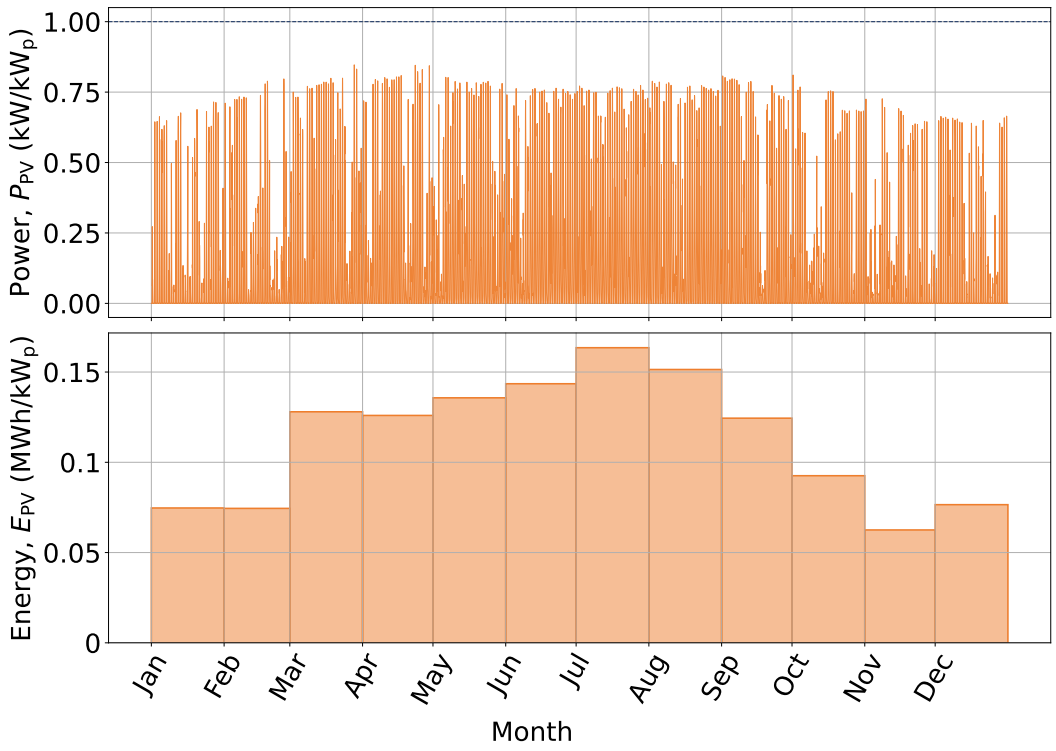

Fig. 2.6 Estimated specific photovoltaic generation per unit of installed power for Turin (Northern Italy). The top subplot depicts the hourly generation throughout the year, normalized per unit of installed capacity. The bottom subplot shows the corresponding monthly energy generation per installed power unit as a bar plot.

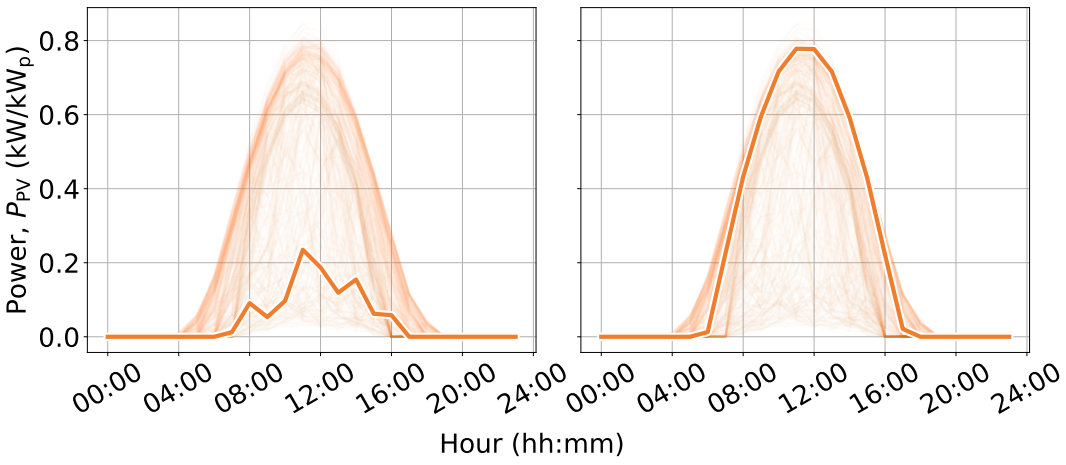

Fig. 2.7 Daily profiles of photovoltaic generation per unit of installed power in Turin (Northern Italy). The left and right subplots show a day with lower and higher photovoltaic generation, respectively. The background depicts the generation profiles in lighter shades for all days of the year.

Table 2.2 Physical characteristics of the reference building [11, 46].

Quantity	Value	Unit	Description
η_d	0.86	–	Distribution system efficiency
b	0.4	–	Correction factor for unheated spaces
n	1.67×10^{-4}	h^{-1}	Air exchange rate
S_{ext}	2514	m^2	External wall surface area
S_g	325	m^2	Ground surface area
S_i	770	m^2	Internal wall surface area
S_r	325	m^2	Roof surface area
S_w	407	m^2	Window surface area
U_{ext}	1.10	W/m^2K	External wall thermal transmittance
U_g	1.56	W/m^2K	Ground thermal transmittance
U_i	1.13	W/m^2K	Internal wall thermal transmittance
U_r	1.65	W/m^2K	Roof thermal transmittance
U_w	4.90	W/m^2K	Window thermal transmittance
V_{net}	6815	m^3	Net heated volume
Other parameters			
$N_{apartments}$	40	–	Number of apartments
N_{floors}	8	–	Number of floors
S/V	0.46	m^{-1}	Surface-to-volume ratio

Table 2.3 Seasonal and daily limits of heating system operations for different Italian climatic zones. Limits specific to the studied case (Turin, Northern Italy) are in bold.

Climatic zone	HDDs	Max daily hours	Heating season (dates in dd-mm)	Operating hours
A	0–600	6	from 01-12 to 15-03	7:00-10:00 18:00-21:00
B	601–900	8	from 01-12 to 31-03	7:00-11:00 17:00-21:00
C	901–1400	10	from 15-11 to 31-03	7:00-12:00 17:00-22:00
D	1401–2100	12	from 01-11 to 15-04	6:00-10:00 12:00-16:00 18:00-22:00
E	**2101–3000**	**14**	**from 15-10 to 15-04**	**5:00-10:00 12:00-16:00 18:00-23:00**
F	>3000		No Limitations	

where ρ_{air} and $C_{p,air}$ are air density (1225 kg/m^3) and specific heat capacity (1005 J/kgK), respectively. The physical characteristics of the reference building are detailed in Tab. 2.2.

A temperature of 20 °C was assumed for the internal environment of the building, while external temperature data $T_{a,h}$ were sourced for Turin using the typical meteorological year (TMY) dataset from the JRC [47]. The heating demand was adjusted according to Italian regulations for heating schedules based on climatic zones, identified by the heating degree days (HDDs) values [11], as detailed in Tab. 2.3.

The estimated heating demand profiles for the reference residential building in Turin are presented in Fig. 2.8 and Fig. 2.9. Fig. 2.8 provides an overview of the seasonal variations in heating demand throughout the year, including the hourly profile and a bar plot of monthly (or half-month) heating consumption. Fig. 2.9 focuses on typical daily variations in heating demand: the left subplot shows a day with lower heating consumption, while the right subplot presents a day with higher consumption. The external air temperature is also shown to contextualize the heating demand throughout the day. The total heating consumption over the year was estimated at **276.9 MWh** for the 40 apartments in the reference building.

2.4 Energy prices

The analysis of energy prices for electricity is based on the market price for Italy known as "*prezzo unico nazionale*" (PUN), which is the average among hourly prices ("*prezzo zonale orario*") of the 7 Italian market zones [48]. Fig. 2.10 shows the evolution of PUN from 2019 to October 2024, highlighting key events that influenced price fluctuations. In 2020, a substantial drop in market prices was observed, directly linked to the COVID-19 pandemic and subsequent lockdown measures. This trend reversed sharply in 2022 due to geopolitical conflicts, while in the second half of 2023 and 2024, the price stabilized, although at a higher average value than before and with more pronounced variations.

Given these significant price fluctuations, only the most recent year (October 2023 to October 2024) was used for the subsequent analyses. Due to the hourly frequency of electricity price variations, the analysis required a method to avoid potential biases when comparing prices with energy load profiles, especially since

the load data were sourced from different years. To address this, the following method was employed to process the PUN data:

1. For each month in the selected year, an hourly median price profile was calculated by averaging the prices at each hour across all days of that month.

2. These monthly median profiles were repeated for all days within their respective months, reconstructing a full year-long price profile.

It is worth noting that using a median profile as representative for each month results in some information loss regarding individual daily variations, particularly on Saturdays, Sundays, and holidays, when price profiles may differ significantly. A self-correlation analysis of the price data was conducted to assess the extent of this loss. As shown in Fig. 2.12, the highest correlation values occur at lags of 24 and 168 hours (i.e., 1 day and 1 week), indicating a clear weekly seasonality. Despite this, a single representative day was adopted for each month for simplicity in the subsequent analyses.

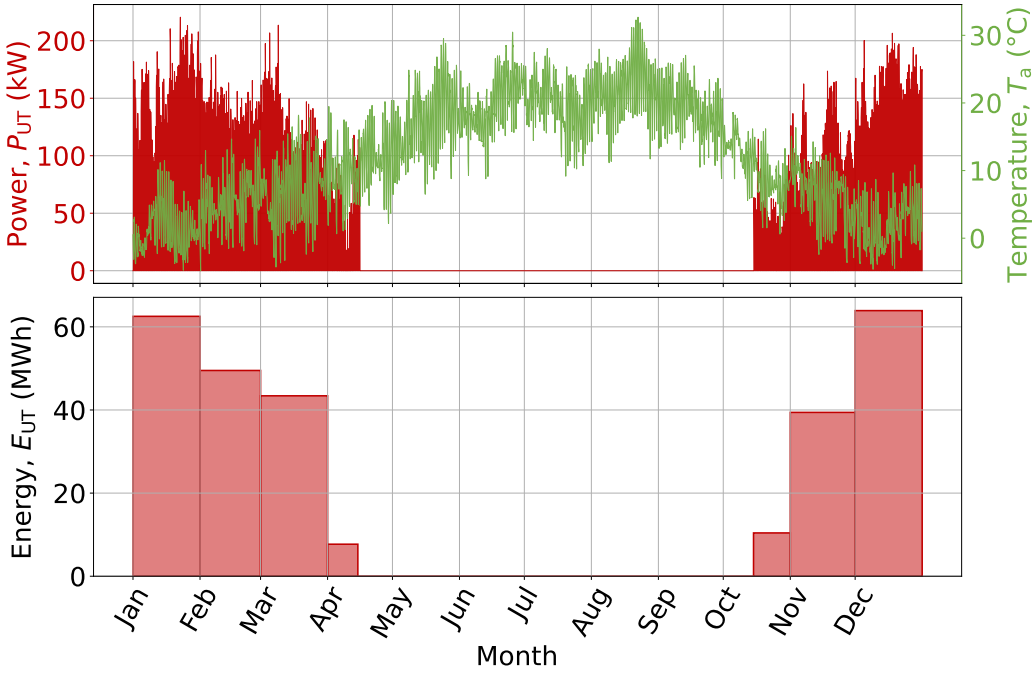

Fig. 2.8 Estimated space heating demand for the 40-apartment residential building in Turin (Northern Italy). The top subplot depicts the hourly heating demand profile throughout the year, showing the external air temperature for reference. The bottom subplot shows the corresponding monthly (or half-monthly) heating energy consumption as a bar plot.

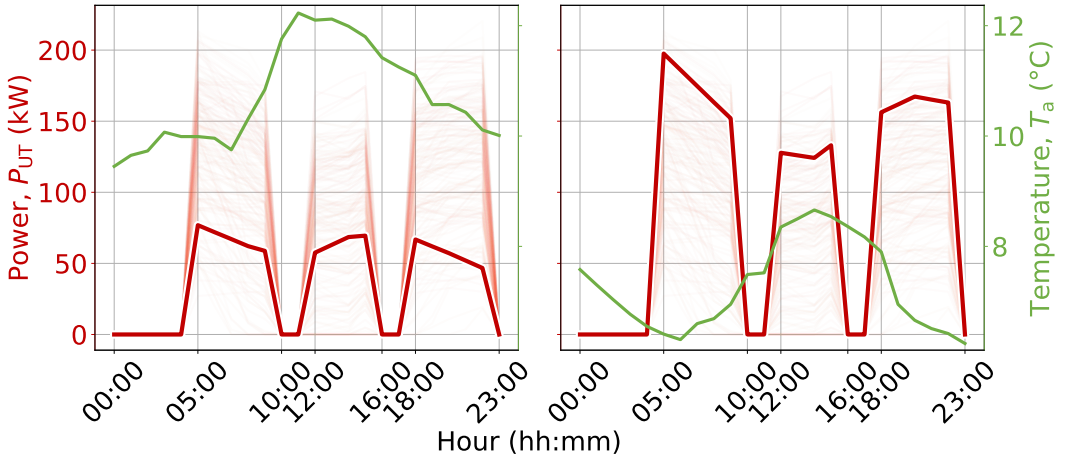

Fig. 2.9 Daily profiles of estimated hourly space heating demand for a residential building in Turin (Northern Italy). The left and right subplots show a day with lower and higher heating consumption, respectively. The external air temperature is shown for reference, providing context for the variation in heating load. The background depicts the heating demand profiles for all days within the heating season in lighter shades.

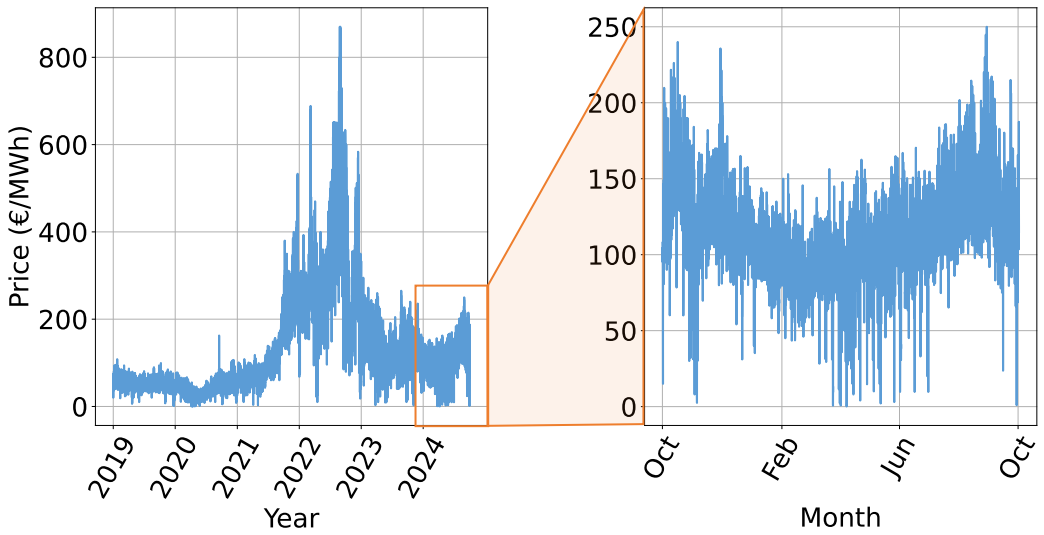

Fig. 2.10 Trend of the Italian hourly market price (PUN) from 2019 to October 2024. The left plot shows the full period, while the right plot provides a magnified view of the last available year (October 2023 to October 2024), highlighting more recent variations.

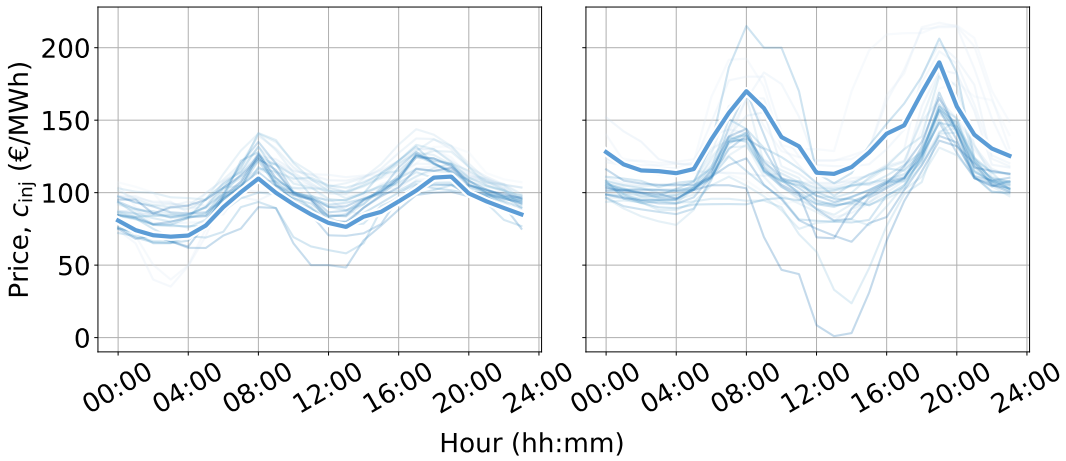

Fig. 2.11 Electricity market price in two months with small (left) and large (right) intra-day price fluctuations. The plots show the median hourly profiles, with all daily profiles of each month shown in the background for comparison.

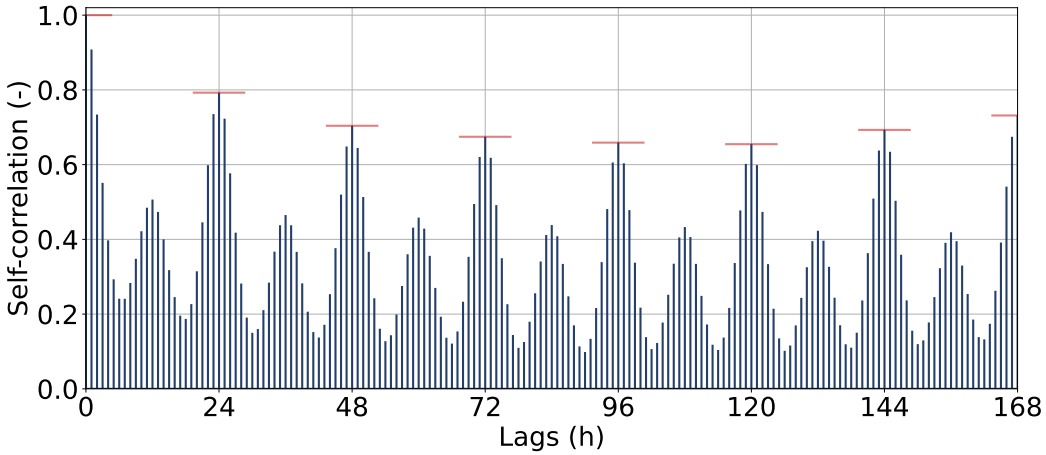

Fig. 2.12 Self-correlation of the electricity retail price in the last available year (October 2023 to October 2024), at different time lags from 1 to 168 hours (i.e., 1 week).

Fig. 2.11 presents the electricity market price data for two months, with small and larger intra-day price fluctuations. Each subplot shows the median hourly price profile, which is used as the injection price (c_{inj}) in the subsequent analyses, with the profiles of all days in the corresponding month displayed in the background for context.

In addition to the market price for electricity, incentives for shared energy and retail prices for energy withdrawals are considered.

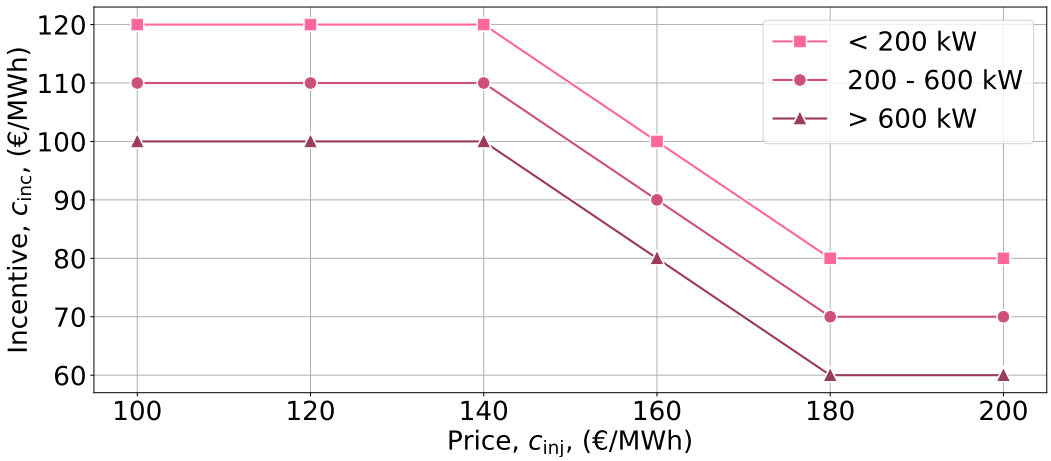

Fig. 2.13 Relation between market price and incentive on the shared energy according to the plant nominal power, as shown in (2.2) and Tab. 2.4.

Shared energy incentive The shared energy incentive consists of a fixed and a variable part, which depends on the hourly market price c_{inj}. In particular, the variable part ranges between 40 (when the market price is below 140 €/MWh) and 0 (when the market price is higher than 180 €/MWh) [32]. Globally, the incentive, c_{inc}, is calculated through the following relationship:

$$c_{inc} = c_{base} + \min\left(40; \max\left(0; c_{inj} - 140\right)\right). \tag{2.2}$$

Here, c_{base} is the fixed part of the incentive, determined by the installed capacity of the PV plant as indicated in Tab. 2.4.

Fig. 2.13 shows how the shared energy incentive varies according to the market price. For simplicity, the first range was adopted for all analyses, even in scenarios where the installed PV capacity exceeded 200 kW. Moreover, an average value across each month was calculated for c_{share}, using the mean market price from the hourly profiles calculated earlier.

Table 2.4 Base value of the incentive for shared energy based on the plant nominal power.

$\mathbf{c_{base}}$ **[€/MWh]**	**Plant nominal power [kW]**
80	<200
70	200 – 600
60	≥ 600

Table 2.5 Average value and variations range (when applicable) of the energy prices in the considered year.

Energy price	Mean value [€/MWh]	Variation range [€/MWh]
c_{inj}	108.6	(50.0 – 190.4)
c_{share}	141.6	n.a.
c_{with}	312.8	(285.2 – 347.3)
c_{gas}	160.0	n.a.

An additional incentive of 10 €/MWh is applied for regions in Northern Italy, along with a network tariff reimbursement of 11.57 €/MWh. Therefore, the total economic value of the shared energy, c_{share} is given by $c_{inc} + 21.57$ €/MWh.

The electricity retail price can vary significantly based on user type, consumption levels, and individual supplier agreements. Therefore, a simplified method was used to calculate the retail electricity price, by summing the incentive and the injection price for each month and multiplying by a factor of 1.25 to account for system charges and distribution fees. Therefore, the price used for electricity grid withdrawals, c_{with}, was calculated as follows:

$$c_{with} = 1.25 \times (c_{share} + c_{inj}). \tag{2.3}$$

This assumption aligns with the rationale that the incentive is designed to cover the difference between the market and retail price, apart from general system fees. Moreover, it is noted that while real-time pricing is theoretically possible, fixed pricing structures are more prevalent in Italy, making this constant approach representative of actual market conditions. The resulting value of around 300 aligns with the average retail price for end users in the liberalized market in 2024 [35].

The yearly trends of the processed electricity market price used for grid injections (c_{inj}), shared energy value (c_{share}), and retail price for grid withdrawals (c_{with}) are shown in Fig. 2.14. The figure also shows the natural gas price (c_{gas}) considered in this thesis [49]. Finally, the average value and variations range (when applicable) of the energy prices in the considered year are shown in Tab. 2.5.

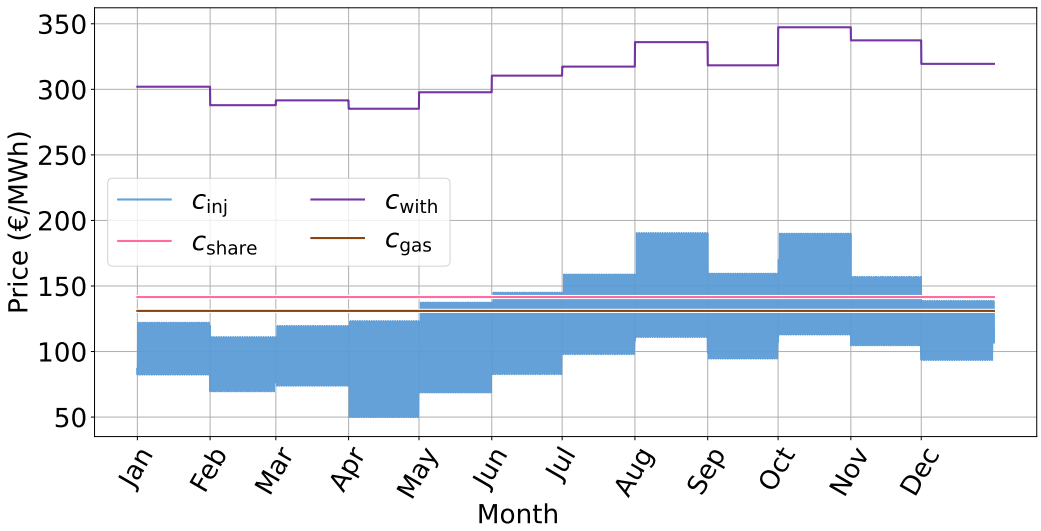

Fig. 2.14 Yearly trends of the energy prices considered in this thesis for grid injections (c_{inj}) –market price– and withdrawals (c_{with}) –retail price–, for shared energy valorization (c_{share}), and natural gas (c_{gas}).

2.5 Technologies data

Tab. 2.6 reports the emission factors considered for calculating the emissions of the ICES, distinguishing between operational and lifecycle emissions. Similarly, Tab. 2.7 presents the parameters used for evaluating the KPIs, including unit prices for the installed technologies and their useful lifetimes. These values are crucial for calculating lifecycle emissions using (1.17) as well as capital expenditures and residual values as defined in (1.22) and (1.23).

Table 2.6 Emission factors used for ICES emission calculations, including both operational emissions (e.g., electricity and gas consumption) and lifecycle emissions of installed technologies.

Quantity	Value	Unit of measure	Source
$\epsilon^{\text{with,el}}$	0.250	$kg_{CO_2}eq/kWh$	[50]
$\epsilon^{\text{inj,el}}$	0		(see Section 1.4)
$\epsilon^{\text{with,gas}}$	0.200		[51]
ϵ^{PV}	1700	$kg_{CO_2}eq$/unit of capacity	[39]
ϵ^{HP}	n.a.		
ϵ^{BESS}	175		[4]
ϵ^{HTS}	n.a.		

Table 2.7 Cost parameters and useful lifetimes for installed technologies in the ICES. These values are used in the calculation of lifecycle costs and residual values.

Quantity	Value	Unit of measure	Source
c_{PV}	1500	€/unit of capacity	[32]
c_{HP}	750		[11]
c_{BESS}	400		[4]
c_{HTS}	50		[14]
n_{PV}	25	years	[14]
n_{HP}	15		[14]
n_{BESS}	n.a.[7]		
n_{HTS}	20		[14]
n	20		
r	6	%	

[7] Calculated based on BESS utilization, as shown in (2.4).

The useful life of most technologies is fixed, but for the BESS, it accounts for the degradation of its state of health (SOH), influenced by both calendar aging and utilization. Calendar aging (ΔSOH^{cal}) depends only on the elapsed time, while utilization degradation (ΔSOH^{use}) is modeled through energy throughput, which represents the total energy processed by the BESS over its lifetime compared to the energy it can process before failure (throughput).

The total battery degradation (ΔSOH) at each year t is calculated as follows [40] (the BESS superscript is omitted in the equations for readability):

$$\begin{aligned} \Delta SOH_t &= \Delta SOH_t^{cal} + \Delta SOH_t^{use}, \\ \Delta SOH_t^{cal} &= 1 - \exp(-c_{cal}\, t), \\ \Delta SOH_t^{use} &= \sum_t \frac{E_t^{in} + E_t^{out}}{ET} \Delta SOH^{fail}, \end{aligned} \tag{2.4}$$

where c_{cal} is the calendar aging coefficient, approximately 1.3×10^{-4} h^{-1} [40], ΔSOH^{fail} is the SOH at failure (0.2), and ET is the energy throughput, defined as:

$$ET = 2 n_{cycles} \Delta SOC^{max} S^{BESS}. \tag{2.5}$$

Here, n_{cycles} is the number of cycles until failure, and ΔSOC^{max} is the maximum depth of discharge (assumed equal to 5000 cycles and 0.8, respectively).

Finally, the useful life of the BESS is evaluated by finding the year t at which the total degradation ΔSOH_t reaches the value at failure, ΔSOH^{fail}.

2.6 Preliminary assessment

This section presents a preliminary evaluation of an ICES, utilizing the data described in this chapter and applying the modeling and assessment methods detailed in Section 1.4. The objective is to provide a baseline assessment of the case while highlighting key features of the adopted assessment framework. As anticipated in Section 1.3, these KPIs are calculated over the one-year time horizon identified by the available input data. However, for environmental and economic KPIs requiring a longer time horizon, ICES performance in this year is taken as the reference year over a 20 years horizon.

In this initial assessment, the ICES consists of two nodes: one active node with photovoltaic (PV) generation and one aggregated node representing the passive consumers. At first, the analysis focuses solely on households and considers only electricity consumption, excluding any sector coupling.

A reference PV size, $S_{PV,0}$, is determined by balancing the annual ICES consumption and generation to establish a baseline, as follows:

$$S^{PV,0} = \frac{\sum_{j,h} P^{UE}_{j,h}}{\sum_{h} P^{PV}_{h}}, \tag{2.6}$$

where $P^{UE}_{j,h}$ represents the hourly consumption of each end user, described in Section 2.1, and P^{PV}_{h} corresponds to the estimated hourly generation per unit of PV system capacity, described in Section 2.2 (in kW/kW_p).

Considering the household end users only, this reference PV capacity is approximately 44 kW_p. Starting from this reference size, multiple scenarios are analyzed by varying the PV size within $10 \div 200$ kW_p. Fig. 2.15 illustrates the energy produced, consumed, and shared in the ICES for different PV capacities. As the PV size increases, the shared energy saturates but does not reach the total consumption.

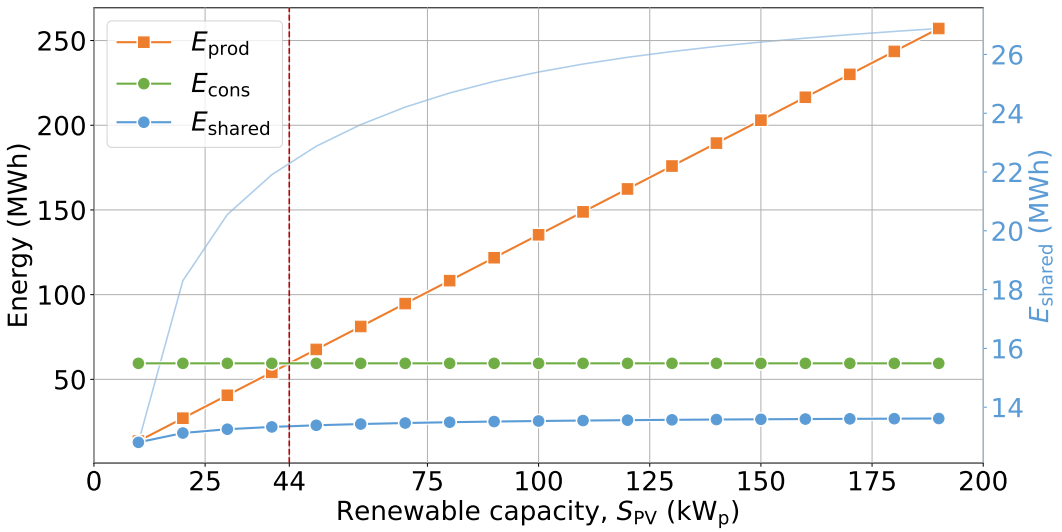

Fig. 2.15 Trend of the produced, consumed, and shared energy with varying PV capacity in the preliminary assessment of the ICES with only household end users as electric loads. The shared energy is also shown on the background using the secondary axis to highlight its asymptotic trend. The vertical dashed line indicates the reference PV size, at which yearly consumption and production are balanced.

2.6.1 Energy KPIs

To compare shared energy with production and consumption, Fig. 2.16 illustrates the self-consumption (SC) and self-sufficiency (SS) rates for varying PV capacities. Consistent with the observed energy values, SS increases with PV size but eventually saturates below 100%. This is explained by the energy consumption that occurs outside PV production hours, which cannot be addressed by simply increasing the size of the PV system. Conversely, SC decreases as the shared energy does not scale proportionally with the total generation.

The analysis of SS and SC highlights how these two KPIs cannot be simultaneously improved by just increasing the renewable capacity installed (in the case of PV) due to the inherent mismatch between production and consumption at various time scales, such as hourly or seasonal. As shown in Chapter 5, flexibility resources like storage systems can enhance both KPIs simultaneously, though typically at the expense of economic performance.

The analysis of SS and SC shows how these two KPIs cannot be simultaneously improved by just acting on the renewable capacity installed (in the case of photovoltaic), due to the inherent mismatch between production and consumption at various time scales –e.g., hourly or seasonal. As shown in Chapter 5 flexibility

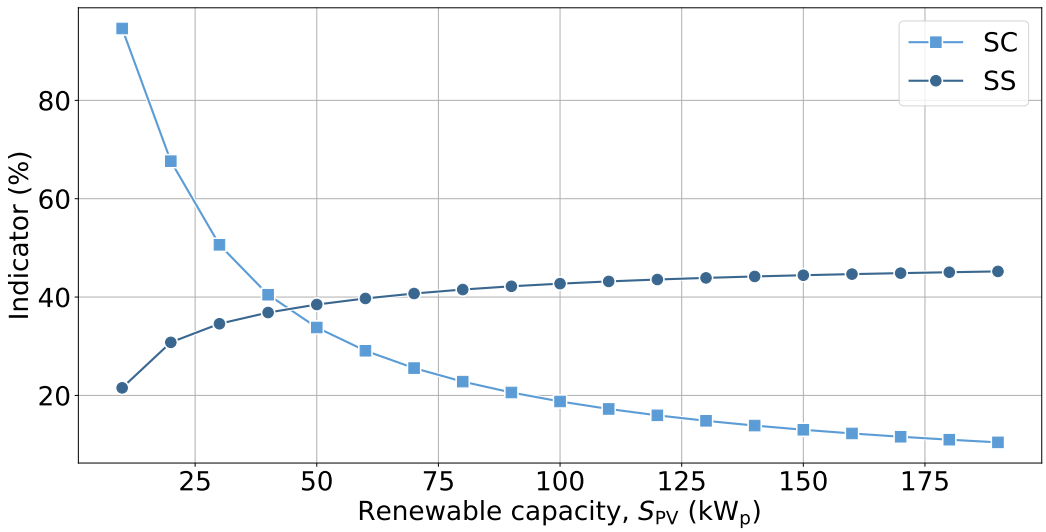

Fig. 2.16 Trend of the self-consumption (SC) and self-sufficiency (SS) rates with varying PV capacity in the preliminary assessment of the ICES with only household end users as electric loads.

resources like storage systems can improve both simultaneously, generally at the expense of economic performance.

The reference size at which the production equals the consumption calculated from yearly values was 44 kW_p, which translates into a PV size of roughly 1.4 kW_p per household since they are 31 in the dataset. This changes significantly when hourly values are considered. For example, from the point of view of self-consumption, this value drops to approximately 0.3 kW_p per household.

2.6.2 Environmental KPI

Fig. 2.17 illustrates the emissions reduction KPI (ER) trend for varying PV sizee. Three lines are shown, corresponding to three different methods of calculating ICES emissions: 1. as proposed in (1.18), which incorporates both operational and life-cycle assessment (LCA) emissions; 2. excluding LCA emissions and 3. including avoided emissions for energy produced but not shared.

When using the calculation proposed in (1.18), there is a PV size that maximizes emissions reduction (20 kW_p in this case). Beyond this point, further increases in PV capacity result in oversized installations relative to the ICES's needs –in the absence of flexibility technologies. This leads to an increase in

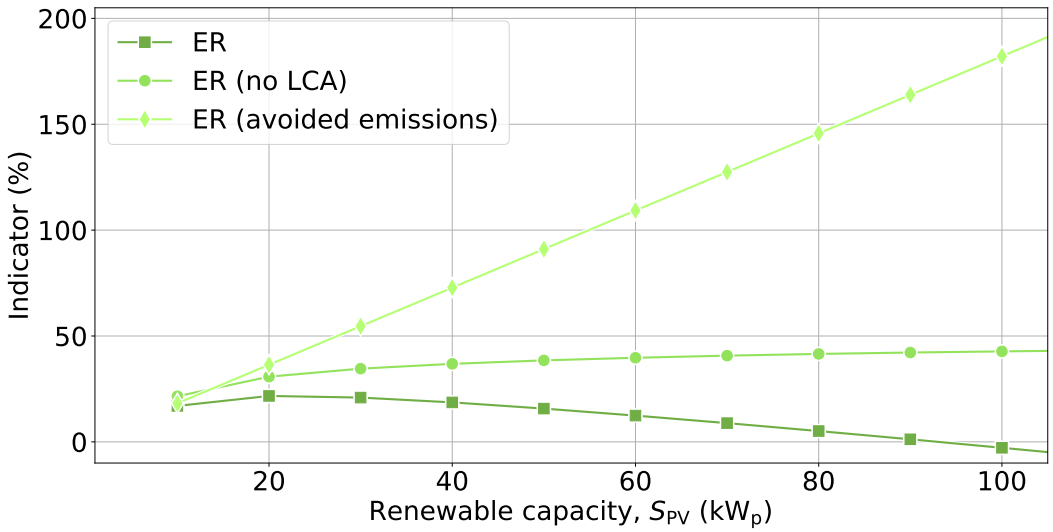

Fig. 2.17 Trend of the emissions reduction (ER) KPI with varying PV capacity in the preliminary assessment of the ICES with only household end users as electric loads. The KPI is evaluated using three methods of calculating ICES emissions: as proposed in (1.18), excluding LCA emissions (no LCA), and including avoided emissions for energy produced but not shared (avoided emissions). The figure is truncated at 100 kW_p to enhance visibility.

ICES emissions, eventually surpassing the emissions of the base case, due to the significant contribution of PV system LCA emissions.

If LCA emissions are excluded, the emissions reduction saturates, similarly to the self-sufficiency rate –the two KPIs would be in fact correlated. Conversely, when avoided emissions for unshared energy are considered, the emissions reduction increases consistently with PV size, eventually surpassing 100%. This approach is not deemed suitable for this thesis, which stresses the local scope of ICES and RECs, thus justifying the adoption of the emissions calculation from (1.18).

2.6.3 Economic KPIs

Fig. 2.18 shows the trends of two economic KPIs: total actualized cost reduction (CR) and internal rate of return (IRR). CR, similarly to ER, initially exhibits an increasing trend, reaching a maximum at 20 kW_p, before decreasing. In contrast, IRR consistently decreases, achieving its maximum at the smallest PV size. These trends are interconnected, as when the CR falls below 0 –indicating TAC higher

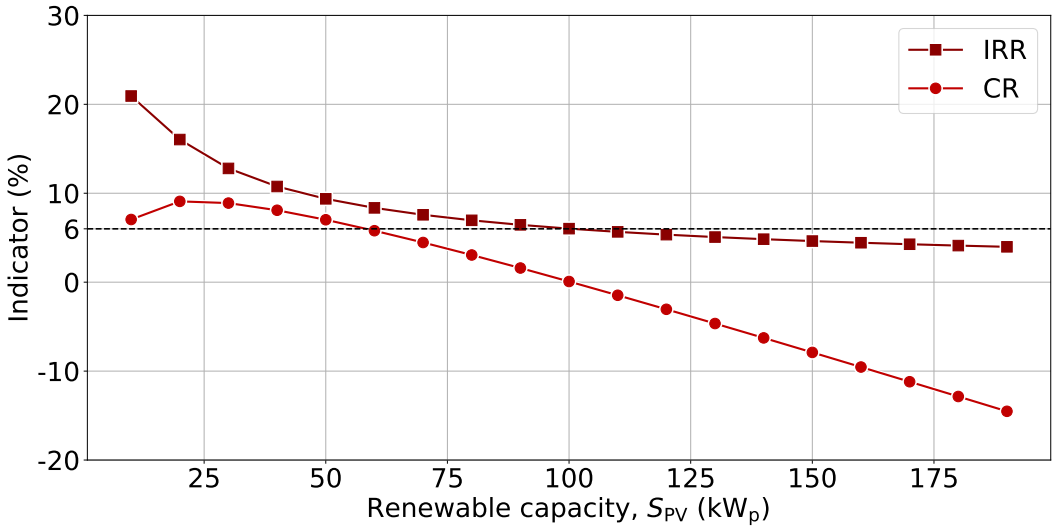

Fig. 2.18 Trend of the total actualized cost reduction (CR) and internal rate of return (IRR) with varying PV capacity in the preliminary assessment of the ICES with only household end users as electric loads. The horizontal dashed line shows the value assumed for the discount factor r in the actualization of costs.

than in the base case– the IRR drops below the discount factor r assumed for actualizing costs, i.e., 6%.

Finally, Fig. 2.19 presents the trends of the other two economic KPIs: net present value (NPV) and pay-back time (PBT). The NPV follows a trend similar to CR; it can be proven that CR can be calculated by dividing the NPV by the TAC in the base case. Being a normalized KPI, however, CR provides more intuitive results. Conversely, PBT consistently increases with the PV size and is not shown for sizes larger than 100 kW$_p$, as it exceeds the considered horizon of 20 years. This size is the same as the one at which IRR drops below the discount factor r.

2.6.4 End user type

Fig. 2.20 shows the trend of self-sufficiency rates in the case of only household end users compared to non-domestic ones, as presented in Section 2.1. The figure reports on the x-axis the renewable capacity normalized to the reference PV size for both cases. For non-domestic end users, with higher consumption, the reference PV size is 255 kW$_p$. It is noted that, in the case of non-domestic end users, the self-sufficiency rate is generally higher. This is due to the different consumption profiles, which can be observed in Fig. 2.5.

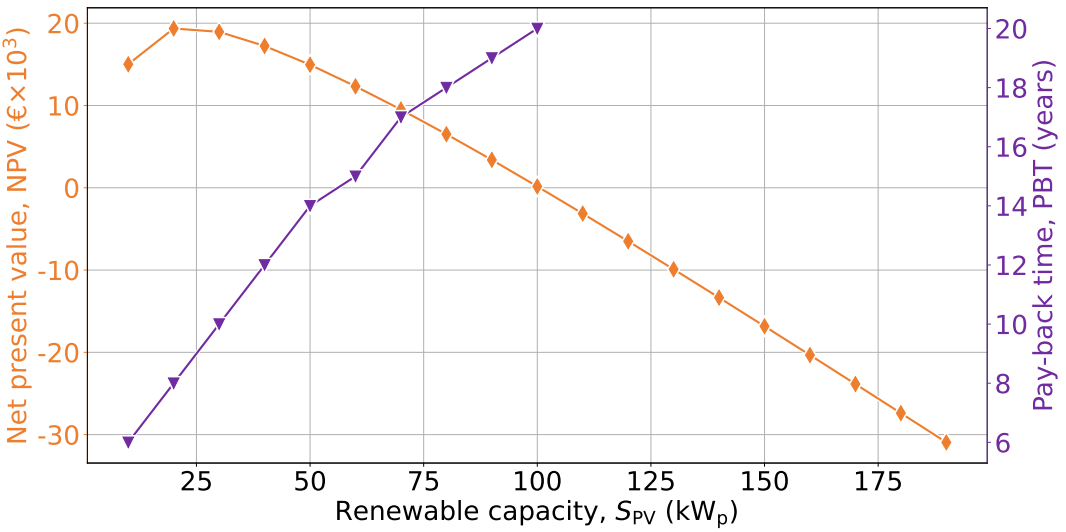

Fig. 2.19 Trend of the net present value (NPV) and pay-back time (PBT) with varying PV capacity in the preliminary assessment of the ICES with only household end users as electric loads.

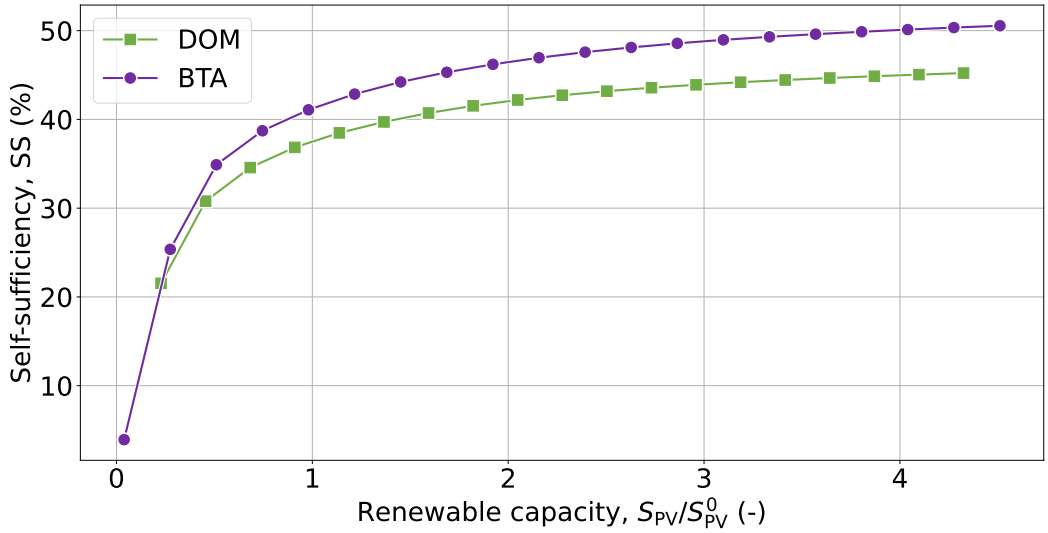

Fig. 2.20 Trend of the self-sufficiency rate (SS) with varying PV capacity in the preliminary assessment of the ICES with only household end users (DOM) versus non-domestic ones (BTA).

Non-domestic end users, especially offices, factories, and commercial activities, often have opening hours during the central hours of the day, when the PV generates more energy. Conversely, households have their largest consumption peak at night.

Chapter 3

Optimal energy management of multi-node, multi-energy systems

Summary

The preliminary assessment from Chapter 2 demonstrated that improving ICES performance relying only on photovoltaic generation is limited. To address these limitations, including energy storage, sector coupling, and other flexibility resources is critical. However, these additions increase the complexity of ICES operations, particularly when considering many interconnected multi-energy nodes and energy sharing. Optimization is a useful instrument to assess the optimal performance of ICES, providing a basis for evaluating KPIs and informing decision-making. This chapter formalizes the optimization of ICES energy flows as a mixed-integer linear programming (MILP) problem and tests its applicability to ICES optimization across a comprehensive set of scenarios.

Key objectives

- Formalizing a comprehensive optimization framework for the operational assessment of ICES, addressing their multi-node and multi-energy nature.
- Discussing key modeling choices, including energy storage modeling in the context of energy sharing, individual versus collective node optimization strategies, and multi-node modeling.

- Benchmarking the impacts of these choices in ICES optimization, including objective function, KPIs, and computational performance.

The chapter is structured as follows. Section 3.1 reviews existing approaches to ICES modeling and optimization and details the contributions of this chapter. Section 3.2 completes the ICES modeling by presenting the equations used to describe the behavior of the components. Section 3.3 formalizes this model as a MILP optimization problem, focusing on minimizing operational energy costs while adhering to physical and regulatory constraints. Section 3.4 outlines the test cases designed to evaluate the model, including simple configurations for initial insights and a comprehensive test set based on real-world data from Chapter 2. Results are presented in Section 3.5 and discussed in Section 3.6, particularly focusing on the effects of collective versus individual node optimization, multi-node modeling, and the complexity of the optimization problem.

Key insights

- Collective optimization consistently outperforms individual node optimization, enhancing energy sharing by leveraging flexible resources effectively.
- Multi-node modeling is essential for properly evaluating economic KPIs in settings where technologies are distributed among multiple end users. However, energy and environmental KPIs remain largely unaffected, as the energy consumed locally within the node remains constant.
- Increasing the number of active nodes and collective node optimization significantly increase complexity and computational demand, with solution times rising by orders of magnitude.
- The trends in collective versus individual and single-node versus multi-node optimization results suggest a potential for data-driven approaches to approximate optimal solutions while reducing the computational burden.

3.1 Literature review and contribution

The literature on the modeling of multi-energy systems is wide and well-established. An extensive review of existing approaches is presented in [52] while [53] focuses

on tools. Both highlight key characteristics and limitations of the investigated models. Relevant elements characterizing these models include geographical scope (ranging from national to building-level systems), temporal resolution (commonly hourly or finer), and the integration of different energy carriers such as electricity, heat, and gas [9]. Among the most desirable features in modeling tools is the adoption of optimization techniques for simulating the operations of complex energy systems.

MILP is widely used for such problems, as it balances mathematical rigor and computational tractability, making it adaptable to various applications [54]. However, since real-world ICES optimization problems are inherently nonlinear, alternative methods such as evolutionary algorithms and swarm intelligence (genetic, particle swarm, etc.) and hybrid techniques have also been explored [55]. Despite being powerful optimization tools, these "metaheuristics" are not deterministic, requiring careful implementation to avoid common pitfalls [55]. For this reason, MILP is often preferred when the problem remains computationally tractable and an exact solution is desirable.

While multi-energy system modeling is well developed, its application to ICES and RECs remains relatively sparse, due to their recent emergence. For instance, [56] reviews modeling and optimization works in the context of RECs. Early studies, such as [4], employ simpler models, e.g., representing REC as a single-node system with aggregated electricity demand, a shared PV plant, and a collective storage unit. A more advanced multi-node approach was presented in [57], where individual users owned PV systems, but storage remained a shared asset. Similarly, [58] introduced a multi-node framework but limited its scope to electricity-only systems. Expanding beyond electricity, [59] incorporated both electrical and thermal energy but restricted the model to a single active node.

The coupling of electricity, heat, and gas systems has been explored in the broader energy systems literature. For instance, [60] demonstrated the cost-effectiveness of integrating diverse storage technologies and polygeneration units in local energy communities. However, such approaches often overlook the specific regulatory requirements of RECs, especially in the Italian context.

In [61], a detailed MILP model is introduced to integrate sector coupling in REC optimization by means of EV charching and demand response. They also include the perspectives of environmnyl and comfort goals in the optimization of operation and design. In [62], multi-energy RECs are considered, where users

are interconnected by means of district heating and cooling networks other than electricity. A significant step toward multi-node, multi-energy REC modeling was made in [63], where individual nodes could host multiple generation, conversion, and storage technologies. Their analysis, however, was limited to cases up to three nodes.

Contributions

This chapter formalizes and tests a comprehensive MILP framework for ICES operation optimization. This model extends the REC modeling capabilities of the open-source tool previously developed by the author [64], adopting a multi-node and multi-energy approach and improving its compatibility with the Italian regulatory framework. Unlike previous studies that were restricted to small-scale cases (e.g., up to three nodes in [63]), the proposed framework is designed to handle larger ICES configurations, allowing for a more detailed and scalable analysis of multi-node interactions

The key contributions are as follows.

MILP optimization framework Building on state-of-the-art energy system modeling, a MILP optimization problem is formalized considering key features, including the multi-node model and energy sharing mechanism. This model extends beyond previous REC optimization frameworks (e.g., [61], [62]) by integrating both electricity and thermal networks while ensuring compliance with Italian regulations on energy storage and sharing. Particular attention is given to modeling electricity storage systems, ensuring compliance with Italian regulations [65]. Specifically, renewable and non-renewable electricity are treated separately in storage calculations.

Comprehensive testing and assessment Unlike previous studies that tested limited configurations, this work evaluates diverse scenarios with varying PV/storage capacities and different optimization strategies, systematically analyzing computational trade-offs for larger ICES sizes. This analysis explores and benchmarks key modeling choices such as single-node vs. multi-node configurations, collective vs. individual optimization strategies, and simplified vs. detailed storage modeling. Finally, the analysis provides results related to computational challenges associated with increasing node counts and problem sizes.

3.2 Components modeling

This section completes the ICES model described in Section 1.3, by presenting the mathematical models adopted for the individual components typically found within an energy node.

A component is modeled as an entity that handles inflow and outflow powers of various energy carriers, which can be converted between different energy carriers, and also stored and released in a subsequent time step. A qualitative representation of such a component is shown in Fig. 3.1. This general approach increases the model's flexibility, allowing it to simulate a wide range of technologies that are typically found in an ICES. RES-based generators –such as PV and solar thermal– are sources with imposed output powers. Similarly, loads are sinks with imposed input power flows. Conversion units –such as boilers and cogenerators– convert a natural gas inflow into heat and heat/electricity with given efficiencies. Heat pumps instead convert electricity into thermal energy with a certain coefficient of performance (COP). Electrochemical batteries and hot water tanks do not perform any energy conversion[1] but can store energy for subsequent use.

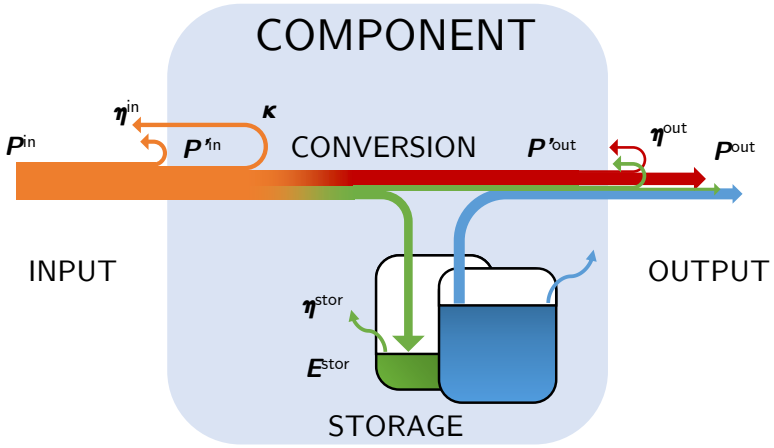

Fig. 3.1 Qualitative representation of a generic component. (Adapted from [16]).

Inflows and Outflows. Each component has associated inflows and outflows of energy carriers, which "cross" its boundaries, with input and output efficiencies, $\eta^{in} \leq 1$ and $\eta^{out} \leq 1$, respectively, as follows:

[1] It could be argued that batteries convert electric into chemical energy (and back). However, this phenomenon is not modeled in the scope of this chapter, hence neglected and approximated through the charge, discharge, and storage efficiencies.

$$P'^{\text{in}} = \eta^{\text{in}} P^{\text{in}}, \tag{3.1}$$

$$P'^{\text{out}} = \frac{1}{\eta^{\text{out}}} P^{\text{out}}, \tag{3.2}$$

where P^{in} and P^{out} are the inflow and outflow powers for a specific energy vector v (whose superscript has been omitted), and P'^{in} and P'^{out} are the related powers after crossing the component's boundaries.
For instance, the charge and discharge of electrochemical batteries can be described using these efficiencies.

Energy conversion. Generally, power flows can be converted between different energy carriers within components. A conversion factor $\kappa^{\text{v}' \to \text{v}''}$ governs the relationship between the input and output powers[2], as follows:

$$\kappa^{\text{v}' \to \text{v}''} P'^{\text{in,v}'} = P'^{\text{out,v}''}, \tag{3.3}$$

where the subscript v is shown to highlight the different energy carriers of the quantities involved.
For example, the conversion of natural gas into heat and heat/electricity in boilers and cogenerators, respectively, can be described utilizing efficiencies as conversion factors. For heat pumps, the conversion factor is their COP.

Energy storage. In some cases, energy can be stored within components, and used in subsequent time steps. Energy storage requires an energy balance between subsequent time steps; a storage efficiency, $\eta^{\text{stor}} \leq 1$, is considered to account for self-discharge phenomena, as follows:

$$E^{\text{stor}}_{\text{h+1}} - \eta^{\text{stor}} E^{\text{stor}}_{\text{h}} = \left(P'^{\text{in}}_{\text{h}} - P'^{\text{out}}_{\text{h}} \right) \Delta t_{\text{h}} \tag{3.4}$$

where the subscript h is shown to highlight the different time steps of the quantities involved; Δt_{h} is the length of the time steps.

[2] Conversion factor is not necessarily an efficiency –and its value can be larger than 1–, as in the case of reverse-cycle machinery such as heat pumps.

Generalized matrix representation. The previous equations can be generalized to represent, in principle, any component with a single equation. If a single energy carrier is involved, without any conversion (for instance, in an electrochemical battery), the generalized equation is obtained by merging (3.1) and (3.4), as follows:

$$E^{\text{stor}}_{\text{h+1}} - \eta^{\text{stor}} E^{\text{stor}}_{\text{h}} = \left(\eta^{\text{in}} P^{\text{in,}}_{\text{h}} - \frac{1}{\eta^{\text{out}}} P^{\text{out}}_{\text{h}}\right) \Delta t_{\text{h}}.$$

If conversion between two energy carriers is also present, two equations would be needed, obtained by including (3.3) in the previous one, as follows:

$$\begin{aligned}
&E^{\text{stor,v}'}_{\text{h+1}} - \eta^{\text{stor,v}'} E^{\text{stor,v}'}_{\text{h}} = \\
&\quad \left(\left(\eta^{\text{in,v}'} P^{\text{in,v}'}_{\text{h}} + \kappa^{\text{v}'\rightarrow\text{v}''} \eta^{\text{in,v}''} P^{\text{in,v}''}_{\text{h}}\right) - \frac{1}{\eta^{\text{out,v}'}} P^{\text{out,v}'}_{\text{h}}\right) \Delta t_{\text{h}}, \\
&E^{\text{stor,v}''}_{\text{h+1}} - \eta^{\text{stor,v}''} E^{\text{stor,v}''}_{\text{h}} = \\
&\quad \left(\left(\eta^{\text{in,v}''} P^{\text{in,v}''}_{\text{h}} + \kappa^{\text{v}''\rightarrow\text{v}'} \eta^{\text{in,v}'} P^{\text{in,v}'}_{\text{h}}\right) - \frac{1}{\eta^{\text{out,v}''}} P^{\text{out,v}''}_{\text{h}}\right) \Delta t_{\text{h}}.
\end{aligned}$$

A generalized matrix form can link inflows, outflows, and stored energy in any component. In this representation, input and output powers, stored energy, and related efficiencies are expressed as vectors, while conversion factors are organized into a matrix (see Tab. 3.1). In this matrix, diagonal elements represent self-conversion (i.e., no conversion between carriers), while off-diagonal elements contain conversion factors between different energy carriers. The generalized matrix equation is the following (column vectors are considered unless transposed):

$$\mathbf{E}^{\text{stor}}_{\text{h+1}} - \boldsymbol{\eta}^{\text{stor}} \circ \mathbf{E}^{\text{stor}}_{\text{h}} = \left(\boldsymbol{\kappa} \cdot \left(\boldsymbol{\eta}^{\text{in}} \circ \mathbf{P}^{\text{in}}_{\text{h}}\right) - \boldsymbol{\eta}^{\text{out}^{\circ(-1)}} \circ \mathbf{P}^{\text{out}}_{\text{h}}\right) \Delta t_{\text{h}}, \tag{3.5}$$

where the operator $\circ$ is the element-wise product between vectors or matrices of the same size (i.e., the Hadamard product [66]) –similarly, $^{\circ(-1)}$ is the element-wise reciprocal–, while operator $\cdot$ is the classic scalar (or matrix) product; the terms in bold font are the vector/matrix representations of the quantities defined previously.

Operative constraints. Usually, additional constraints must be enforced to represent the components' behavior properly. For instance, power and energy quantities must be bounded to minimum and maximum values, which depend on the size of the component. Some components may require enforcing mutual

Table 3.1 Conversion factors matrix. The matrix may not be square, as the input and output powers can correspond to different energy vectors. If the same energy vector is involved for both input and output, the corresponding cell takes a value of 1.

		Input				
		v_1	$\cdots$	v_k	$\cdots$	$v_{in,V}$
Output	v_1	1	$\cdots$	$\kappa^{v_1 \to v_k}$	$\cdots$	$\kappa^{v_1 \to v_V}$
	$\vdots$	$\vdots$	$\ddots$			$\vdots$
	v_k	$\kappa^{v_k \to v_1}$		1		$\kappa^{v_k \to v_V}$
	$\vdots$	$\vdots$			$\ddots$	$\vdots$
	v_V	$\kappa^{v_V \to v_1}$	$\cdots$	$\kappa^{v_V \to v_k}$	$\cdots$	1

exclusivity between quantities in the same time step (e.g. charge and discharge of electrochemical batteries).

3.2.1 Storage and energy sharing

Energy storage systems (ESS) are given particular attention when modeling the ICES. Classically, ESS stores excess energy generation within an individual energy node. This energy can come from both renewable and non-renewable energy sources. Also, ESS units can store energy withdrawn from the energy networks, for instance, to improve the local consumption (i.e., within the ICES) by sharing excess energy injected by another node. The stored energy can later be used locally or re-injected into the network.

Nonetheless, national regulations may impose additional restrictions on the sharing of stored energy. For instance, only energy produced from RES is usually eligible for sharing. Additionally, the Italian regulation for RECs does not allow the sharing of electricity stored after being withdrawn from the grid, even if injected by another node of the ICES [65]. Such regulatory constraints make the integration of ESS into ICES more complex, and hence these components must be modeled carefully so as not to hinder their potential.

ESS is divided into two fictitious separate subsystems, as in Fig. 3.2. A 'renewable' storage r accounts for energy stored from RES-based generators, while a 'non-renewable' one, nr, accounts for energy stored from non-RES-based generators. When further constraints are necessary –as in the case of the Italian regulation [16]–, the non-renewable storage can be extended, for instance, to include electricity from the grid.

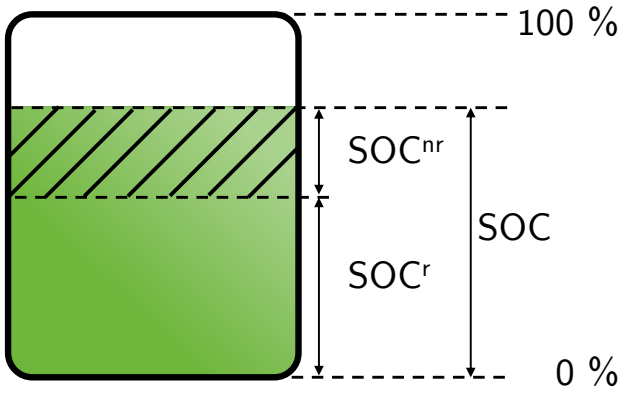

Fig. 3.2 Energy storage split into renewable and non-renewable storage subsystems. (Adapted from [16]).

The input power to the renewable storage subsystem, $P^{\mathrm{ESS_r,in}}$, is calculated as follows:

$$P^{\mathrm{ESS_r,in}} = \min\left(P^{\mathrm{ESS,in}}; P^{\mathrm{r}}\right), \tag{3.6}$$

where $P^{\mathrm{ESS,in}}$ is the total input power of the component, and P^{r} is a term accounting for the renewable energy storable. For instance, if only renewable energy produced within an individual node can be shared, this term is the sum of the locally-produced renewable energy.

Balance equations like (3.4) are included separately for both subsystems. The input and output powers and the stored energy are the sum of the related renewable and non-renewable quantities so that the whole ESS balance holds.

The output power of the non-renewable subsystem, $P^{\mathrm{ESS_{nr},out}}$, is then used to calculate the shareable energy injected by an energy node. The latter is a part of the total injected energy and is calculated as follows:

$$P^{\mathrm{inj,sh}} = \max\left(0; P^{\mathrm{inj}} - \sum_{i \in I^{\mathrm{stor}}} P^{\mathrm{i_{nr},out}}\right) \tag{3.7}$$

where I^{stor} is the set of ESS components in the energy node. Even though the related subscripts and superscripts are omitted, this equation is written separately for each energy vector (whose network injections and sharing are possible), each energy node, and naturally each time step.

The shareable energy injection replaces the actual injections in (1.2), which is then rewritten as follows:

$$P^{\text{shared}} = \min\left(\sum_{\text{j}} P_{\text{j}}^{\text{inj,sh}}; \sum_{\text{j}} P_{\text{j}}^{\text{with}}\right). \tag{3.8}$$

3.3 Optimization problem

An ICES is generally a complex multi-node and multi-energy system, and its energy performances (and, consequently, environmental, economic, etc.), are not trivial to assess. Optimization techniques can provide benchmarks of an ICES performance for the operation over a certain time horizon. The model described in the previous section can be implemented into an optimization problem, to find the power values that maximize or minimize an objective function, for each time step in the considered time horizon.

A minimization problem –with a single objective function– can be generally written as follows:

$$\begin{aligned} \underset{\mathbf{x}}{\text{minimize}} \quad & f(\mathbf{x}) \\ \text{subject to} \quad & h_{\text{i}}(\mathbf{x}) = 0, \quad i = 1, \dots, m, \\ & g_{\text{j}}(\mathbf{x}) \leq 0, \quad j = 1, \dots, p, \\ & \mathbf{x} \in X \subseteq \mathbb{R}^{\text{n}}, \end{aligned} \tag{3.9}$$

where $\mathbf{x}$ is the vector of decision variables, in the decision space X, f is the objective function, and h_{i} and g_{j} are, respectively, equality and inequality constraints.

The objective function and the constraints can have any shape. In case they are all linear functions, the problem is said to be linear and can be re-written according to a standard form:

$$\begin{aligned} \underset{\mathbf{x} \in \mathbb{R}^{\text{n}}}{\text{minimize}} \quad & \mathbf{C}^{\intercal}\mathbf{x} \\ \text{subject to} \quad & \mathbf{A}\mathbf{x} = \mathbf{b}, \\ & \mathbf{x} \geq 0, \end{aligned} \tag{3.10}$$

where $\mathbf{C} \in \mathbb{R}^{\text{n}}$ is the so-called cost vector, and $\mathbf{A}, \in \mathbb{R}^{\text{m}\times\text{n}}$ and $\mathbf{b} \in \mathbb{R}^{\text{m}}$ are the coefficient matrix and known-terms vector of the equality constraints.

Linear optimization problems can be solved deterministically, utilizing Linear Programming (LP) techniques, such as the simplex method [67]. When the de-

cision vector includes integer variables (e.g., binary) $x_i, \dots x_j \in \mathbb{Z}$, Mixed-Integer Linear Programming (MILP) techniques can be used, as the well-known branch-and-bound algorithm [67].

The details of implementing the ICES model into a MILP optimization problem are described in the following.

3.3.1 Auxiliary binary variables

As stated above, the objective function and all the constraints in an optimization problem must be linear to use MILP. This is not true for the ICES model described in Section 3.2. Indeed, while linear models are used to describe the behavior of the components in the system, non-linear equations are necessary to model the ICES properly. For instance, in (1.2) the calculation of the shared energy involves a min function, while imposing mutual exclusivity between variables –such as concurrent injections and withdrawals into/from the electricity grid– requires logical constraints.

Auxiliary binary variables can be introduced to linearize such constraints, allowing the implementation of the adopted ICES model into a MILP optimization problem.

Min, max constraints. In general, a constraint involving min function –e.g., $z_1 = \min(x_1, y_1)$– can be linearized as follows:

$$\begin{aligned} & z_1 \leq x_1, \\ & z_1 \leq y_1, \\ & z_1 \geq x_1 - \delta_1 M_1, \\ & z_1 \geq y_1 - (1-\delta_1) M_1, \end{aligned} \tag{3.11}$$

where $\delta_1 \in \{0,1\}$ is the auxiliary binary variable, and $M_1 \in \mathbb{R}$ is the so-called 'big-M parameter', a number large enough such that $x_1, y_1 < M_1$ for all x_1 and y_1 in the design space. While the first two inequalities enforce z_1 to be smaller-equal than both x_1 and y_1, adding the last two enforces z_1 to be larger-equal than the minimum between the two. As a consequence, the only possibility is that z_1 is exactly equal to the minimum between the two values[3]. Constraints involving

[3]For instance, assuming $x, y \geq 0$, if $\delta_1 = 0$, then $z_1 \leq x_1$ and $z_1 \geq x_1 - \delta_1 M_1 \rightarrow z_1 \geq x$, hence $z = x$, meaning that $x = \min(x, y)$ otherwise the problem would be unfeasible since $x_1 = z_1 < y_1$.

max functions –e.g., $z_2 = \max(x_2, y_2)$– can be linearized similarly, as follows:

$$\begin{aligned} z_2 &\geq x_2, \\ z_2 &\geq y_2, \\ z_2 &\leq x_2 + (1-\delta_2)M_2, \\ z_2 &\leq y_2 + \delta_2 M_2, \end{aligned} \tag{3.12}$$

Logical constraints Binary optimization variables are also useful to impose that two variables cannot be larger than zero at the same time. Mutual exclusivity between two variables, x_3 and y_3 can be enforced by using once again an auxiliary variable $\delta_3 \in \{0,1\}$, together with big-M parameters $M_{x_3} > x_3 \forall x_3, M_{y_3} > y_3 \forall y_3$ as follows:

$$\begin{aligned} x_3 &\leq \delta_3 M_{x_3}, \\ y_3 &\leq (1-\delta_3) M_{y_3}. \end{aligned} \tag{3.13}$$

For instance, mutual exclusivity between injections and withdrawals into/from the electricity grid, or charge and discharge of electricity storage systems within the same time step can be enforced using (3.13). In these cases, the big-M parameters could be set as, respectively, the maximum injections and withdrawals, and the maximum charge and discharge powers.

3.3.2 Objective function

Different possibilities are available concerning the objective function. For instance, maximizing the energy consumed within the ICES or minimizing energy exchanges outside the ICES, have been proposed in the literature [4]. These approaches have the advantage of decoupling the results from the variability of energy prices, which, as shown in Section 2.4, can fluctuate significantly over time. However, in settings involving multiple energy vectors, they cannot account for the varying importance of different energy carriers unless appropriate weighting is applied. Similarly, they do not distinguish between physical self-consumption and virtual energy exchanges, assigning them equal value in a purely energy-based objective function.

For this reason, the objective of the optimization is set as the minimization of the total operational costs over the considered time horizon, specifically the

The constraint $z_1 \geq y_1 - (1-\delta_1)M_1$ becomes $z_1 \geq y_1 - M_1 \leq 0$ since M_1 is always larger than y_1. This is already true since $z_1 \geq 0$ in the decision space.

energy costs, as defined in Section 1.4. A tentative generalization of these costs in an ICES, C, can be the following:

$$C = \sum_{\mathrm{h}} \left(\sum_{\mathrm{v}} \left(P^{\mathrm{with,v}}_{\mathrm{ICES,h}} c^{\mathrm{with,v}}_{\mathrm{h}} - P^{\mathrm{inj,v}}_{\mathrm{ICES,h}} c^{\mathrm{inj,v}}_{\mathrm{h}} + P^{\mathrm{shared,v}}_{\mathrm{h}} c^{\mathrm{sh,v}}_{\mathrm{h}} \right) \Delta t_{\mathrm{h}} \right). \tag{3.14}$$

In (3.14), for energy vector having a network interconnecting the energy nodes, only exchanges outside of the ICES are considered as costs (for withdrawals) and revenues (for injections), respectively, at $c^{\mathrm{with,v}}_{\mathrm{h}}$ and $c^{\mathrm{inj,v}}_{\mathrm{h}}$. A cost for the shared energy may be introduced $c^{\mathrm{sh,v}}_{\mathrm{h}}$, for instance, due to the utilization of a public distribution grid. If energy sharing on a certain network is not allowed, $P^{\mathrm{shared,v}}_{\mathrm{h}}$ for that vector will always be 0 and, according to (1.4) and (1.5), the ICES exchanges with the outside coincide with the total injections and withdrawals of the energy nodes. Similarly, if injections in an energy network are not allowed, the term $P^{\mathrm{inj,v}}_{\mathrm{ICES,h}}$ will always be zero (as well as $P^{\mathrm{shared,v}}_{\mathrm{h}}$).

The energy costs depend strongly on the legal structure of the ICES and the national rules adopted for these configurations. For instance, as described in Section 1.2, the Italian regulation for RECs states that electricity can be shared using the public distribution grid. Shared energy is economically incentivized but each member's withdrawals (and injections) are paid at the retail (market) price. The cost in (3.14) can be adapted to better reflect this situation, by using the relations in (1.4) and (1.5). The energy costs can then be re-written as:

$$\begin{aligned} C = \sum_{\mathrm{h}} \Bigg(\sum_{\mathrm{v}} \Bigg(& \sum_{\mathrm{j}} P^{\mathrm{with,v}}_{\mathrm{j,h}} c^{\mathrm{with,v}}_{\mathrm{h}} - \sum_{\mathrm{j}} P^{\mathrm{inj,v}}_{\mathrm{j,h}} c^{\mathrm{inj,v}}_{\mathrm{h}} + \\ & - P^{\mathrm{shared,v}}_{\mathrm{h}} \left(c^{\mathrm{with,v}} - c^{\mathrm{inj,v}}_{\mathrm{h}} + c^{\mathrm{sh,v}}_{\mathrm{h}} \right) \Bigg) \Bigg) \Delta t_{\mathrm{h}}, \end{aligned} \tag{3.15}$$

where the shared energy term appears as a revenue (negative sign), valued at $c^{\mathrm{with,v}} - c^{\mathrm{inj,v}}_{\mathrm{h}} + c^{\mathrm{sh,v}}_{\mathrm{h}}$, representing an incentive to cover the difference between retail and market price for the energy produced locally and collectively self-consumed, increased by a certain cost for using the public distribution grid.

The rewritten cost function in (3.15) maintains full consistency with the general formulation in (3.14), while explicitly incorporating REC regulatory framework within the ICES. Therefore, this refined formulation serves as a reference for the subsequent analysis.

3.3.3 Collective versus individual optimization

The energy costs in (3.15) highlight how shared energy represents an additional revenue compared to the individually-acting energy nodes. Indeed, two distinct approaches can be adopted when considering an ICES with multiple energy nodes: the individual optimization of each node or a collective optimization of the nodes.

In the individual approach, each energy node acts independently (as a single player in a game) and is therefore unaware of the other nodes in the ICES during optimization. This can be achieved by removing the term of shared energy from the objective function in (3.15) and minimizing

$$\sum_{\mathrm{h}}\left(\sum_{\mathrm{v}}\left(\sum_{\mathrm{j}}\left(P_{\mathrm{j,h}}^{\mathrm{with,v}}c_{\mathrm{h}}^{\mathrm{with,v}}-P_{\mathrm{j,h}}^{\mathrm{inj,v}}c_{\mathrm{h}}^{\mathrm{inj,v}}\right)\right)\right)\Delta t_{\mathrm{h}},$$

instead[4]. While this minimizes the costs of the individual energy nodes, it does not account for the potential benefits of energy sharing or collective resource management. Consequently, system-wide performance is often suboptimal, as opportunities for collective use of flexible resources such as storage systems are missed.

Conversely, collective optimization considers the ICES as a whole, with each node aware of the other nodes, and their decisions mutually influenced. This allows for a more effective utilization of resources, enhancing the overall performance of the ICES. For example, excess generation at one node can be stored or utilized elsewhere in the system, and nodes coordinate to balance supply and demand across the ICES. The downside of collective optimization is that considering all nodes and their interactions in a single optimization problem is computationally more demanding.

While collective optimization improves the system-wide objective, the need to optimize all energy nodes concurrently poses questions about its practical application. For instance, a robust infrastructure for data sharing among the nodes and a central controller to manage operations would be required. Also, the acceptance of centralized decision-making by all participants is not straightforward. These aspects are crucial in real-world cases, but not in the scope of this chapter, where

[4] Removing the shared energy term from the objective function *de facto* decouples the optimization of the individual energy nodes. One optimization problem for each node can be solved instead of a single, larger problem. While the complexity of the individual problems decreases, this might not always be computationally efficient in practice, due to fixed costs of creating and solving each single problem, unless they are parallelized.

optimization is primarily used to provide performance benchmarks for ICES performances. Nonetheless, the results obtained for the test cases presented in the following are meant to explore any different results in the cases of individual and collective optimization.

3.3.4 Time periodicity

As mentioned in Section 1.3 optimization is performed over a one-year time horizon, serving as a reference period for evaluating the ICES performance. For this reason, periodicity constraints are put to time-coupling quantities –e.g., energy stored in ESS– so that they assume the same value at the beginning and the end of this period. Considering the generalized matrix representation from (3.5), the periodicity constraint over the considered time horizon can be imposed as follows:

$$\mathbf{E}_0^{\text{stor}} - \boldsymbol{\eta}^{\text{stor}} \circ \mathbf{E}_{\text{H}}^{\text{stor}} = \left(\boldsymbol{\kappa} \cdot \left(\boldsymbol{\eta}^{\text{in}} \circ \mathbf{P}_{\text{H}}^{\text{in}} \right) - \boldsymbol{\eta}^{\text{out}^{\circ(-1)}} \circ \mathbf{P}_{\text{H}}^{\text{out}} \right) \Delta t_{\text{h}}, \tag{3.16}$$

where 0 and H refer, respectively, to the first and last time steps in the time horizon. Such a long periodicity implies perfect knowledge of the entire year, i.e., a perfect forecast of the input quantities, such as prices, energy generation, and consumption patterns, which seems unrealistic in real-world operational scenarios. Once again, these details about the real-world implementation of the proposed optimization problem as a controller for the ICES fall outside the scope of this chapter, where optimization is rather intended as a benchmark of its performance.

3.4 Test cases

A series of test cases is designed to analyze the multi-node ICES model and its optimization using the MILP problem described before. These test cases (summarized in Fig. 3.3) are structured to assess the key features of the proposed ICES model and some relevant aspects briefly introduced in the previous section, mainly:

- Multi-node modeling of the ICES.
- Collective versus individual nodes optimization (see Section 3.3.3).
- Storage modeling for energy sharing (see Section 3.2.1).

Test	Nodes		ICES model		Optimization strategy		BESS model		Multi-energy	Time horizon
	Active	Total	Single node	Multi-node	Individual	Collective	Simple	Detailed		
3-node ICES	2	3	-	✓	-	✓	✓	✓	-	1 day
50-node ICES	40	50	-	✓	✓	✓	-	✓	✓	1 day
Comprehensive set	1-5-10-15	103	✓	✓	✓	✓	-	✓	-	1 year

Fig. 3.3 Overview of the test cases conducted on the optimal energy management of multi-node and multi-energy ICES.

First, two 'exploratory test cases' are considered, highlighting the different power profiles in a one-day time horizon concerning: 1. collective versus individual optimization; and 2. simple versus renewable/non-renewable storage modeling. Then, a more comprehensive analysis is conducted, using the data described in Chapter 2, with scenarios designed to investigate different PV and storage capacity availability. In all tests, the ICES model is used to represent a REC according to the Italian regulation. Therefore, only electricity can be shared, using the public distribution grid. Consequently, the economic scheme described in Section 1.2.3 is used to evaluate energy costs in the objective function. In some tests, sectors-coupling is included, locally within single energy nodes, by using heat pumps to supply heating demand.

3.4.1 Three-node ICES

A simple ICES with three energy nodes is considered, as follows:

- Active node 1, prosumer with larger PV generation and small battery ESS capacity.
- Active node 2, pure producer with larger battery ESS capacity but smaller PV generation.
- Passive node, pure electricity consumer.

Despite not representing a likely real-world situation, this test highlights the different storage utilization in an ICES setup when split into renewable and non-renewable sub-systems and the simple case where energy from any source can

Table 3.2 Composition of the ICES with 50 nodes.

Combination of components				
PV	**BESS**	**HP**	**HTS**	**N. nodes**
✓	✓	-	-	11
-	-	-	-	10
✓	-	-	-	8
-	✓	-	-	8
✓	✓	✓	✓	6
-	-	✓	✓	4
-	✓	✓	✓	3
			Total	50

be stored, without restrictions. In particular, the Italian regulation on RECs is considered, according to which energy coming from the grid cannot be stored and then re-injected for sharing, even if it comes from another renewable generator in the ICES. For this reason, differently from (3.6), the non-renewable (i.e., non-shareable) input to the ESS is defined, as follows: $P_{\mathrm{j}}^{\mathrm{BESS_{nr},in}} = \min\left(P_{\mathrm{j}}^{\mathrm{BESS,in}}, P_{\mathrm{j}}^{\mathrm{with}}\right)$, preventing energy from the grid (even if injected by another node) to be stored in the renewable sub-system.

3.4.2 Fifty-node ICES

A larger ICES is considered, composed of fifty energy nodes. All nodes have a certain electricity demand and a combination of the following technologies – that are selected randomly–, as detailed in Tab. 3.2: photovoltaic generator (PV), battery energy storage system (BESS), heat pump (HP), heat thermal storage (HTS). Both individual and collective optimizations are run, highlighting how collective use of the flexible technologies can achieve minimum overall costs against the case in which each node minimizes its costs individually.

3.4.3 Comprehensive test scenarios

For this set of tests, the electricity end users described in Chapter 2 are considered as part of an ICES, again in a REC setup. Different scenarios are identified by varying the PV and BESS capacities, to cover a series of possible situations, as follows:

- Undersized PV, in relation to the reference size $S^{\mathrm{PV},0}$ from(2.6) that would cover the total demand in one year (i.e., without considering hourly fluctuations).
- Reference PV size, theoretically sufficient to meet annual energy demands but with seasonal discrepancies in generation and consumption.
- Oversized PV, potentially saturating energy consumed locally within the ICES.
- No storage, therefore without the possibility to modify the injection or withdrawal profiles.
- Gradually increasing from moderate to high storage capacity, particularly relevant with higher PV sizes, to store excess energy and reduce exchanges with the grid outside the ICES.

As reported in Chapter 2, the reference PV size, $S^{\mathrm{PV},0}$, is equal to 300 $\mathrm{kW_p}$ considering all end users present in the dataset.

Then, twelve scenarios are defined, by combining the PV size, S^{PV}, and BESS size, S^{BESS}, as follows:

$$S^{\mathrm{PV}} = \{0.5, 1, 1.5\} \times S^{\mathrm{PV},0} \qquad [\mathrm{kW_{peak}}],$$
$$S^{\mathrm{BESS}} = \{0, 1, 1.5, 2\} \times S^{\mathrm{PV}} \qquad [\mathrm{kWh}],$$

Single active node For each scenario, an initial configuration is considered, consisting of:

- One active node, holding the totality of PV and BESS capacity in the ICES.
- One passive node, given by aggregating all the end users in the ICES.

Multiple active nodes The number of active nodes in the ICES is varied, to investigate differences introduced by the multi-node approach, both in terms of objective function and computational complexity. Given the number of active nodes, N_{active}, the total PV and BESS capacity are uniformly spread among them. Hence, the composition of the ICES becomes the following:

- N_{active} active nodes, each with

  - electric power consumption randomly extracted from the set of available end users measures,
  - PV size equal to $\frac{S^{\text{PV}}}{N_{\text{active}}}$,
  - BESS size equal to $\frac{S^{\text{BESS}}}{N_{\text{active}}}$.
- One passive node, given by aggregating the end users not selected for the active nodes.

Since the electric load of the active nodes is assigned randomly, 10 different runs are performed for each N_{active} value, varying the selected end users.

Metrics Rather than power profiles, this comprehensive analysis focuses on more general metrics to assess the optimization results and ICES performance:

- Optimal objective function, i.e., minimum total energy costs found by solving the optimization problem.
- Computational complexity, i.e., time required by the solver to minimize the objective function.
- Energy, environmental, and economic KPIs, as detailed in Section 1.4.

3.5 Results

This section presents the results of the test presented in the previous section. In all cases, the MILP optimization problem was written in `Python`, using the `PuLP` package; afterward, the optimization problem was solved using `Gurobi`, under an academic license. Concerning the two 'exploratory test cases', a time horizon of one day was considered, to show the optimal power profiles in the considered cases. In the comprehensive test scenarios, a one-year time horizon was optimized in a single MILP problem, using the data described in Chapter 2.

3.5.1 Simple versus detailed energy storage

Fig. 3.4b and Fig. 3.4a show the optimized electric power flows for the passive node and Active node 1, which has a relatively small BESS compared to its PV size.

The passive node relies entirely on grid withdrawals to meet its electricity demand, while Active node 1 must inject much of its PV generation into the grid due to the limited BESS capacity, allowing only partial local PV utilization. This

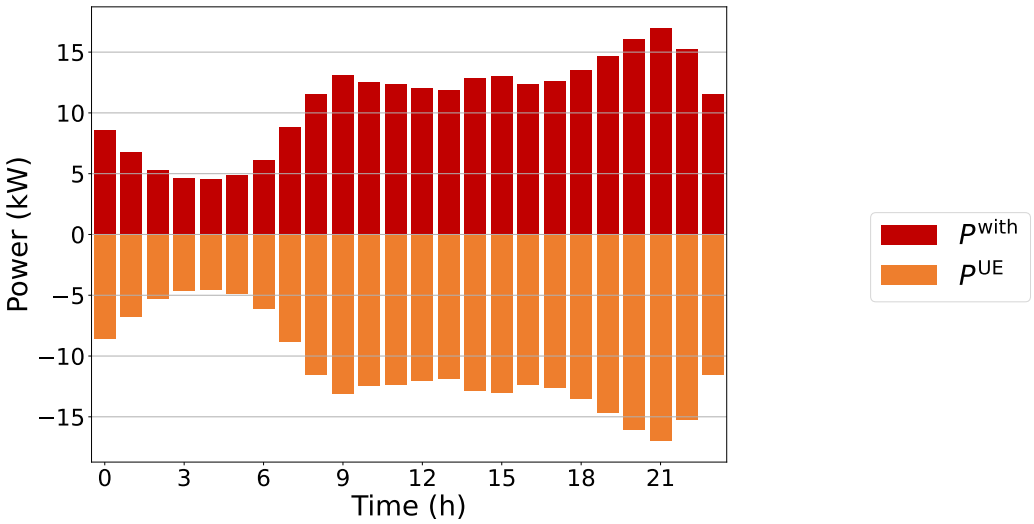

(a) Passive node

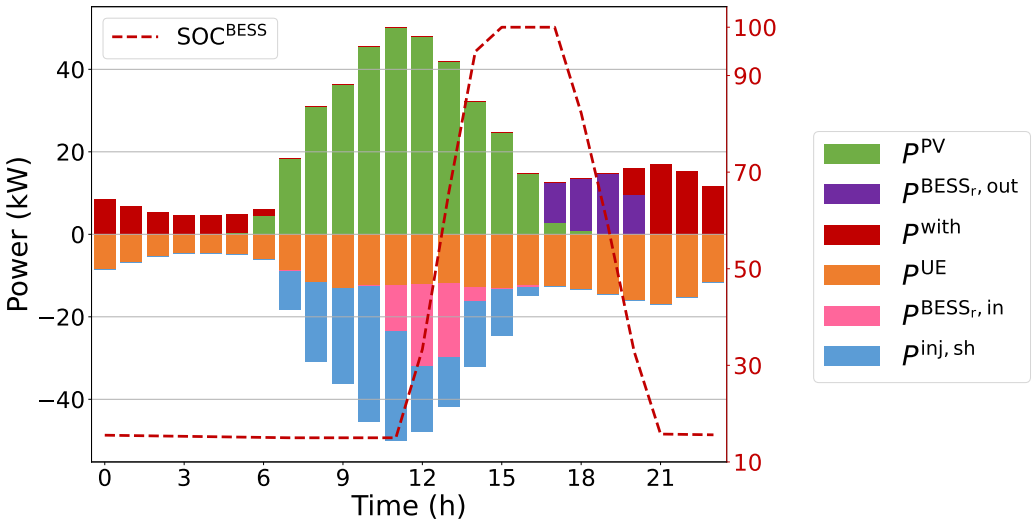

(b) Active node 1

Fig. 3.4 Optimized electric power flows over a one-day horizon for the Passive node and Active node 1 (large PV capacity, small BESS) within the three-node ICES. Power values are positive, with components outflows and grid withdrawals plotted above the x-axis, and inflows and grid injections below. Total inflows, including grid injections, always balance total outflows, including grid withdrawals, as the power balance requires.

behavior remains consistent when using the simplified BESS model that does not differentiate between renewable and non-renewable subsystems.

Active node 2, having a larger BESS capacity available, exhibits a more interesting behavior, withdrawing energy from the grid when surplus from Active node 1. However, the optimization only stores this energy locally if it will be used locally, as shown in Fig. 3.5a –in this case only to compensate self-discharge losses since there are no loads in the node. In general, when using a renewable/non-renewable BESS model, only energy discharged from the renewable subsystem can be shared via the grid, reducing overall BESS utilization and limiting energy-sharing potential (Fig. 3.6a). By contrast, the simplified BESS model treats all stored energy equivalently. As shown in Fig. 3.4a, Active node 2 charges its BESS from surplus injected by Active node 1, later re-injecting this energy into the grid to enhance sharing within the ICES (see Fig. 3.6b).

While the simplified BESS model increases the shared energy, this benefit can be misleading. Shared energy must be recalculated to exclude energy not originating from the same node, as grid-withdrawn energy re-injected into the grid does not qualify for compensation, ultimately increasing costs. The renewable/non-renewable BESS model better reflects regulatory constraints[5]. If energy and environmental goals are prioritized, the simplified model may still be advantageous by maximizing energy sharing, despite its higher associated costs.

3.5.2 Collective versus individual optimization

Fig. 3.7a and Fig. 3.7b show the optimization results for the entire fifty-node ICES, which is structured as described in Tab. 3.2. The figures present, respectively, the outcomes of the two distinct approaches, collective and individual nodes optimization. To compare the two approaches, only the electricity balances across the ICES electricity distribution grid are shown, highlighting the total grid injections and withdrawals of the nodes and energy shared within the ICES.

In the collective approach, energy nodes adjust their injection and withdrawal profiles to increase shared electricity within the ICES. This flexibility is enabled by the distributed storage systems, heat pumps, and heat storage systems across the nodes. As shown in Tab. 3.3, the energy processed by these components –

[5]This model is still an approximation of real-world behavior, as physical subsystems do not exist; instead, the model assumes separate subsystems and decides when to discharge one or the other.

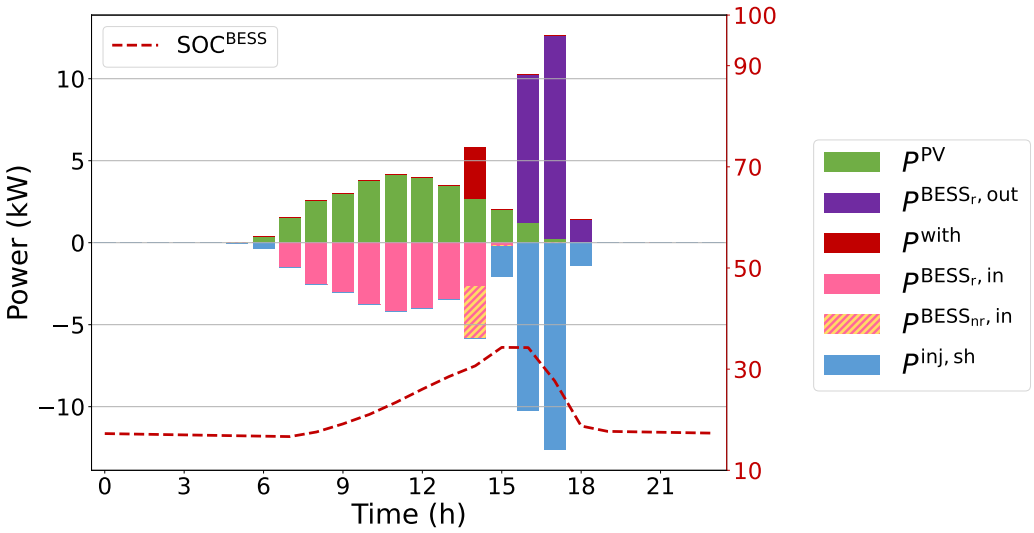

(a) Renewable/non-renewable BESS model

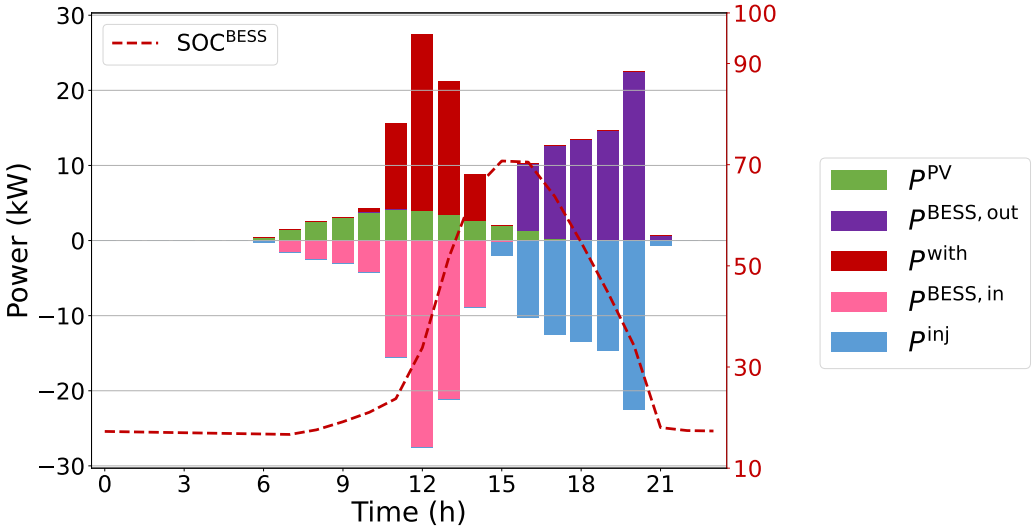

(b) Simple BESS model

Fig. 3.5 Optimal electric powers over a one-day horizon for Active node 2 (smaller PV capacity, larger BESS) within the three-node ICES. Power values are positive, with components outflows and grid withdrawals plotted above the x-axis, and inflows and grid injections below. Total inflows, including grid injections, always balance total outflows, including grid withdrawals, as the power balance requires.

especially BESS– increases under the collective strategy, leading to a higher level of shared energy than the individual optimization.

However, the total injections and withdrawals over the time horizon do not vary significantly between the two cases. Thus, the benefit arises from the strate-

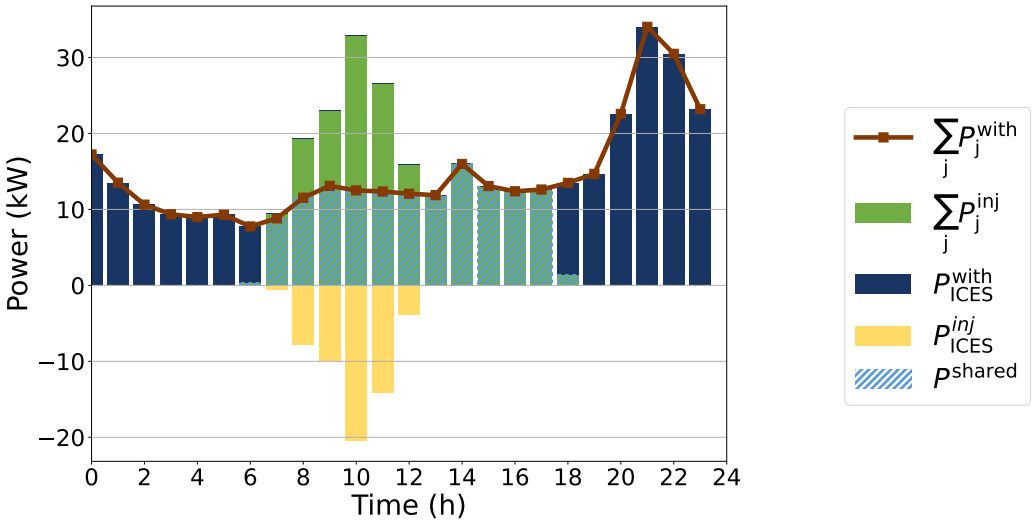

(a) Renewable/non-renewable BESS model

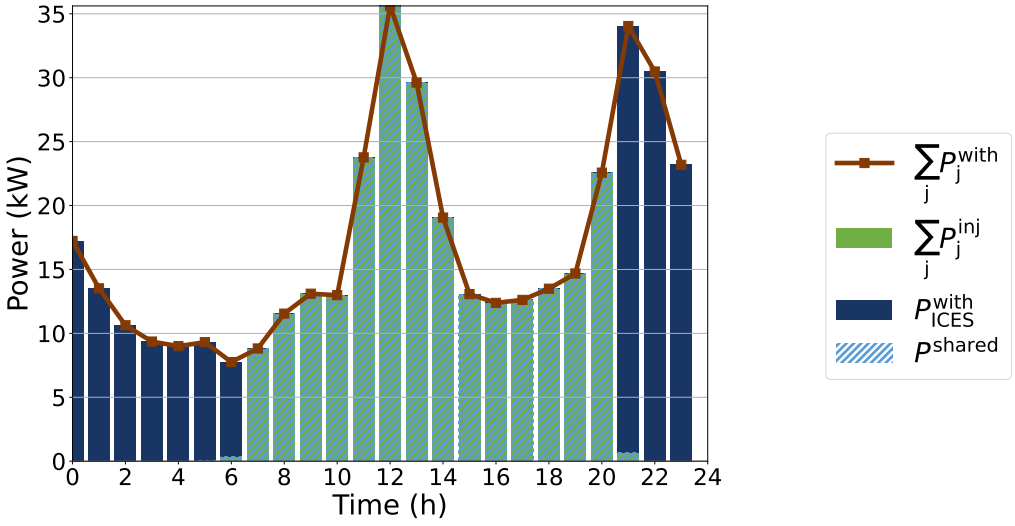

(b) Simple BESS model

Fig. 3.6 Optimal electric power profiles over a one-day horizon for the entire three-node ICES. Total injections from the nodes into the grid and withdrawals from outside the ICES are displayed above the x-axis, and compared to the total nodes withdrawals (brown line), highlighting shared power within the ICES. Injections outside the ICES are shown below the x-axis.

gic timing of electricity injections and withdrawals of the energy nodes, which collectively leverage these flexibility sources to minimize overall energy costs. The table shows that self-consumed energy within each node remains unchanged between the two approaches, indicating that the collective optimization does not

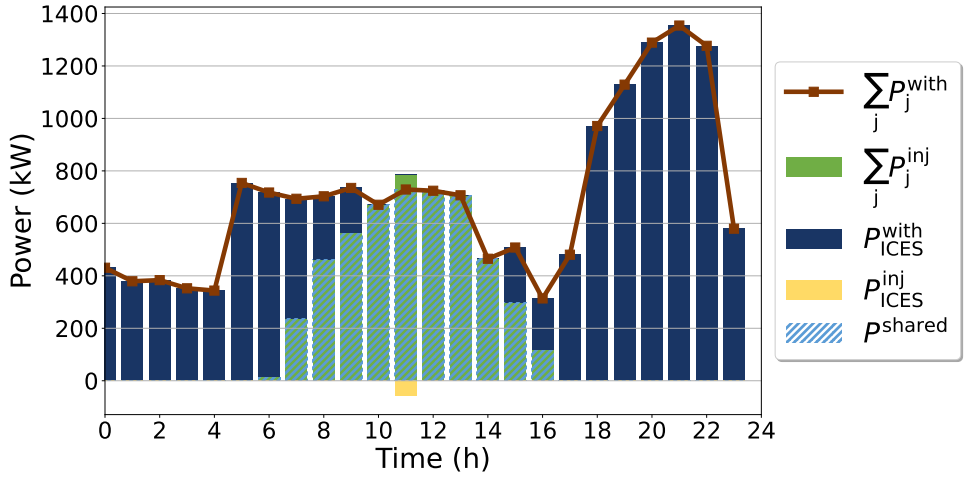

(a) Collective optimization

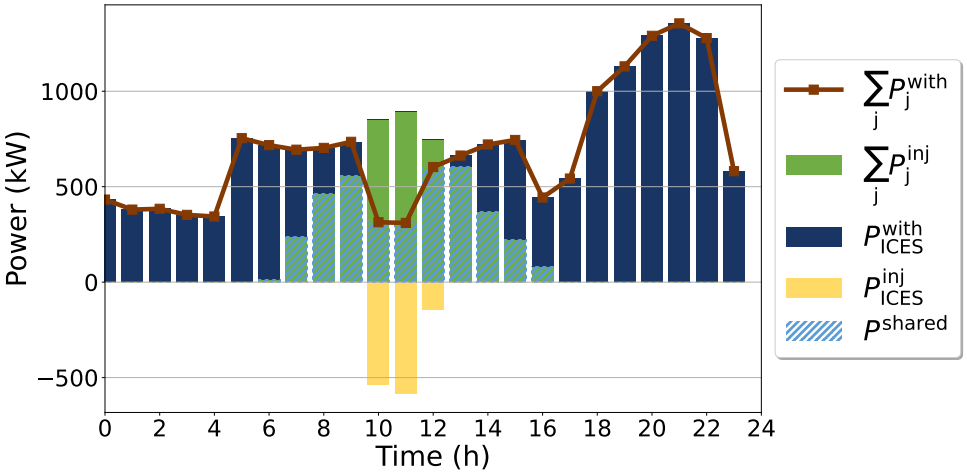

(b) Individual optimization

Fig. 3.7 Optimal electric power profiles over a one-day horizon for the entire fifty-node ICES. Total injections from the nodes into the grid and withdrawals from outside the ICES are displayed above the x-axis, and compared to the total nodes withdrawals (brown line), highlighting shared power within the ICES. Injections outside the ICES are shown below the x-axis.

compromise the single-node benefits. In contrast, under the individual nodes optimization, each node operates based on its local conditions, without aligning injections and withdrawals of electricity with optimal times. Consequently,

Table 3.3 Optimal energy values over a one-day horizon for the entire fifty-node ICES.

Quantity (MWh)	Optimization	
	Collective	Individual
E^{shared}	4.99	3.78
$\sum_j E_{\text{j}}^{\text{inj}}$	5.05	5.05
$\sum_j E_{\text{j}}^{\text{with}}$	16.7	16.5
$\sum_j E_{\text{j}}^{\text{selfcons}}$	4.71	4.71
$\sum_j E_{\text{j}}^{\text{BESS,in}}$	1.50	0.75
$\sum_j E_{\text{j}}^{\text{HP,in}}$	8.03	7.92
$\sum_j E_{\text{j}}^{\text{HTS,in}}$	2.52	2.17

shared electricity is more limited, hindering achieving economic, energy, and environmental objectives.

These findings are further validated by the results of the comprehensive test scenarios, which compares collective and individual optimization of the same configurations. Fig. 3.8 illustrates the optimal objective values across all PV-BESS combinations, with varied node counts and optimization runs, as detailed in the following section. The comparison clearly shows that the optimal objective is consistently lower (i.e., better) under collective optimization.

3.5.3 Multi-node versus aggregated modeling

This section presents the optimization results from the comprehensive test scenarios described in 3.4.3. In particular, the focus is on the trends of key metrics –optimal objective, time complexity, and other KPIs– as the total PV and BESS capacity in the ICES are distributed among an increasing number of active nodes (namely, 1, 5, 10, and 20). Twelve scenarios are considered, each varying the total PV and BESS capacity in the ICES, as described in 3.4.3.

Fig. 3.9 provides an overview of the optimal objective found by solving the MILP optimization problem across various scenarios. Each scenario in the figure is identified in terms of PV ratio (i.e., total PV capacity relative to the reference PV size $S^{\text{PV,0}}$) and BESS ratio (i.e., total BESS size relative to total PV capacity). It is noted that no results are available for scenarios with higher PV and BESS capacities when 20 nodes are considered; this is due to the calculator running out of memory because of the large problem size and complexity.

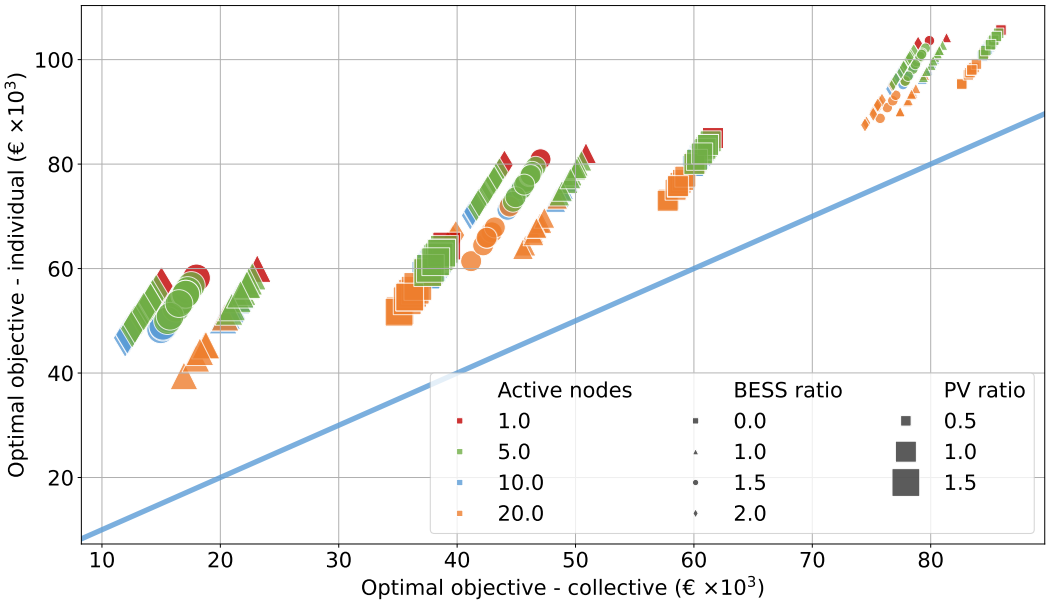

Fig. 3.8 Optimal objective for collective versus individual nodes optimization, across different scenarios in the detailed test set. Scenarios are distinguished by marker sizes (PV ratio) and shapes (BESS ratio), with color indicating the number of active nodes. The reference blue line represents the identity function.

As expected, the optimal objective decreases (i.e., improves) with increasing total PV and BESS capacities in the ICES, as evident from the scales of the different subplots. This trend is readily explainable, given that the energy costs minimized in the objective function account only for operational expenses. More notably, the results show that the optimal objective consistently decreases in all combinations as the number of active nodes distributing the total PV and BESS capacity increases.

To further analyze this effect, the previous results are rearranged into a single plot showing the percentage difference in the optimal objective relative to its value with only one active node (see Fig. 3.10). The figure indicates that the improvement in the objective function grows with both the total PV and BESS capacities, reaching up to a 25% reduction. Additionally, a significant spread is observed in the optimization results across different runs, highlighting variability in improvement with the number of active nodes.

It is particularly insightful to analyze the configurations without BESS capacity (i.e., where the BESS ratio equals 0). Optimization results are trivial in these cases since the only available degrees of freedom are the grid exchanges of each energy

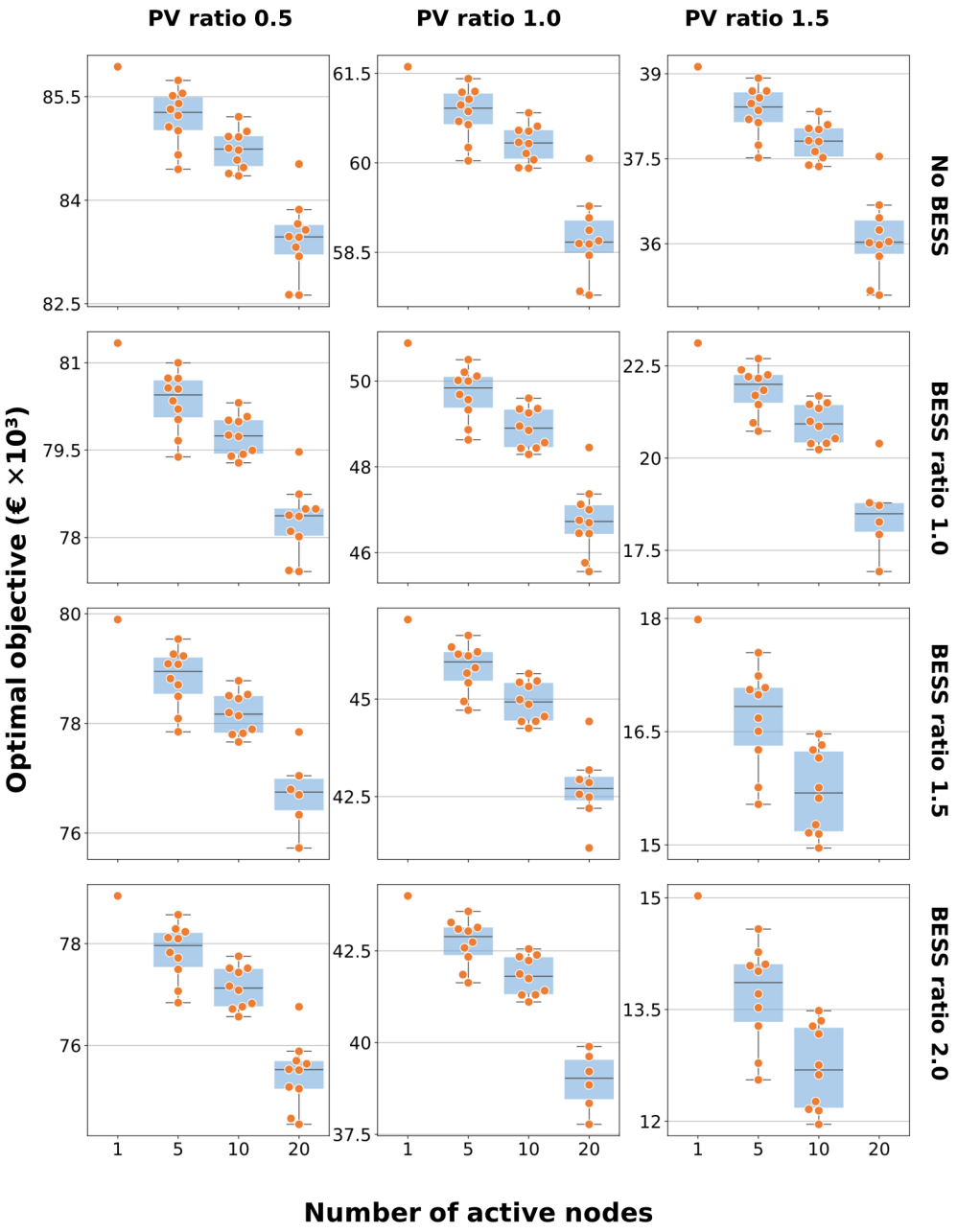

Fig. 3.9 Overview of the optimal objective –i.e., energy costs over a one-year time horizon– across the different scenarios of the detailed test set. Scenarios are identified by combinations of the PV ratio (i.e., total PV size over the reference PV size $S^{\mathrm{PV},0}$) and BESS ratio (i.e., total BESS size over total PV size). For each combination, the total PV and BESS capacity are spread over an increasing number of active nodes. When more than one active node, the results from 10 runs, obtained by varying the power consumption profile, are shown as a boxplot and swarm-plot.

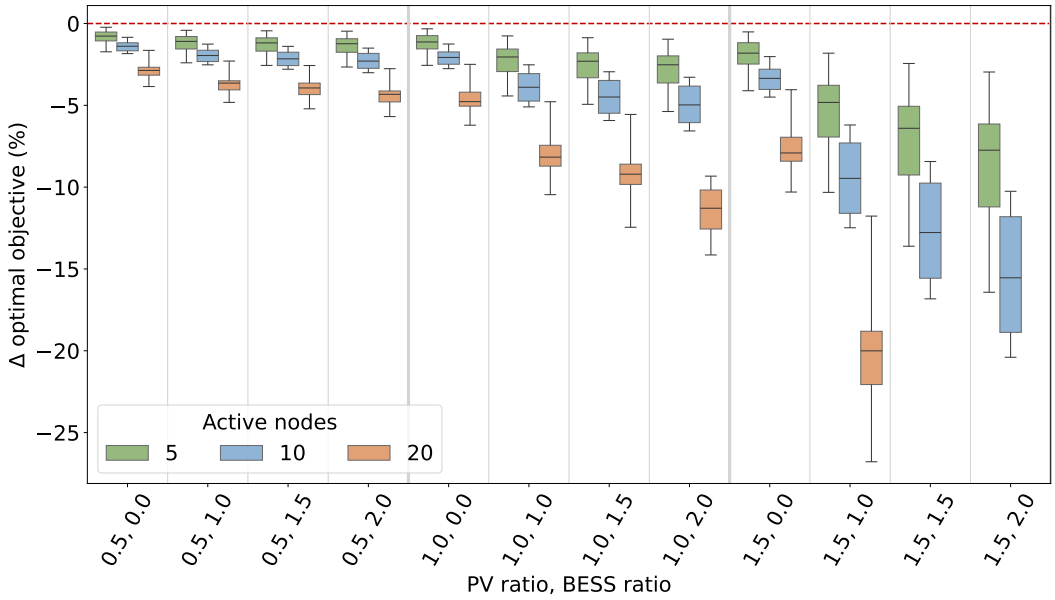

Fig. 3.10 Percentage difference between the optimal objective and its value when only one active node is considered, across the different scenarios of the detailed test set. When more than one active node is considered, the boxplot refers to the 10 optimization runs obtained by varying the power consumption profile.

node, which are imposed by the electricity balances. However, an improvement in the optimal objective is still observed in these configurations. This can be attributed to the fact that, as the number of nodes increases, it becomes possible to distinguish between energy that is self-consumed within individual nodes and energy that is shared between nodes. These two quantities carry different economic values, which explains this variation in energy costs.

Fig. 3.11 expands on this analysis across all scenarios, showing for each number of active nodes the amount of energy shared over the time horizon and the amount of energy self-consumed within nodes. While these two values vary with the number of nodes –shared energy decreases as self-consumption increases– their sum remains constant.

Fig. 3.12, Fig. 3.13, Fig. 3.14, and Fig. 3.15 conclude this analysis by presenting the percentage difference between the single active node case and those with 5, 10, and 20 active nodes for four KPIs: self-consumption and self-sufficiency rates, SC and SS, CO_2 emissions reduction, ER, and cost reduction, CR (see 1.4 for detailed calculations). SC and SS depend directly on the sum of the energy self-consumed within individual nodes and the energy shared among nodes. These indicators

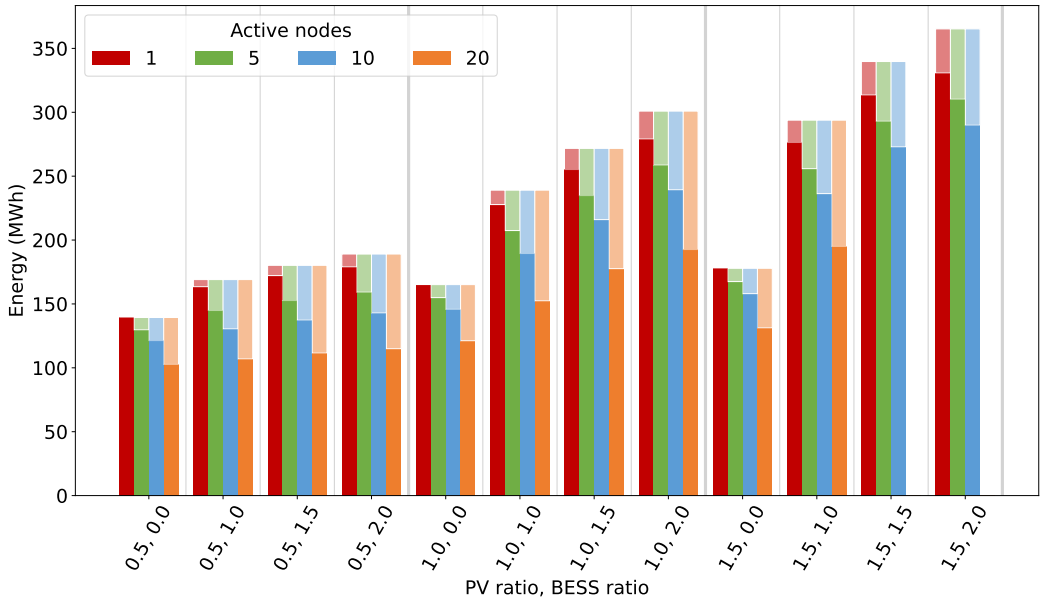

Fig. 3.11 Energy self-consumed within nodes –top bars, lighter shade– and shared between nodes –bottom bar, darker shade– across the different scenarios in the comprehensive test set. When more than one active node, the median value across the 10 optimization runs is shown.

Fig. 3.12 Self-consumption rate (SC) variation with increasing numbers of active nodes, compared to the single active node case. Median values are displayed as a heatmap and shown numerically along with the range of variation in brackets (where applicable).

show minimal to no variation with the number of active nodes in most scenarios, as the sum of self-consumption and shared energy remains stable.

Fig. 3.13 Self-sufficiency rate (SS) variation with increasing numbers of active nodes, compared to the single active node case. Median values are displayed as a heatmap and shown numerically along with the range of variation in brackets (where applicable).

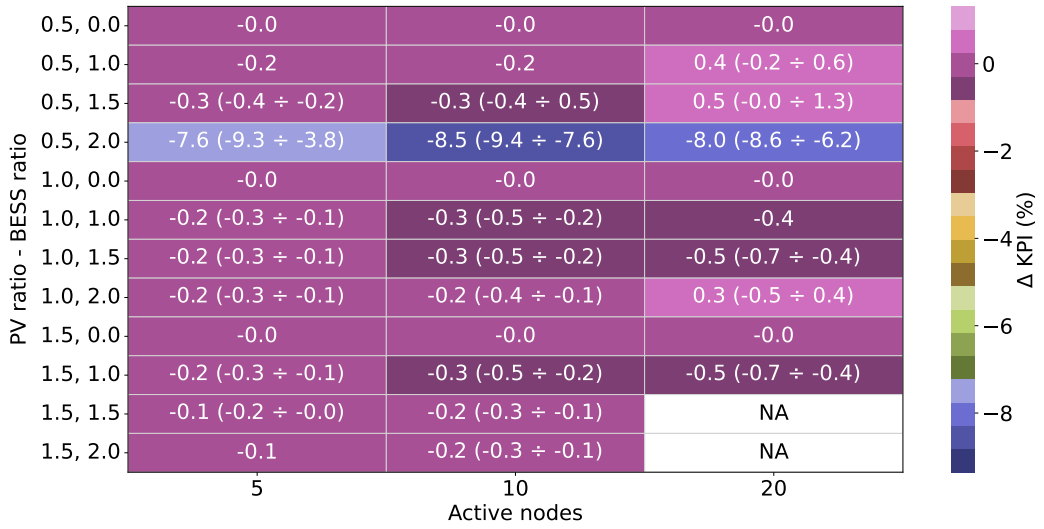

Fig. 3.14 Emissions reduction (ER) variation with increasing numbers of active nodes, compared to the single active node case. Median values are displayed as a heatmap and shown numerically along with the range of variation in brackets (where applicable).

ER also shows little variation, although notable changes appear in cases with small PV and large BESS capacities, likely due to emissions associated with BESS. This aspect requires further investigation. Conversely, the CR displays substantial variations with more active nodes (up to a 300% difference against then case with

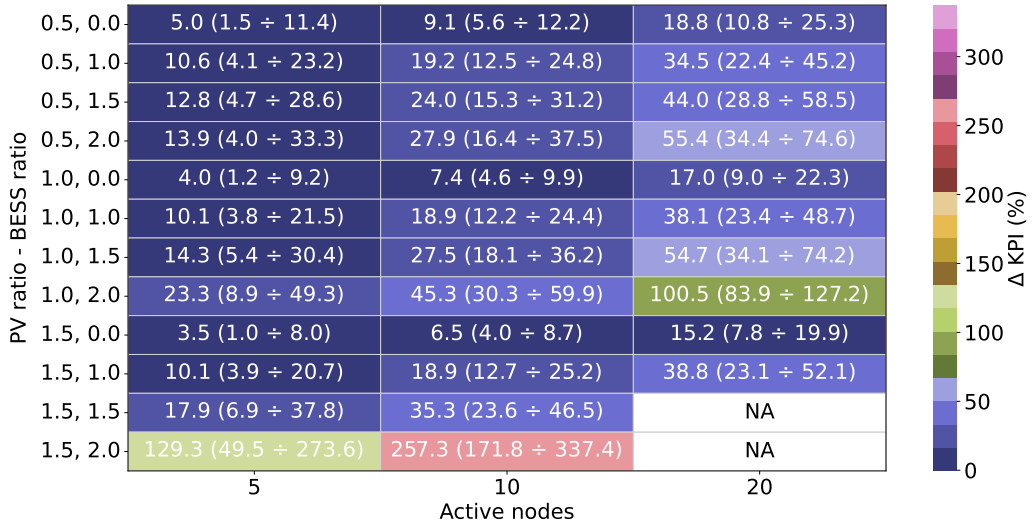

Fig. 3.15 Cost reduction (CR) variation with increasing numbers of active nodes, compared to the single active node case. Median values are displayed as a heatmap and shown numerically along with the range of variation in brackets (where applicable).

one active node), which is attributable to its direct dependence on energy cost reductions achieved through optimized energy sharing and resource use.

Also in this case, the results of the analysis are rearranged to plot the cost reduction (CR) for configurations with multiple active nodes (5, 10, 20) compared to the single-node case, across all scenarios and optimization runs. It is interesting to note that these values are highly correlated, displaying a nearly linear trend.

3.5.4 Computational complexity

Fig. 3.17 shows boxplots of the computation time required by the solver to minimize the objective function across different scenarios, compared against the number of active nodes. The left subplot corresponds to collective optimization, while the right one represents the individual case.

On average, increasing the number of active nodes from one to 20 results in a two-order-of-magnitude increase in solution time. Notably, computation times are already high with just one active node, especially when BESS are included. This is largely attributed to the optimization problem covering a full year, increasing both the size and computational complexity. While configurations with more active nodes remain solvable, they present substantial computational demands

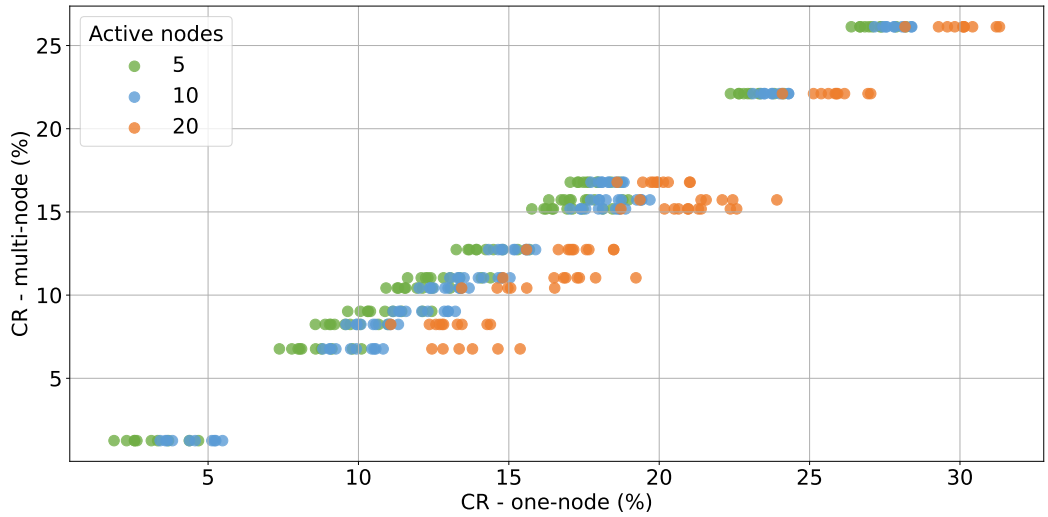

Fig. 3.16 Cost reduction (CR) for configurations with multiple active nodes (5, 10, 20) compared to the single-node case, plotted across all scenarios and optimization runs.

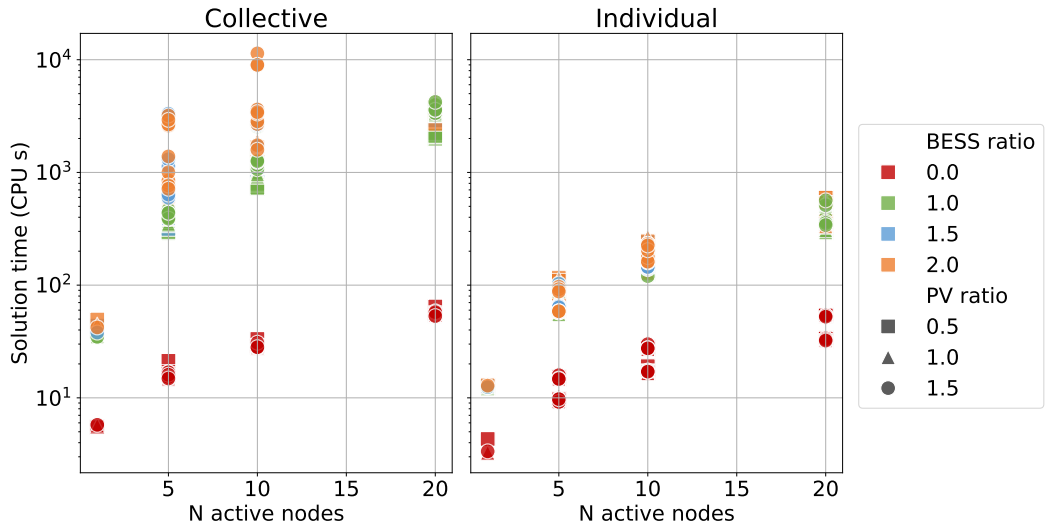

Fig. 3.17 Optimization solution time against number of active nodes, across the different scenarios in the detailed test set, in log scale. Scenarios are distinguished by marker shape (PV ratio) and color (BESS ratio). The left plot shows the value for collective optimization, the right one for the individual case.

that could limit their feasibility for practical applications, such as operational optimization as part of design optimization.

When comparing collective and individual optimizations, the latter generally requires less computation time, except in specific cases –e.g., when there is only one active node or no BESS. In scenarios with multiple nodes and BESS, the

time difference is significant—often by one order of magnitude—suggesting that individual optimization could be a more computationally efficient alternative, despite potential trade-offs in objective performance.

3.6 Discussion

The results presented in this chapter highlight the significant impact of modeling choices on the optimal energy management of ICES, emphasizing the need for tailored models that reflect the unique characteristics of these systems.

Energy storage plays a crucial role in ICES performance, due to the inherent mismatch between renewable generation and energy consumption. While this chapter focuses on storage's impact on operational optimization, its role in ICES design is explored further in Chapter 5. The key modeling decision here is the inclusion of virtual energy sharing, which enables "collectively" managed storage. Dividing storage into renewable and non-renewable subsystems improves performance evaluation by aligning more closely with regulatory constraints and providing more accurate energy cost estimates. However, this approach limits storage's use for energy sharing, reducing energy and environmental KPIs.

When multiple active nodes are present, collective optimization consistently outperforms individual node optimization, where nodes are considered independently and shared energy is calculated *a posteriori*. However, the collective approach is computationally demanding, especially for larger systems, limiting its feasibility.

As the number of active nodes increases, ICES performance improves in terms of energy costs, though this is not due to greater energy efficiency. The benefit arises from distinguishing between physical and virtual self-consumption, each having distinct economic values. Yet, this advantage comes at the cost of increased computational complexity, which grows with the number of nodes and presents challenges for scaling up.

In both collective vs. individual optimization and single vs. multi-node modeling, a strong correlation in results suggests that data-driven approximations could replicate collective and multi-node optimizations with reduced complexity, addressing scalability issues.

Overall, the results of this analysis highlight that MILP provides a robust framework for ICES optimization, but detailed modeling is crucial for accurately esti-

mating KPIs, particularly economic metrics. However, this comes at the cost of high computational demands, limiting its scalability for large or long-horizon problems. Future work should explore machine-learning-based approaches to approximate ICES KPIs and reduce computational costs.

Chapter 4

Data-driven prediction of typical hourly load profiles

Summary

This chapter addresses the challenge of predicting hourly electricity consumption profiles for end users whose measurements are unavailable (unobserved), using limited input data such as aggregated monthly energy bills. Accurate load and generation profiles are a crucial input for the operational optimization of ICES, as introduced in Chapter 3, and are critical for sizing renewable energy systems (RES), storage, and energy conversion technologies.

While historical data for energy prices is widely available, accurate measurements of renewable generation and loads are often scarce. In such cases, physical or data-driven models can provide a valuable alternative. Existing and consolidated methodologies exist for estimating renewable generation (see Section 2.2), while obtaining data for a large number of consumers with different energy uses remains a challenge, especially when limited inputs are available.

To address this, this chapter proposes a data-driven approach using time-of-use (ToU) energy bills to predict load profiles, leveraging a k-nearest neighbors (k-NN) regression model. This method is scalable and applicable across different end-user categories, offering significant improvements to ICES design and operational performance.

Key objectives

- Developing a data-driven methodology for predicting hourly electricity load profiles from ToU energy bills, addressing the needs of unobserved end users.
- Comparing the performance of the proposed k-NN regression approach against established benchmarks, including standard load profiles (SLPs) and other data-driven methods.
- Evaluating the applicability of the predicted load profiles for ICES assessment and design, particularly in scenarios with diverse end-user categories.

The chapter is organized as follows. Section 4.1 reviews the state of the art in load profile modeling and prediction, focusing on data-driven approaches, and highlighting the need for scalable methods using limited data. Section 4.2 introduces the mathematical definitions and notation, while Section 4.3 formalizes the direct and inverse mappings between energy bills and load profiles. The proposed k-NN regression approach is detailed in Section 4.4, alongside two benchmark methods. The dataset of consumption data obtained from Chapter 2 and used for testing is described in Section 4.5. Results are presented in Section 4.6, including a comparison of prediction accuracy and an application-specific assessment for ICES optimization. Finally, Section 4.7 reflects on the findings and potential improvements for the proposed methodology.

Key insights

- The proposed k-NN regression method consistently outperforms benchmarks in predicting load profiles, particularly for non-residential end users.
- Prediction errors are higher when comparing instantaneous time-step values but significantly lower for aggregated statistics such as duration curves.
- Despite individual-level prediction errors, the proposed method achieves high accuracy in ICES assessment and design tasks.
- The reliance on widely available ToU energy bills makes the proposed approach scalable and practical for managing large and heterogeneous end-user portfolios, beyond ICES applications.

4.1 Literature review and contribution

This chapter contributes to the energy use modeling domain [68], focusing on fine-resolution electricity consumption data for heterogeneous end users including residential, commercial, and public offices. These data are particularly relevant in contexts such as RECs, where accurate load profiles are critical for energy management but often unavailable due to the lack of granular SM data.

Historically, SLPs derived from measurement campaigns have been widely employed by energy companies to model consumption. For instance, the H0 SLP is commonly used for residential customers in Germany and Austrias [69], while non-residential customers are given SLPs based on energy use intensity or activity types [70, 71]. In Italy, the GSE applies SLPs to end users in RECs when SM data are unavailable [72]. Despite their widespread use by industry and regulatory bodies, SLPs are increasingly criticized for relying on outdated data and failing to account for evolving consumption patterns or intra-category variations [69, 70].

To address these limitations, researchers have proposed models to generate synthetic load profiles, typically categorized as bottom-up or top-down approaches [73]. Bottom-up models can produce accurate load profiles but require extensive input data [69], while top-down models utilize larger-scale data and are typically better suited for modeling aggregated energy consumption [69, 73].

The recent proliferation of advanced metering infrastructure, including SMs, allowed the development of data-driven models [74–76]. These models utilize machine learning and data mining techniques to extract insights from hourly or sub-hourly consumption time series [77]. While applications of data-driven models range from fault detection to load forecasting, this chapter focuses on their use in load management [78], which encompasses energy benchmarking and customer segmentation.

Clustering methods are widely used for customer segmentation and have been applied to identify energy-saving opportunities [79–81] and enable demand response programs [82–84]. Studies consistently show that data-driven clustering approaches outperform traditional classification methods based on typologies or energy use intensity [85, 70, 86, 87].

Clustering techniques typically rely on unsupervised learning [88] to group users with similar consumption patterns, associating each cluster with a representative load profile. Comprehensive review studies in this field focus on clustering methodologies [74], their applications to customer classification [89],

and evaluation metrics [71]. Few studies include a post-clustering phase, which applies supervised learning [88] to classify or predict the load profiles of new or unobserved customers.

This post-clustering phase can serve dual objectives: inferring end-user characteristics from their load profiles or predicting the load profile class of unobserved users based on known attributes. The latter, which is the focus of this study, has received limited attention in prior literature [82, 84].

Existing works in this area often rely on specific end-user attributes to classify new or unobserved customers. For instance, survey data –such as demographics– were used for households in [83], alongside limited SM data (up to 10 weeks). Non-residential consumers were classified in [82] using internal company data, municipal open data, and others. Piscitelli et al. [84] adopted a simpler approach, relying on easily obtainable data like monthly energy consumption and business hours to classify commercial and industrial end users. Differently from this clustering-classification approach, Granell et al. [90] used regression, predicting hourly load profiles of supermarkets based on attributes like floor area.

However, these approaches often target specific customer categories and require significant data collection, limiting their scalability across diverse end users. As the number and diversity of end users increases, these methods become cumbersome and inefficient, stressing the need for approaches that balance accuracy and practicality.

4.1.1 Contributions

This chapter introduces a streamlined methodology to overcome these challenges, focusing on scalable load modeling using only ToU energy bills. The contributions of this chapter are threefold:

Utilization of ToU energy bills only Unlike the other state-of-the-art methods, the proposed approach relies solely on ToU energy bills, which are widely available and easily obtainable. While Piscitelli et al. [84] have also considered energy bills, their analyses depended on additional data specific to certain customer types and focused primarily on weekdays. This chapter expands the scope to account for a broader range of day types, including weekends and holidays.

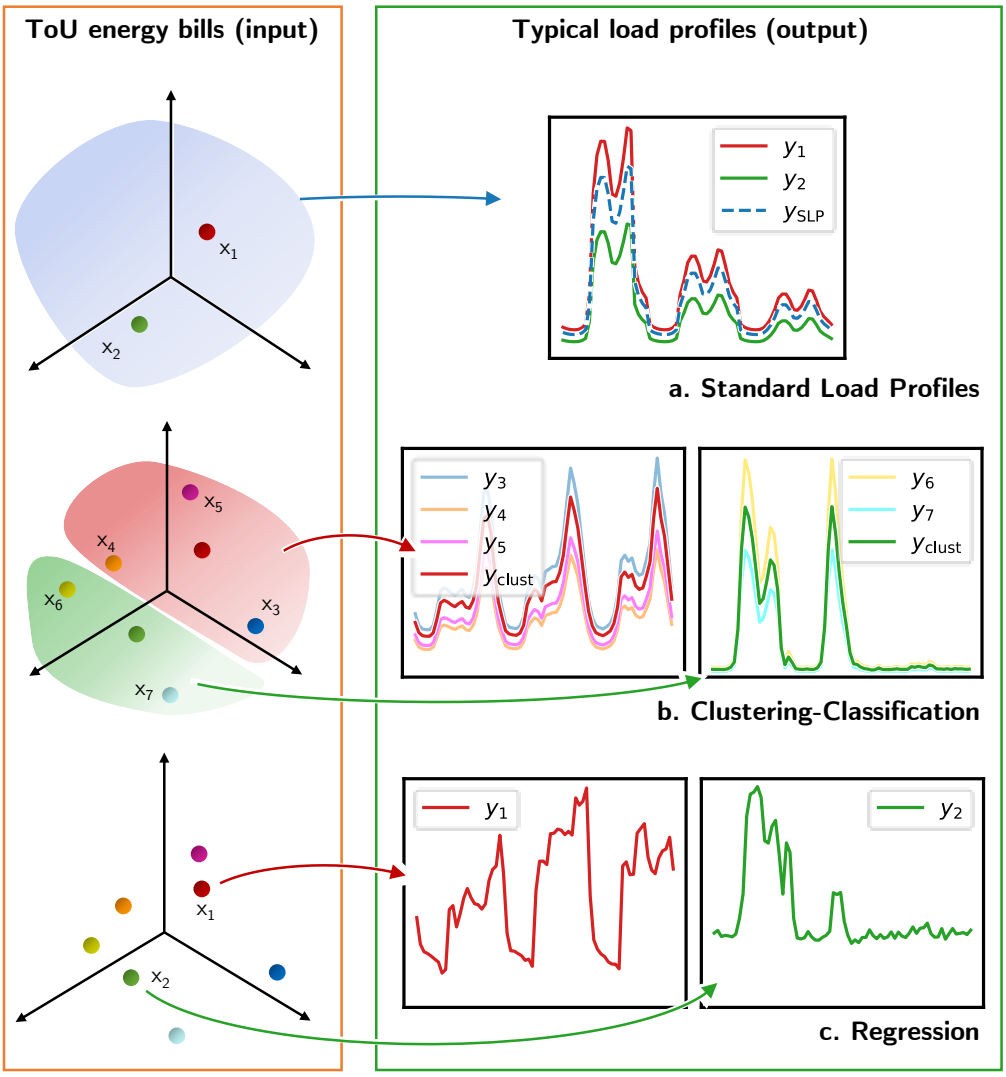

Fig. 4.1 Qualitative representation of three approaches for mapping energy bills (points in the x-space) to their corresponding typical load profiles (lines in the y-space). Detailed definitions of these quantities are found in Section 4.2. (a) SLP-based mapping –on top– assigns all energy bills within a category with the same load profile, with only the total consumption ("magnitude") scaled to match the energy bill. (b) Clustering-classification mapping –in the center– divides the x-space into clusters, assigning each energy bill to a representative load profile corresponding to the cluster center. (c) Regression-based mapping –at the bottom– treats each energy bill individually, providing a continuous relationship between the energy bill values and the load profiles using k-NN. (Adapted from [13]).

Regression-based prediction The methodology adopts a regression-based framework for predicting hourly load profiles directly from ToU energy bills. Unlike SLPs, which assign uniform profiles scaled to match energy bills [72], or clustering-classification methods, which map bills to discrete representative profiles, the proposed approach employs k-Nearest Neighbors (k-NN) regression. This enables a continuous mapping between bills and profiles, capturing subtle variations among users while maintaining scalability (see Fig. 4.1).

Evaluation across diverse end-user categories The proposed approach is evaluated across diverse end-user categories –including residential, commercial, and public office users–, to demonstrate its versatility and scalability. Additionally, the methodology's performance is benchmarked against two established alternatives: a standard SLP-based method and a clustering-classification approach from the literature.

4.2 Definitions and notation

This section introduces the mathematical notation used throughout the chapter, which relies on various sets and their associated indices, summarized in Tab. 4.1. Sets are represented by uppercase letters –e.g., X–, with their indices shown in lowercase –e.g., x. The cardinality of a set, representing the number of its elements, is denoted as |X| or N_x. For clarity and brevity, this section defines key terms and symbols that will be used extensively in the chapter. As all considerations are performed individually for each month, the subscript m is omitted to simplify the notation.
The quantities introduced in the following are based on the ToU tariff scheme implemented in the Italian regulation [91] shown in Fig. 4.2. In particular, three

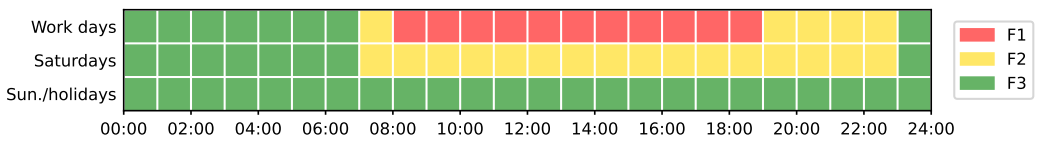

Fig. 4.2 ToU tariffs structure adopted in Italy. The central hours of work days are on-peak (tariff F1, in red); early morning and evening of work days (Monday-Friday) and day hours of Saturdays are mid-peak (tariff F2, in yellow); night, Sundays, and major holidays are off-peak hours (tariff F3, in green).

Table 4.1 Sets and indices used in the notation.

Name	Index	Description	Cardinality	Elements
H	h	Time steps in a day	24	1, 2, ..., 24
D	d	Day types	3	Work day, Saturday, Holiday
M	m	Months	12	January, ..., December
$L_{d,m}$	l	Days of day type d in month m	$nd_{d,m}$	-[8]
G	g	Time indices of the typical load profile	72	Work day-1, ..., Holiday-24[9]
F	f	Time-of-Use tariffs	3	F1, F2, F3

[8] Depends on the month and day type; [9] G = D × H.

different tariffs are defined for electricity (F1, F2, F3), respectively, for on-peak, mid-peak, and off-peak hours. According to these ToU tariffs, three types of days can be identified, each characterized by a different subdivision of the hours into ToU tariffs: work days, from Monday to Friday; Saturdays; and Sundays/holidays (just 'holidays', in the followings).

Load profile A load profile is defined as a time series representing energy consumption across uniformly spaced time steps, which in this chapter have an hourly resolution. The average uniform power demand, denoted as P, is used, which is derived from the energy consumption in each time step. The load profile is represented as a vector, as follows:

$$\begin{aligned} \mathbf{p} &= \{P_k\}_{k=1,\ldots,N_k}, \\ \text{where } P_k &= \frac{E_k}{\Delta t_k}. \end{aligned} \tag{4.1}$$

Here, E_k is the energy consumed during time step k and Δt_k its duration; N_k is the total number of time steps.

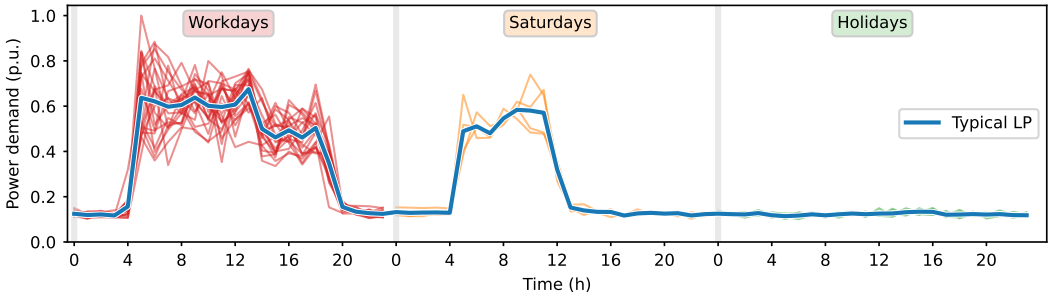

Fig. 4.3 Visual example of the averaging process and creation of a typical load profile in one month. A month-long load profile is first chunked into day-long sequences, which are arranged by day type (in red are the load profiles of all work days, in yellow those of all Saturdays, and in green holidays); then, an average load profile is evaluated for each day type; these profiles are finally put in a sequence to obtain the typical load profile (the blue, continuous line). The data used here originate from a commercial end user, which explains the lower consumption on Saturdays and the base load on Sundays. (Source [13]).

Average load profile An average load profile is a time step-by-time step average with the same length and shared characteristics. In this case, average load profiles are calculated monthly for each day type (work days, Saturdays, holidays). For a given month, the load profile time series can be rearranged into day-long sequences, and sorted by day type. Given the set of day-long load profiles of day type d, L_{d}, the corresponding average load profile $\bar{\mathbf{p}}_{\mathrm{d}}$ is evaluated as:

$$\begin{aligned} \bar{\mathbf{p}}_{\mathrm{d}} &= \{\bar{P}_{\mathrm{d,h}}\}_{\mathrm{h}\in\mathrm{H}}, \\ \text{where } \bar{P}_{\mathrm{d,h}} &= \frac{1}{\mathrm{nd}_{\mathrm{d}}} \sum_{\mathrm{l}\in\mathrm{L}_{\mathrm{d}}} P_{\mathrm{l,h}}. \end{aligned} \tag{4.2}$$

Typical load profile A typical load profile condenses a month's three average load profiles into a single sequence (see Fig. 4.3). The average load profile $\bar{\mathbf{p}}_{\mathrm{d}}$ in each day type d is concatenated to form the typical load profile $\mathbf{y}$, as follows:

$$\mathbf{y} = \{Y_{\mathrm{g}}\}_{\mathrm{g}\in\mathrm{G}} = \{\bar{P}_{\mathrm{d,h}}\}_{\mathrm{h}\in\mathrm{H}}^{\mathrm{d}\in\mathrm{D}}. \tag{4.3}$$

As shown in Tab. 4.1, the typical-load-profile length is 72, since there are 3 day types and 24 time steps for each of them.

Energy bill An energy bill is a vector that records the monthly energy consumption in the three time-of-use (ToU) tariffs F1, F2, F3 (rather than the expenditure):

$$\mathbf{x} = \{E_{\mathrm{f}}\}_{\mathrm{f}\in\mathrm{F}}, \tag{4.4}$$

where E_{f} represents the energy consumption in tariff f.

Spaces of energy bills and typical load profiles Energy bills can be conceptualized as points in a three-dimensional space (one dimension for each ToU tariff), the "x-space". Similarly, typical load profiles exist in a space referred to as the "y-space", where each dimension corresponds to a time step in the profile.

4.3 Direct and inverse mapping

Given a typical load profile **y**, the elements E_{f} of the energy bill vector **x** associated with it are calculated as follows:

$$E_{\mathrm{f}} = \sum_{\mathrm{d}\in\mathrm{D}} \mathrm{nd}_{\mathrm{d}} \left(\sum_{\mathrm{h}\in\mathrm{H}} \bar{P}_{\mathrm{d,h}} \Delta t_{\mathrm{h}} \delta_{\mathrm{f}}(d,h) \right), \forall f \in \mathrm{F}. \tag{4.5}$$

Here, $\delta_{\mathrm{f}}(d,h)$ is a binary auxiliary variable, defined as follows:

$$\delta_{\mathrm{f}}(d,h) = \begin{cases} 1, & \text{if } h \text{ in day type } d \text{ belongs to tariff } f, \\ 0, & \text{otherwise} \end{cases}, \tag{4.6}$$

whose values can be directly obtained from Fig. 4.2.

'Direct mapping' refers to calculating an energy bill from a given typical load profile, as formalized in (4.5). This relationship is deterministic and explicitly defined, relying on the known structure of ToU tariffs and the distribution of time steps across day types. The example provided in Fig. 4.4 illustrates this process qualitatively.

On the other hand, inverse mapping seeks to estimate a typical load profile from a given energy bill. Unlike direct mapping, this relationship is not explicitly defined and must be inferred based on observed patterns in the data. An initial analysis of measured data suggests that end users with similar energy bills in the x-space tend to exhibit structurally similar load profiles in the y-space. This phenomenon is illustrated qualitatively in Fig. 4.5, which shows three pairs of

energy bills selected randomly from six different end users, that are pairwise close in the x-space Their respective typical load profiles reveal similar consumption patterns, including the timing and magnitude of peak demand, base load levels, and general usage trends. However, discrepancies within the same ToU tariff can still occur due to differences in instantaneous consumption or behavioral patterns of individual end users.

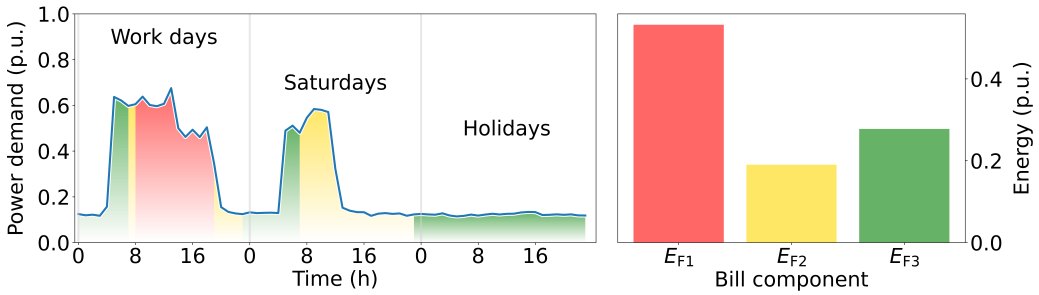

Fig. 4.4 Visual example of the bill calculation from a typical load profile in one month. The blue line shows the typical load profile. The subdivision of the time steps into ToU tariffs is also shown (F1, in red, F2, in yellow, and F3, in green). The colored bars represent the three components of the bill, i.e., the consumption in each ToU tariff. The arrow's width is proportional to the number of days of each day type in the month. (Source [13]).

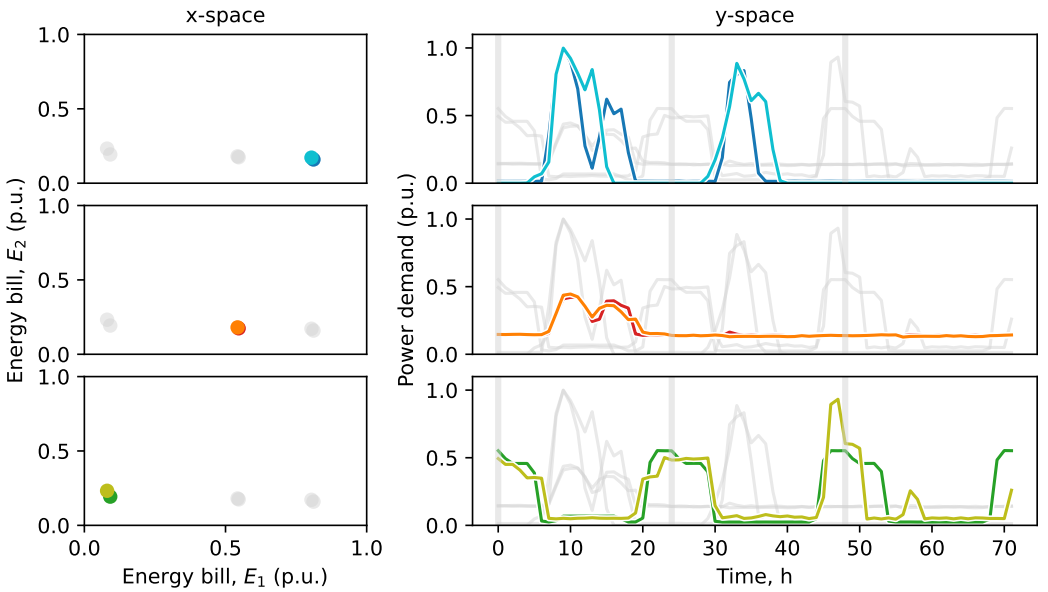

Fig. 4.5 Visual examples of the similarity between monthly ToU energy bills and typical hourly load profiles. In particular, three pairs of points (i.e., energy bills) are shown, which are pair-wise close in the x-space. The respective "lines" in the y-space (i.e., typical load profiles) exhibit similar shapes. (Source [13]).

These observations, while promising, are based on qualitative assessment and intuition, forming the basis for an exploratory analysis. Validating the extent to which this inverse relationship holds across broader datasets is a key objective of this chapter.

4.4 Methods

The following section details the methodology proposed to quantify and model the inverse mapping, enabling the prediction of typical load profiles for unobserved end users. The first part outlines the construction of the training data set, detailing how monthly bill and profile pairs are derived from year-long load data. Next, normalization procedures are presented to ensure comparability across end users with varying consumption magnitudes while preserving the mathematical relationships underlying the analysis. These methods form the foundation for the modeling and evaluation processes discussed in the subsequent sections.

4.4.1 Training data and normalization

The data-driven approach proposed in this chapter requires a collection of paired energy bills ($\mathbf{x}$) and corresponding typical load profiles ($\mathbf{y}$). Aligning with terminology commonly used in machine learning applications, these pairs are referred to as the 'training data set', denoted as {X, Y}. Creating this data set involves extracting paired data from many end users year-long consumption data. For each end user, the procedure involved the following steps:

i. splitting the time series into monthly segments;

ii. applying (4.2), (4.3), and (4.5) for each segment.

This process generates twelve pairs of $\mathbf{x}$ and $\mathbf{y}$ vectors, one per month of the year, for each end user. The complete training data set is then structured such that each row corresponds to a specific month and user combination.

Since {X, Y} incorporates data from multiple end users with varying total energy consumption levels, normalization is used to eliminate the influence of differences in consumption magnitude. For each pair of $\mathbf{x}$ and $\mathbf{y}$ vectors, the energy bill components are normalized so that their sum equals 1. The elements

$\hat{E}_{\mathrm{f}}$ of the normalized energy bill vector $\hat{\mathbf{x}}$ are computed as:

$$\hat{E}_{\mathrm{f}} = \frac{E_{\mathrm{f}}}{\sum_{\mathrm{f}\in\mathrm{F}} E_{\mathrm{f}}}. \tag{4.7}$$

For typical load profiles, normalization methods such as min-max scaling [74], max normalization [87], or z-standardization [85] are commonly employed to ensure that values lie within a standard range or distribution. However, the link between the normalized profile and the corresponding energy bill must be preserved in this chapter. Thus, the normalized load profile elements $\hat{Y}_{\mathrm{g}}$ of $\hat{\mathbf{y}}$ are evaluated as:

$$\hat{Y}_{\mathrm{g}} = \frac{Y_{\mathrm{g}}}{\sum_{\mathrm{f}\in\mathrm{F}} E_{\mathrm{f}}}. \tag{4.8}$$

As a result of this approach, each normalized typical load profile retains a total monthly consumption equal to 1.

The normalized dataset $\{\hat{\mathrm{X}}, \hat{\mathrm{Y}}\}$ is obtained through a "row-wise" normalization is performed, ensuring that all samples can be compared on the same scale. Unlike many machine learning applications, "column-wise" normalization is unnecessary in this context because the individual elements of both the energy bill vector and the load profile vector are inherently comparable.

4.4.2 k-NN based prediction

The proposed approach employs a k-NN algorithm to predict end users' typical load profiles from their monthly energy bills, leveraging the training data set. As a supervised learning method [92], k-NN does not involve a dedicated training phase. Instead, it utilizes the entire training data set during each prediction. The only parameter in this method is the number of neighbors (k) to consider.

Given the normalized training data set set $\{\hat{\mathrm{X}}, \hat{\mathrm{Y}}\}$ and a "test" bill vector $\mathbf{x}^*$, whose corresponding typical load profile $\mathbf{y}^*$ is unknown, the algorithm proceeds as follows:

i. Normalize the test bill vector through (4.7), obtaining $\hat{\mathbf{x}}^*$.

ii. Compute the Euclidean distance between $\hat{\mathbf{x}}^*$ and all $\hat{\mathbf{x}} \in \hat{\mathrm{X}}$.

iii. Identify the k vectors $\hat{\mathbf{x}} \in \hat{\mathrm{X}}$ with the smallest distances from $\hat{\mathbf{x}}^*$ –i.e., the nearest neighbors. The sets of $\hat{\mathbf{x}}$ and $\hat{\mathbf{y}}$ vectors of these neighbors, whose cardinality is k, are denoted as $\mathrm{K_x}$ and $\mathrm{K_y}$, respectively.

iv. Compute the prediction $\hat{\mathbf{y}}_{\text{pred}}$ as the element-wise weighted average of the vectors $\hat{\mathbf{y}} \in \mathrm{K_y}$:

$$\hat{\mathbf{y}}_{\text{pred}} = \frac{1}{k} \sum_{\hat{\mathbf{y}} \in \mathrm{K_y}} \hat{\mathbf{y}}. \tag{4.9}$$

v. De-normalize $\hat{\mathbf{y}}_{\text{pred}}$ by inverting (4.8), to restore the actual magnitude of the typical load profile $\mathbf{y}_{\text{pred}}$.

vi. Assign the predicted vector $\mathbf{y}_{\text{pred}}$ to $\mathbf{y}^*$ as the estimated typical load profile.

This implementation assumes uniform weights for the neighbors. However, alternative weighting schemes can be adopted, such as assigning weights inversely proportional to the distance between $\hat{\mathbf{x}}^*$ and each neighbor [93].

Fig. 4.6 illustrates the k-NN prediction process in the x- and y-spaces. It is worth noting that despite the proximity of neighbors in the x-space, the "predicted" energy bill derived from applying (4.5) to $\mathbf{y}^*$ may not exactly match the original energy bill $\mathbf{x}^*$ across different ToU tariffs, as shown in the figure.

4.4.3 Benchmark approaches

This section presents an overview of the benchmark methods employed to validate the k-NN approach.

Standard Load Profiles This method relies on predefined profiles representing typical consumption patterns for different categories of end users. Specifically, the SLPs outlined by the GSE in [72] are used, distinguishing between domestic (DOM) and non-domestic (BTA) end users (see Fig. 4.7). For an end user with a given monthly energy bill $\mathbf{x}^*$, the corresponding typical load profile $\mathbf{y}^*$ is simply derived through the following steps:

i. A standard load profile $\mathbf{y}_{\text{ref}}$ is selected based on the end user's category;

ii. The selected SLP is scaled to ensure that its total consumption matches the reported value in the energy bill.

Clustering-classification This approach, detailed in works like[83, 82] and specifically [84], follows a clustering-classification framework adapted to predict typical

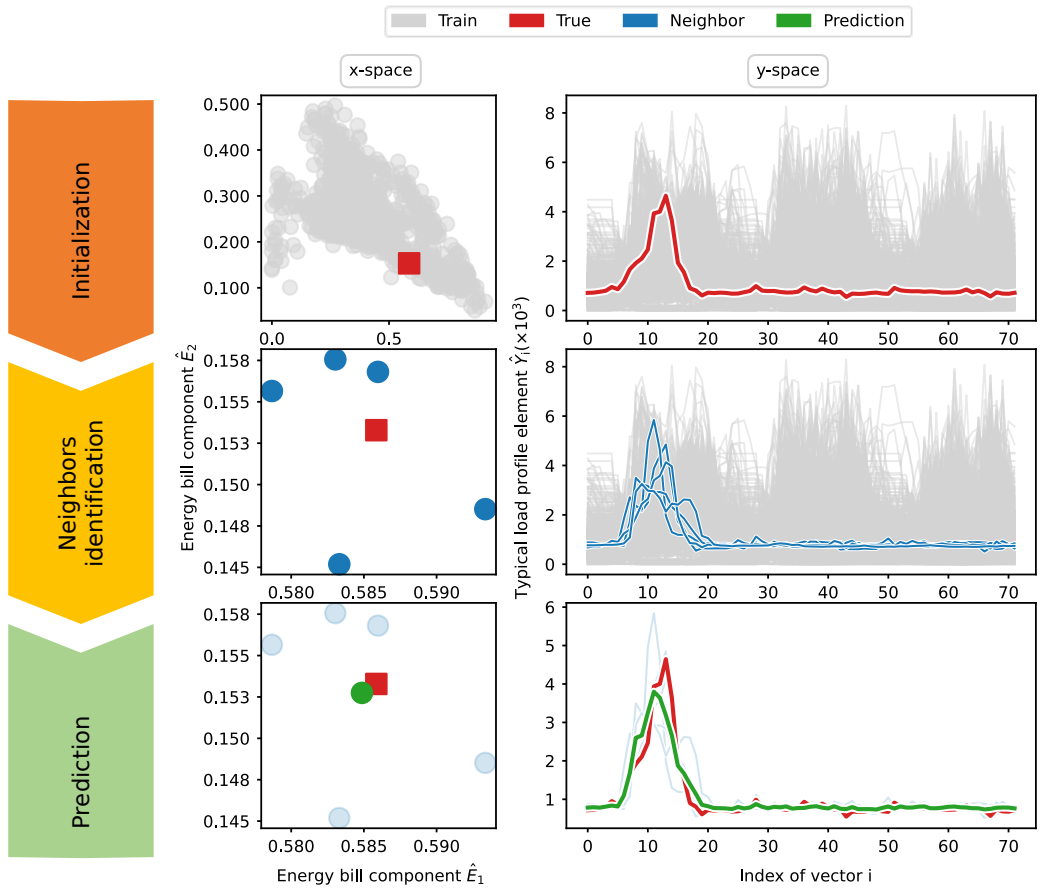

Fig. 4.6 Graphical outline of the k-NN prediction process in the x- and y-spaces. For simplicity, only two components of the bill are shown, enabling a two-dimensional representation of the x-space. The training set consists of ($\hat{\mathbf{x}}$, $\hat{\mathbf{y}}$) pairs. A test pair $\hat{\mathbf{x}}^*$ and $\hat{\mathbf{y}}^*$ is also shown (with $\hat{\mathbf{y}}^*$ typically unknown). To predict $\hat{\mathbf{y}}_{\text{pred}}$ from $\hat{\mathbf{x}}^*$, the k nearest neighbors are identified in the x-space, and $\hat{\mathbf{y}}_{\text{pred}}$ is computed as the weighted average of their corresponding values in the y-space. (Source [13]).

load profiles based on energy bills. A summary of the key steps and algorithms used is provided here.

First, representative load profiles are extracted from the training data set through clustering of the $\hat{\mathbf{y}} \in \hat{\mathrm{Y}}$ vectors. K-means, an unsupervised learning algorithm, is utilized for clustering due to its effectiveness in grouping similar load profiles [80]. The only parameter for the algorithm is the number of clusters. Once the clustering is complete, the training set $\{\hat{\mathrm{X}}, \hat{\mathrm{Y}}\}$ is partitioned into classes, each associated with a representative load profile corresponding the cluster center. Next, a classifier system is trained, using the energy bill vectors $\hat{\mathbf{x}}$ as input features and the cluster labels as target values. As in [84], a Decision Tree classifier is

employed for this supervised learning task. The output of the training phase is a set of decision rules, which can be applied to classify new energy bills into the appropriate clusters. To predict a typical load profile $\hat{\mathbf{y}}^*$ for a new end user with an energy bill $\hat{\mathbf{x}}^*$, the first step is to assign a cluster label based on the decision rules. Then, the typical load profile corresponding to the cluster center is selected, and the magnitude effect is added by inverting (4.8) to match the total consumption with the actual energy bill.

In both benchmark methods, similar to the proposed k-NN approach, the total consumption of the predicted load profile aligns with the energy bill, while the distribution of consumption across the Time-of-Use (ToU) tariff components may not exactly match. This discrepancy arises because the shape of the predicted load profile, determined by the SLP or cluster centers, influences the allocation of energy across the ToU periods.

4.4.4 Validation

The validation of the proposed methods is carried out using a test set of actual hourly consumption data. The process begins by predicting the typical load profiles using the methods described above, followed by a comparison with the real measured profiles.

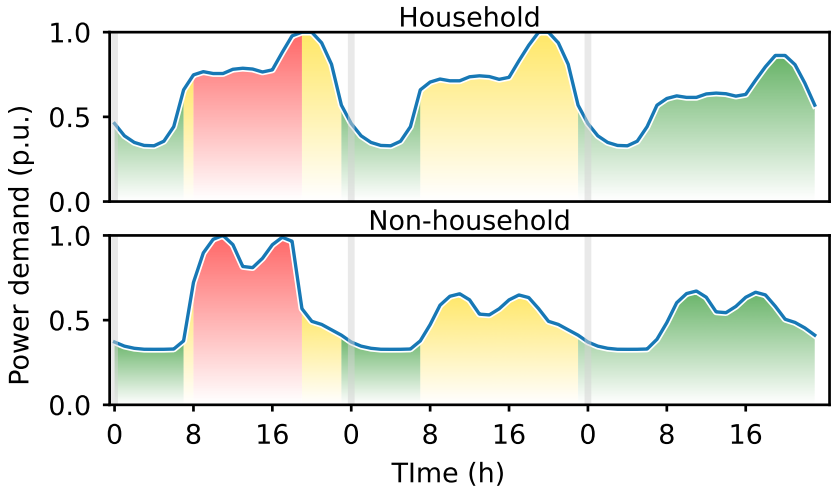

Fig. 4.7 Typical load profiles evaluated from the SLPs adopted by the GSE for household and non-household end users. The subdivision of the time steps into ToU tariffs is also shown (in red, F1, yellow, F2, green, F3). (Source [13], elaboration of data from [72]).

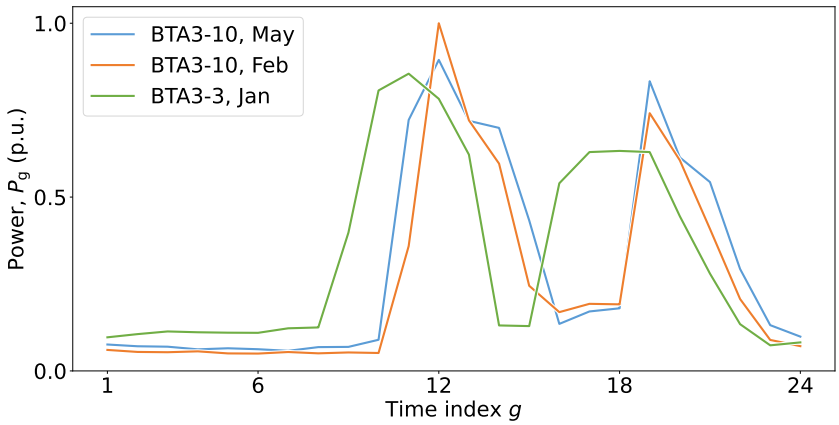

Fig. 4.8 Qualitative representation of the concepts of sameness and similarity. The two profiles in orange and blue originate from the same end user (BTA 3 10) and are the average load profiles for work days in two different months. These profiles are only slightly different, and a measure of sameness would yield a high value. In contrast, the profile in green is from a different end user. A measure of sameness, such as the time step-by-time step difference, would provide a smaller value. However, the profiles exhibit many similar characteristics.

Kohler et al. [73] conducted a comprehensive review of evaluation metrics commonly used to compare predicted or synthetic load profiles with actual ones. In particular, they focus on the distinction between "sameness" and "similarity."

Sameness The concept of sameness refers to the direct equivalence between corresponding time steps of two time series. Commonly used metrics for sameness include the mean squared error (MSE) and the mean absolute error (MAE) [73].

Similarity The concept of similarity is broader, looser, and more challenging to assess. Kohler et al. [73] suggest metrics that examine statistical properties –e.g., minimum, median, and maximum values, standard deviation, and errors in the duration curve–, and others that assess profile complexity, such as the number of peaks and fractal dimension.

Fig. 4.8 provides a qualitative representation of these two concepts, considering three load profiles from two different end users. The two profiles from the same end user are almost identical. Conversely, the profile from the other end user does not coincide with the other two, as the consumption in each time step does not perfectly match. However, the profiles are similar, exhibiting two peaks and a valley in the central hours.

The sameness between predicted and actual load profiles is assessed through a Normalized Cumulative Absolute Error (NCAE). This metric quantifies the deviation between predicted and actual profiles by performing a time step-by-time step comparison for each sample –i.e., the profile of an end user in a month. The errors at each time step are summed and normalized by the total consumption, allowing the comparison of the errors for different end users. To account for the varying contributions of different day types in each month, the NCAE of the typical load profiles is weighted accordingly. The calculation is as follows:

$$\mathrm{NCAE_y} = \frac{\sum_{\mathrm{d}\in\mathrm{D}} \left(\sum_{\mathrm{h}\in\mathrm{H}} \left| \bar{P}^{\mathrm{pred}}_{\mathrm{d,h}} - \bar{P}_{\mathrm{d,h}} \right| \right) \mathrm{nd_d}}{\sum_{\mathrm{f}\in\mathrm{F}} E_{\mathrm{f}}}. \tag{4.10}$$

This metric evaluates how accurately the predicted profiles allocate consumption across the time steps.

On the other hand, similarity is assessed by comparing the duration curve (DC) obtained from the typical load profiles. An equivalent month-long profile is generated by assigning an average load profile to each day, corresponding to its specific day type. Next, the power values across all time steps are sorted to create a duration curve. Finally, the NCAE is computed between the sorted vectors and normalized using the total consumption. This error is denoted as $NCAE_{\mathrm{DC}}$.

All methods predict the load profiles so that the total energy consumption for the month approximates the actual value. However, the consumption across different ToU tariffs is not guaranteed to match the actual values exactly. Consequently, the NCAE between the real and predicted energy bills is also calculated, as follows:

$$\mathrm{NCAE_x} = \frac{\sum_{\mathrm{f}\in\mathrm{F}} \left| \bar{E}^{\mathrm{pred}}_{\mathrm{f}} - \bar{E}_{\mathrm{f}} \right|}{\sum_{\mathrm{f}\in\mathrm{F}} E_{\mathrm{f}}}. \tag{4.11}$$

This metric evaluates how accurately the predicted profiles allocate consumption to the various ToU tariffs, indicating how much of the total monthly consumption is misallocated between ToU tariffs.

4.5 Case study

The proposed and benchmark approaches were tested on the dataset introduced in Section 2.1. This dataset consists of hourly electricity consumption measurements provided by a local multi-utility for 114 end users, spanning April 2021 to

March 2022. Initially, 11 end users were removed due to their significantly higher yearly energy consumption. Additionally, two end users were excluded because their total consumption was equal to 0 during at least one month, which would have compromised the normalization procedure.

The users are classified as either household (DOM) or non-domestic (BTA) and further categorized by their contractual power levels and specific end-user categories (see Tab. 2.1 and Fig. 2.1). As noted in Section 2.1, the DOM1 class was merged with DOM2 to form the DOM1-2 category due to the limited number of users in the former class.

The year-long load profile of each end user in the original dataset was processed as described in Section 4.4.1 to obtain two sets of monthly energy bills and corresponding typical load profiles for each end user.

Fig. 4.9 illustrates the statistics of typical load profiles in absolute values, divided by user class. Additionally, the distributions of the three components of the energy bills across user classes are shown in Fig. 4.11. To address the bias introduced by differences in magnitude, normalized versions of the typical load profiles and energy bills are shown in Fig. 4.10 and Fig. 4.12, respectively.

Regarding typical load profiles, some classes exhibit well-defined intra-cluster characteristics. For example, BTA1, BTA3, BTA4, and households demonstrate narrow interquartile ranges (IQRs) closely aligned with their respective medians. However, other classes, such as BTA2, show significantly wider IQRs, indicating greater variability within the class. Even in cases with a narrow IQR, extreme values (minimum and maximum) may deviate substantially from the median and display varying shapes, as observed in BTA1 and BTA4.

Similarly, some user groups, such as households, exhibit relatively narrow distributions of energy bill components. Conversely, other classes demonstrate considerable dispersion, highlighting the presence of end users with diverse consumption behaviors and energy bill compositions within the same class.

For testing and training the data-driven approaches, a variation of the leave-one-out and k-fold cross-validation (CV) procedure was applied [94]. This approach is denoted as “leave-one-group-out” CV. In this setup, the samples from a single end user served as the test set, while the remaining users constituted the training set, resulting in 101 folds.

All algorithms were implemented in Python using the open-source library `sklearn` [95, 96]. For the clustering-classification approach, the number of clus-

ters was set to 11, while for the proposed k-NN approach, the number of neighbors was set to 9. These parameters were selected to minimize the average error on the predicted load profiles. Default settings from `sklearn` were utilized for training the Decision Tree classifier.

4.6 Results

This section presents the validation results for the proposed and benchmark approaches. In addition to the error metrics detailed in Section 4.4.4, an application-specific assessment is performed. Here, the methods are applied to ICES evaluation and optimization, and their performance is compared against real data.

4.6.1 Error metrics

Fig. 4.14 shows the distributions of the error, $NCAE_x$, between the actual and predicted ToU consumption components for the three tested methods. Half of

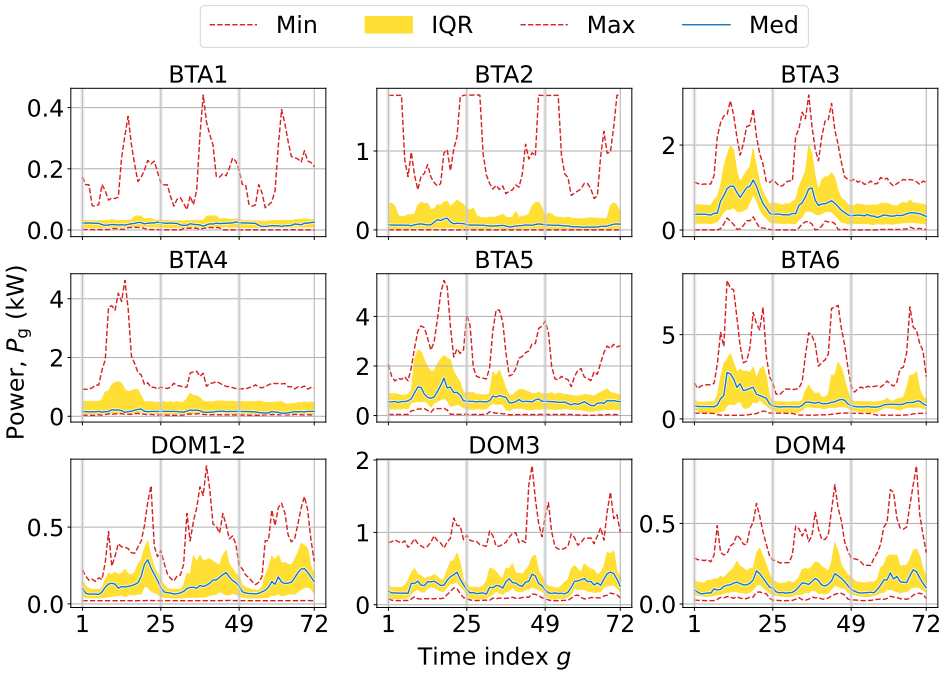

Fig. 4.9 Statistics of the typical load profiles evaluated for the end users divided by class: minimum (i.e., 5th percentile), median and maximum(i.e., 95th percentile), and interquartile range, IQR, (25th-75th percentile) of the consumption in each time step.

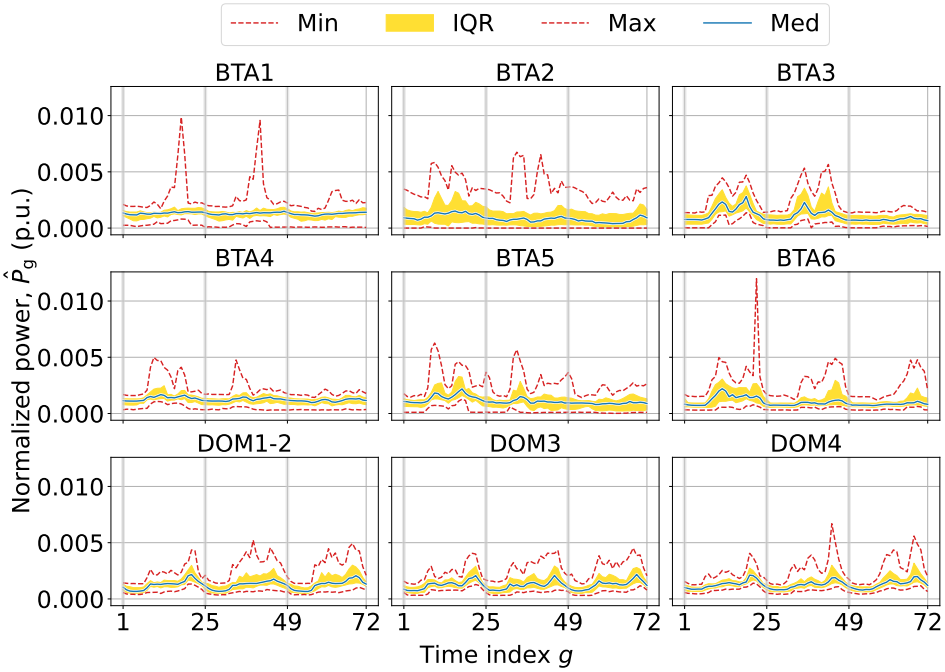

Fig. 4.10 Statistics of the normalized typical load profiles evaluated for the end users divided by class: minimum (i.e., 5th percentile), median and maximum(i.e., 95th percentile), and interquartile range, IQR, (25th-75th percentile) of the consumption in each time step.

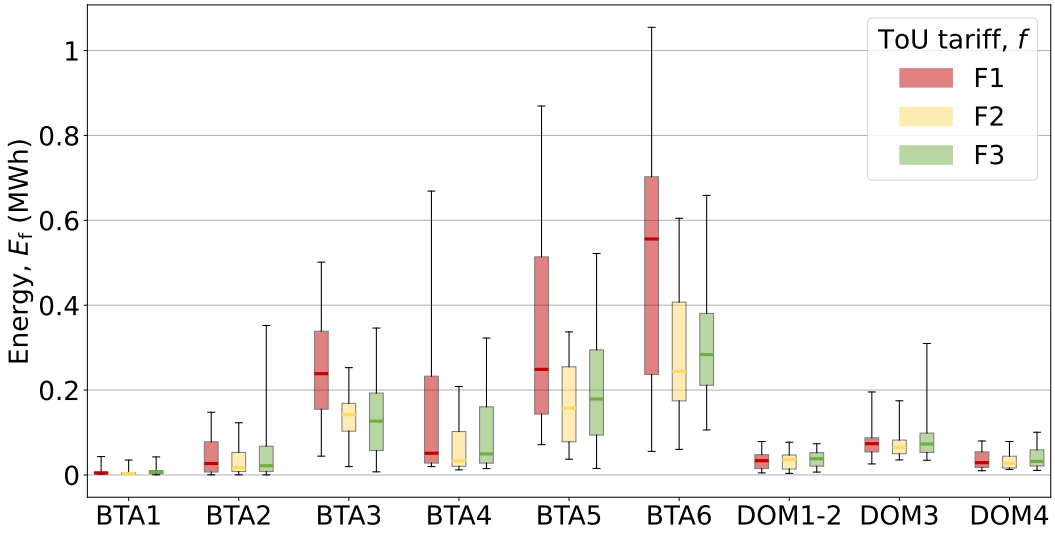

Fig. 4.11 Statistics of the normalized monthly energy bills evaluated for the end users divided by ToU tariff and class. The whiskers are truncated at the 5th and 95th percentile.

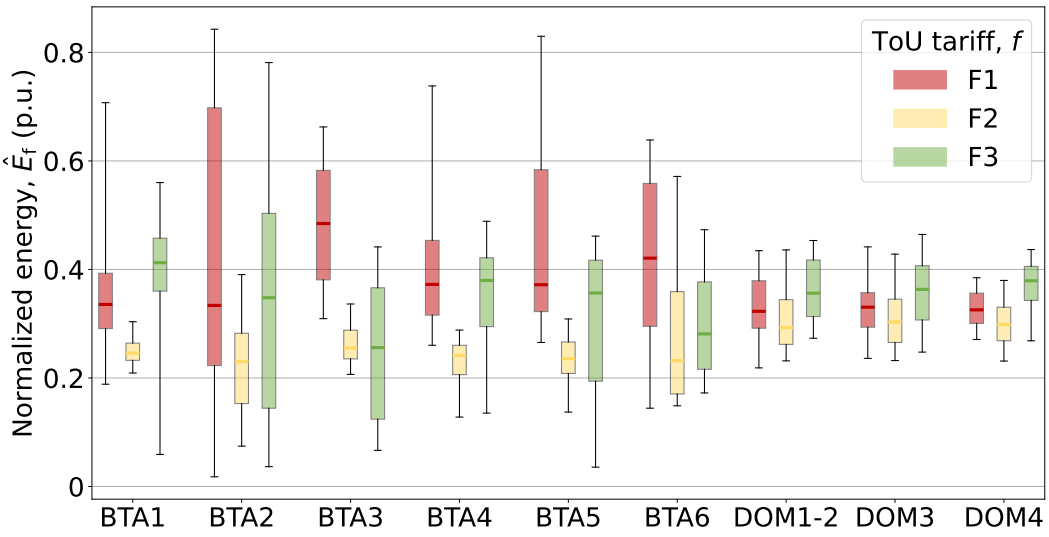

Fig. 4.12 Statistics of the normalized monthly energy bills evaluated for the end users divided by ToU tariff and class. The whiskers are truncated at the 5th and 95th percentile.

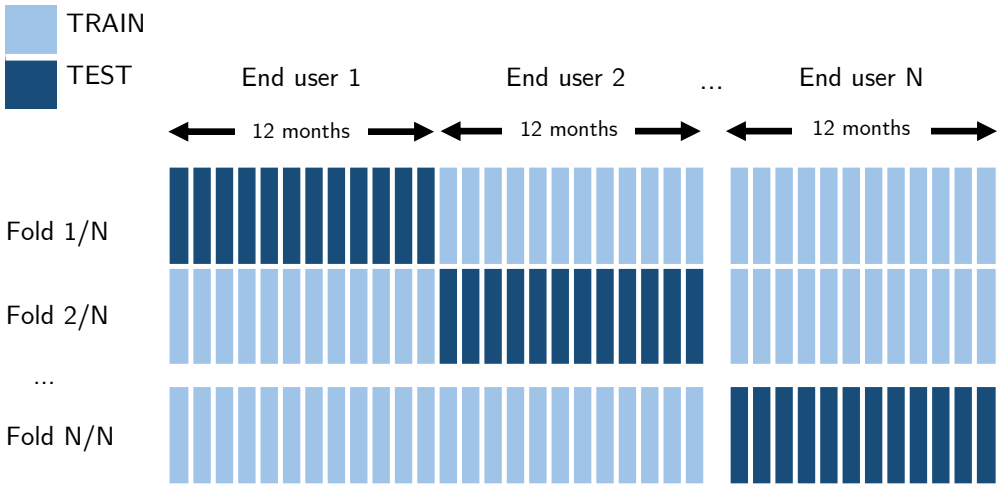

Fig. 4.13 Illustration of the leave-one-group-out cross-validation process adopted. Each fold isolates one user's data for testing, while the remaining data is used for training.

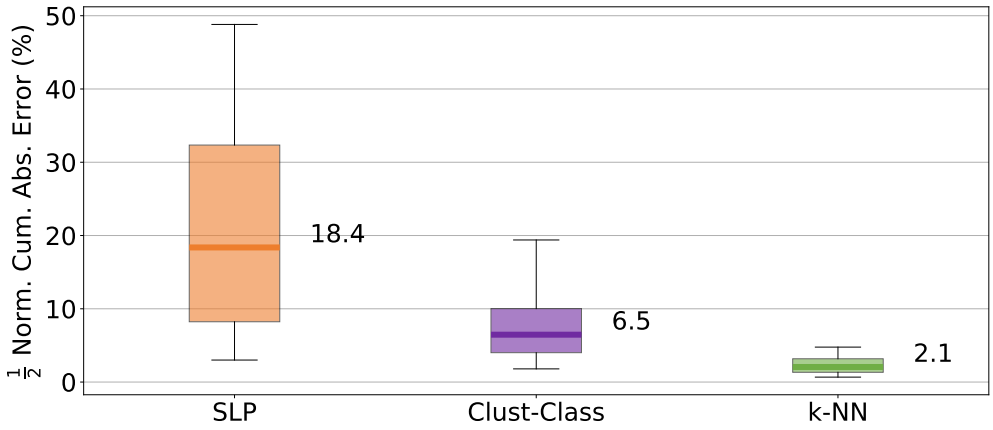

Fig. 4.14 Distribution of the normalized cumulative absolute error on the components of the energy bills, $NCAE_x$, between the actual data and the predictions from the different methods, for all samples. The median error across all samples is also shown.

the total error is reported, as this directly quantifies the proportion of energy misallocated to the incorrect tariff (or time step, in the case of load profiles). In fact, the error ranges from 0% (indicating a perfect prediction) to 200%, corresponding to the total consumption allocated incorrectly.

Thanks to its reliance on proximity in the x-space, the k-NN method achieves the smallest error. In contrast, the clustering-classification approach exhibits a higher error because the predicted energy bill composition is more "rigid", constrained by the shapes of the cluster centers. This effect is even more evident in the SLP approach, which is limited to only two predefined shapes (household and non-household).

Fig. 4.15 depicts the distribution of the error calculated for the typical load profiles, $NCAE_y$. These errors are generally larger as they are assessed instantaneously time step by time step. Once again, the k-NN method demonstrates superior performance, compared to the clustering-classification and SLP approaches.

Fig. 4.16 illustrates the error between the actual and predicted duration curves, $NCAE_{DC}$, which evaluates the similarity between the actual and predicted load profile statistics. As expected, this error is smaller than $NCAE_y$, given that it assesses similarity over aggregated statistics rather than instantaneous deviations.

The radar plots in Fig. 4.17 present the $NCAE_y$ and $NCAE_{DC}$ metrics divided by end-user classes. For households, the SLP approach performs comparably to the data-driven methods. However, for non-household end users, the SLP struggles to characterize load profiles, whereas data-driven approaches, particularly k-NN,

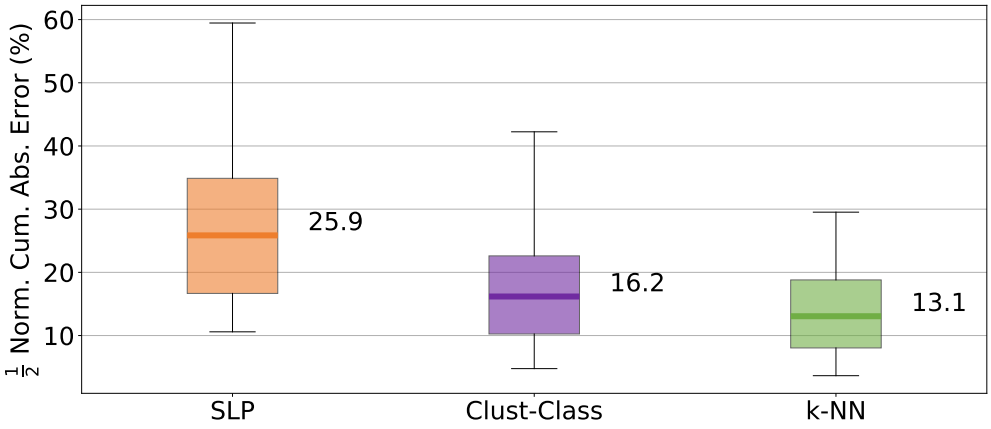

Fig. 4.15 Distribution of the normalized cumulative absolute error on the typical load profiles (weighted by day type), $NCAE_y$, between the actual data and the predictions from the different methods, for all samples. The median error across all samples is also shown.

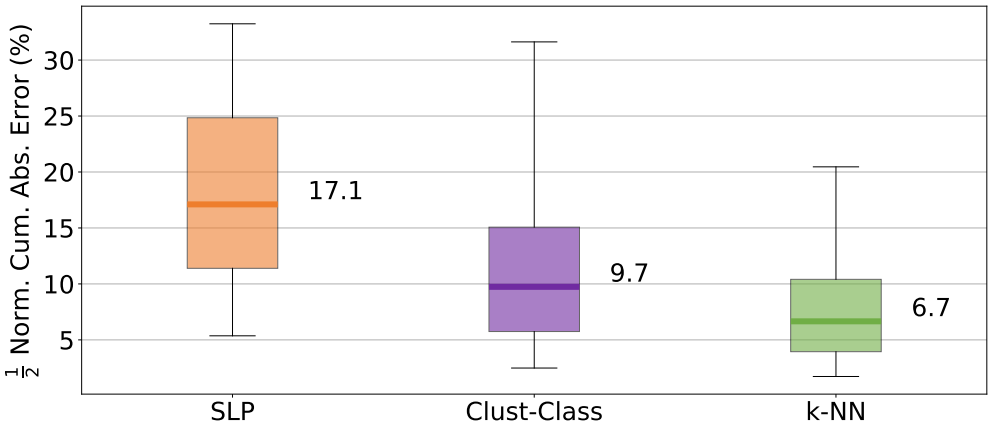

Fig. 4.16 Distribution of the normalized cumulative absolute error on the reconstructed duration curves, $NCAE_{DC}$, between the actual data and the predictions from the different methods, for all samples. The median error across all samples is also shown.

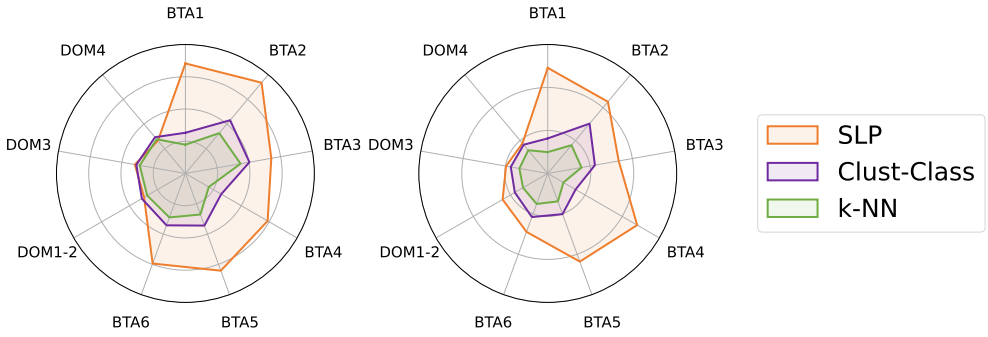

(a) $\frac{1}{2}$ NCAE-y (%) (b) $\frac{1}{2}$ DCE (%)

Fig. 4.17 Median values of: (a) Normalized cumulative absolute error on the typical load profiles ($NCAE_y$) and (b) Normalized cumulative absolute error on the reconstructed duration curves ($NCAE_{DC}$), evaluated for all samples and methods, broken down by end-user categories.

show significantly better performance, achieving results similar to those observed for households. This suggests that the SLP effectively represents typical household load profiles, which exhibit lower within-class variability (see Fig. 4.9). In contrast, non-household customers exhibit diverse consumption patterns that a single SLP cannot capture, while data-driven methods better adapt to the variability using energy bill data.

4.6.2 Application-specific assessment

The three methods were evaluated in an application for ICES assessment and optimization. In particular, the original dataset was split between training and testing sets, with 90-10 % ratios –in terms of end users. The test set was randomly selected, ensuring that the end users were drawn uniformly from all user classes. However, the number of users from each class in the test set was adjusted to mitigate bias due to varying consumption magnitudes. This was done by replicating users within each class as needed, ensuring that each class contributed equally to the test set's overall consumption distribution.

Fig. 4.18 shows the self-sufficiency rate (SS) evaluated on the test set using predicted data from the three methods, compared with actual data, for different renewable generation capacity –i.e., PV size. The results indicate that the k-NN method closely matches the actual SS values, while the clustering-classification

method performs slightly worse, and the SLP method significantly overestimates SS.

The assessment was further extended to examine the impact of different prediction methods on a design problem. Specifically, the MILP setup described in Chapter 3 for operational optimization was applied to an ICES consisting of two nodes: an active node with a PV system coupled to a BESS, and a passive node for the aggregated consumption.

The optimization problem was expanded to also optimize the sizes of the PV system and BESS by introducing two design variables[1]. The objective function was set to minimize the total actualized cost (TAC) while imposing minimum self-sufficiency (SS) as a constraint. Different optimization runs were performed varying the constraint on the self-sufficiency to reflect the need for higher renewable energy contributions.

Fig. 4.19 presents the optimal objectives for the different cases, using consumption data predicted by various methods as well as actual data. As expected, the k-NN method performs the best, especially for higher renewable energy constraints. The clustering-classification method performs slightly worse, while the SLP approach significantly underestimates costs.

[1]The problem was slightly modified to maintain linear constraints. In particular, since the BESS capacity is now a variable, the constraints in (3.13) were removed. This modification does not pose a problem, as mutual exclusivity between BESS charge and discharge is ensured by efficiencies, and the exclusivity between grid injection and withdrawal is guaranteed by different pricing.

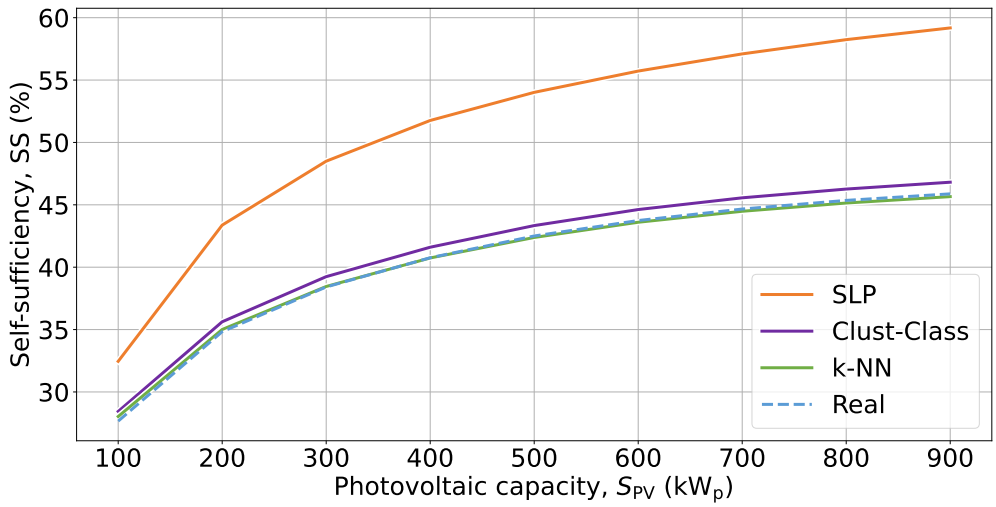

Fig. 4.18 Self-sufficiency rate (SS) evaluated on the test set using the predicted data from the three methods, compared with the actual data, for various PV sizes.

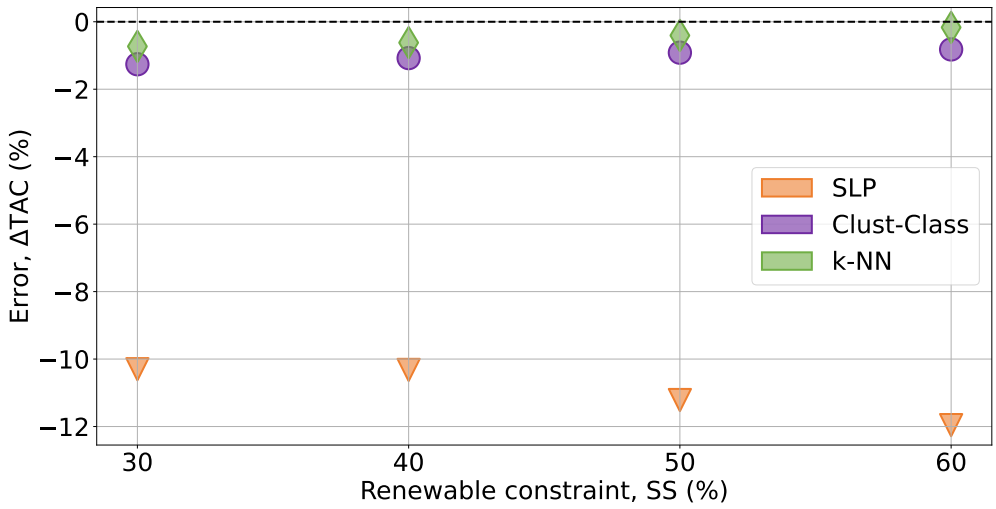

Fig. 4.19 Error on the optimal objectives –total actualized cost, TAC– obtained for different cases using consumption data predicted by various methods, compared to the solution obtained with actual data for each self-sufficiency constraint

It is also worth noting the optimal PV and BESS capacities errors when using different prediction methods, under varying self-sufficiency (SS) constraints. Specifically, the SLP method tends to overestimate PV capacity but shows smaller errors in BESS capacity when the SS requirement is low. As the SS requirement increases, however, the SLP method severely underestimates the BESS capacity, although the PV capacity improves. In contrast, the two data-driven methods consistently perform better or at least comparably in terms of both optimal PV and BESS sizes, except for the case with the smallest SS requirement.

While these results are insightful, they are primarily illustrative at this stage. A deeper understanding of these trends would require further analysis to draw definitive conclusions about the methods' performance in the application. Specifically, implementing a cross-validation procedure would help eliminate any bias arising from the randomly selected test set.

4.7 Discussion

The results reported in this chapter highlight how data-driven methods significantly improve the prediction of typical load profiles from ToU energy bills compared to SLPs. This improvement is especially evident for non-residential end users, where data-driven approaches capture the diversity of consumption

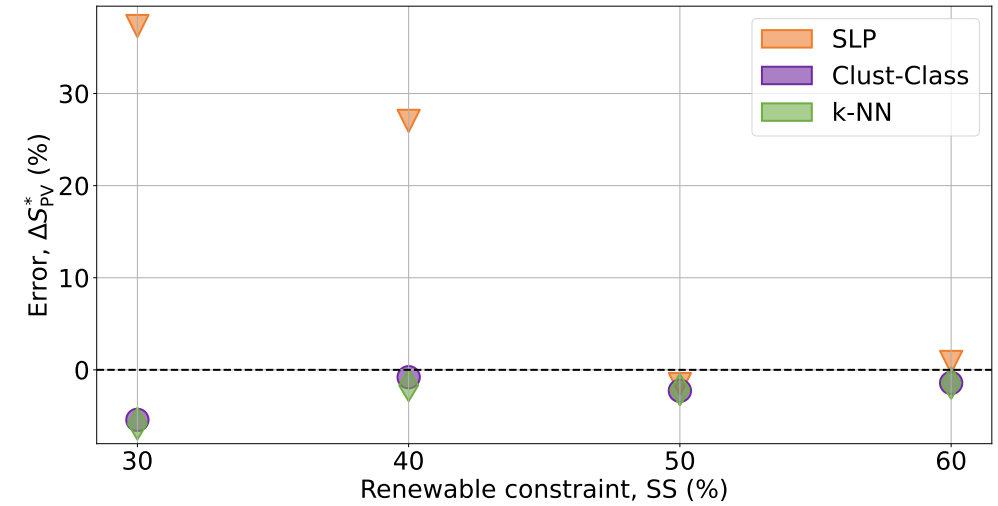

Fig. 4.20 Error on the optimal photovoltaic capacity S_{PV} obtained for different cases using consumption data predicted by various methods, compared to the solution obtained with actual data for each self-sufficiency constraint.

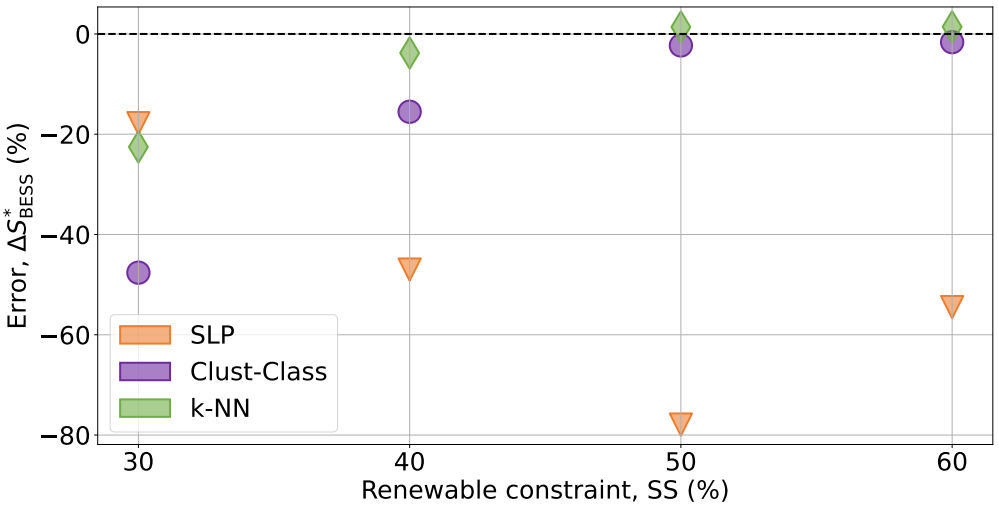

Fig. 4.21 Error on the optimal battery capacity S_{BESS} obtained for different cases using consumption data predicted by various methods, with the solution obtained with actual data for each self-sufficiency constraint..

patterns that traditional approaches often fail to address. Among the two data-driven approaches considered, the regression-based on usingk-NN consistently outperformed the clustering-classification method across multiple metrics. This can be explained by the continuous mapping between the two spaces performed in the regression approach. Instead, the other approach discretizes the energy consumption by clustering data, hence its performance also depends on how data are distributed (other than the clustering technique adopted).

While prediction errors are higher at the time-step level, they are less significant when considering aggregated statistics or ToU data. However, while these metric errors are important, it is also essential to assess the application of these methods in real-world scenarios. In particular, evaluating these prediction methods for ICES assessment shows a strong mitigation of the errors found in individual load profiles. This is largely due to the aggregation of consumption data, which reduces the impact of individual-level inaccuracies.

Limitations and further improvements Generating accurate predictions from minimal input data offers considerable advantages, particularly for large and heterogeneous end-user portfolios. However, the trade-off between prediction accuracy and ease of data collection should not be overlooked. The findings suggest that the proposed method offers a promising solution for predicting a wide variety of load profiles when only limited input data is available, as demonstrated by its successful application in ICES assessment and optimization tasks. Nevertheless, this analysis requires further refinement. For example, while the approach demonstrated here efficiently leverages ToU data, implementing separate models for different end-user categories or seasons could further enhance accuracy as more data become available. Additionally, to fully evaluate the impact of these methods on their application to ICES, a more detailed analysis is required where consumption data are not aggregated, allowing for the assessment of how errors in individual profiles influence final outcomes.

Chapter 5

Towards game theoretic many-objective design optimization

Summary

Building on Chapter 3, where optimal energy management strategies were introduced for evaluating the performance of ICES configurations, this chapter shifts focus to the design phase, where the sizes of active assets –such as renewable generators, storage systems, and sector-coupling components– are determined. In particular, considering the multiple and conflicting ICES objectives (e.g., energy, environmental, and economic KPIs), a many-objective approach is adopted. A simplified case of a collective self-consumption (CSC) system is considered, to capture the multi-energy nature of ICES while avoiding the added complexity of multi-node systems. This chapter adopts an exploratory approach, employing a grid discretization of the design space rather than performing actual optimization. The preliminary analyses aim to characterize the optimization landscape under increasing numbers of conflicting objectives and to investigate scalarization techniques for simplifying many-objective problems. Metrics such as closeness to the Utopia point and the Nash product, the latter inspired by game-theory concepts, are evaluated for their ability to identify balanced compromise solutions.

Key objectives

- Exploring the multi-objective ICES design problem under increasing numbers of objectives.

- Characterizing trade-offs among multiple conflicting objectives, including self-consumption, energy self-sufficiency (electricity and heating), emission reduction, and cost reduction.
- Evaluating the potential of scalarization metrics, such as closeness to the Utopia point and the Nash product, to address challenges in many-objective optimization.

The chapter is structured as follows. Section 5.1 reviews the literature on multi-objective ICES and REC design, alongside traditional multi-objective optimization methods, scalarization, and game-theory-inspired approaches. Section 5.2 presents the formal definition of the multi- (or many-) objective optimization problem (MOOP) and describes the scalarization techniques used to evaluate trade-offs. The CSC configuration is detailed in Section 5.3, including the design variables and performance objectives considered. Preliminary results of the grid analysis are presented in Section 5.4, highlighting the increasing complexity of the Pareto front as the number of objectives grows and comparing the performance of scalarization metrics. Finally, Section 5.5 reflects on the findings, limitations, and potential directions for many-objective ICES optimization.

Key insights

- The grid-based analysis reveals significant trade-offs among energy, environmental, and economic objectives, with the Pareto front becoming increasingly complex as the number of objectives rises.
- Scalarization metrics, such as the Nash product and closeness to the Utopia point, effectively identify balanced compromise solutions.
- The Nash product demonstrates higher selectivity among trade-off solutions, offering promise in optimization settings. However, complementarity with closeness is valuable, especially during initial design phases where exploration is critical.
- While these initial findings offer useful insights, they are far from conclusive. Further studies are necessary to address the complexities of many-objective ICES optimization, particularly in settings with greater system complexity.

5.1 Literature review and contribution

The design of community energy systems is widely discussed in the literature, often considering multiple objectives, such as economic costs, environmental impacts, and energy performance, and addressing the inherent conflicts between these targets. For instance, [97] optimized a local energy community in Valencia (Spain) in terms of battery energy storage capacity, ownership, and community composition, considering costs, emissions, and energy autarchy (a concept similar to self-sufficiency). Similarly, in [98], a multi-objective model determined the optimal energy mix for a community in Okanagan Valley (Canada), taking energy costs and life-cycle environmental impacts into account. In [99], the sizes of photovoltaic, heat pump, fuel cell, and electric energy storage systems were optimized for a community center in Korea using a multi-objective framework addressing economic and environmental goals. Furthermore, [100] presented a multi-criteria evaluation framework incorporating technological, economic, environmental, and societal aspects to plan distributed energy systems for a residential community in Tianjin, China. Closer to the Italian context, [63] explored the optimization of energy production and storage units in an energy community in Padua using a bi-objective approach. [61] presented a three-objective optimization approach (economic, environmental, and social) for an energy community with electric vehicles and demand response. [62] introduced the concept of polygeneration in energy communities through district heating and cooling networks, interconnecting the members of a REC beyond just the electric grid.

The studies above underline how the design of community energy systems inherently involves multiple conflicting objectives, making the problem well-suited for formulation as a multi-objective optimization problem (MOOP). MOOPs are extensively used in energy system optimization to balance trade-offs between objectives [101, 102]. These problems yield a Pareto front of non-dominated solutions, where any improvement in one objective necessitates worsening at least another. Traditional approaches to solving MOOPs involve exploring the entire Pareto front using the ε-constraint method [103], which separates one objective as a target while treating others as constraints, or metaheuristic algorithms, such as the widely used NSGA-II [104]. However, with an increasing number of objectives, these methods encounter significant challenges: navigating the Pareto front becomes computationally intensive, and the Pareto dominance criterion becomes

less effective in distinguishing solutions due to the higher dimensionality of the objective space [105].

One strategy to address this issue is scalarization, where the MOOP is reformulated into a single-objective problem, thereby avoiding the need to explore the entire Pareto front. The most common scalarization method involves creating a weighted sum of the objectives, requiring careful tuning of weights that can significantly influence the resulting solution. Alternatively, reference point-based methods, such as minimizing or maximizing the distance from a defined point in the objective space, offer another scalarization strategy [106, 107]. A notable example is the ideal (or Utopia) point, which combines the optimal values of individual objectives from the design space. Although representing an unachievable solution, this point is generally an important reference in MOOPs.

Game-theoretic concepts have also been explored in MOOP solutions [108]. In these approaches, objectives are treated as players in a cooperative game, and the MOOP is reformulated by seeking an equilibrium point in the game. For instance, the Nash bargaining solution maximizes the Nash product, which measures the distance from a disagreement point where each player achieves their worst outcome [109]. Compared to other reference point-based approaches, game theory-inspired solutions have a strong mathematical foundation and exhibit interesting features. For instance, the Nash bargaining solution ensures Pareto efficiency and introduces specific symmetry properties among the objectives, simplifying the decision-making process [110].

These methods are particularly interesting in the context of community energy systems, where multiple stakeholders are present, and objectives are typically conflicting. For example, non-cooperative and cooperative game theory concepts have been used in [41] to fairly allocate benefits within RECs. Game theory is also frequently applied in the “transactive energy” context to model and optimize peer-to-peer energy exchanges, as well as to design cost-sharing mechanisms or pricing strategies [111]. However, the potential of game theory concepts in multi-objective design problems has not been explored in detail. While applications in aerospace engineering and structural optimization can be found in the literature [112, 110], their use in the energy sector remains limited, particularly in optimizing the size and design of technologies within RECs.

Contributions

This chapter explores the complex problem of multi- and many-objective ICES design, focusing on the challenges posed by an increasing number of objectives, including the growth of non-dominated solutions and the navigation of high-dimensional Pareto fronts. It investigates scalarization metrics as a means to identify balanced compromise solutions without the need to explore the entire Pareto front. Two approaches are analyzed: one traditional, based on closeness to the Utopia point, and another inspired by game theory, the Nash product. By using a simplified case with a limited number of design variables, this study serves as a foundation for future deployment of game theory approaches in more comprehensive many-objective optimizations in complex ICES contexts.

5.2 Multi and many-objective optimization problem

While single-objective optimization problems follow the formulation presented in (3.9), multi and many-objective optimization problems (MOOPs), characterized by multiple conflicting objectives, are defined as follows:

$$\begin{aligned} \underset{\mathbf{x} \in X}{\text{minimize}} \quad & f_1(\mathbf{x}), f_2(\mathbf{x}), \ldots, f_\mathrm{m}(\mathbf{x}) \\ \text{subject to} \quad & g_\mathrm{j}(\mathbf{x}) \leq 0, \quad j = 1, \ldots, q, \\ & h_\mathrm{k}(\mathbf{x}) = 0, \quad k = 1, \ldots, p \end{aligned} \tag{5.1}$$

Here, $\mathbf{x}$ represents the vector of decision variables, X is the design space, and $f_1, \ldots, f_\mathrm{m}$ denote the objective functions.

The distinction between multi-objective and many-objective problems lies in the number of objectives, which directly affects the dimensionality of the objective space. Conventionally, problems with up to three objectives are classified as multi-objective, whereas those with more than three are considered many-objective [113].

Unlike single-objective optimization problems, MOOPs yield a set of optimal solutions instead of a single point. These solutions, known as the Pareto set, consist of non-dominated points where improving one objective necessarily degrades at least one other. The corresponding images in the objective space define the Pareto front. Population-based metaheuristic algorithms are frequently employed to approximate the Pareto front [114]. For instance, NSGA-II [104] is

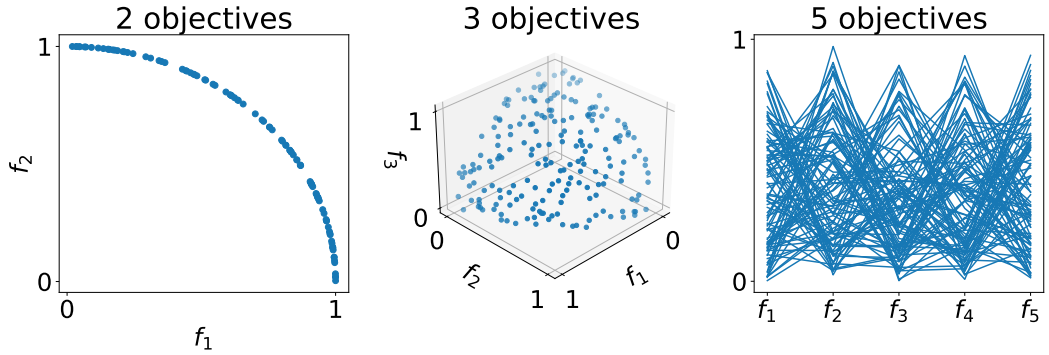

Fig. 5.1 Examples of Pareto fronts in two, three, and five-dimensional spaces.

a genetic algorithm leveraging non-dominated sorting, which generates and iteratively updates a population of solutions until a termination criterion is met. Over time, NSGA-II has proven particularly effective in handling multi-objective optimization problems in different engineering applications [115].

Fig. 5.1 provides a qualitative illustration of Pareto fronts drawn from n-dimensional hypersphere sectors and their visualization in spaces with two, three (multi) and five (many) objectives. In the right-most plot, with more than three dimensions, the objectives are shown using parallel coordinates.

An approximated Pareto front provides a global view of trade-offs among objectives, enabling decision-makers to explore a range of optimal solutions. Nevertheless, selecting a single compromise solution is still necessary. This selection may be guided by subjective preferences, such as assigning relative weights to objectives, or by objective criteria.

5.2.1 Characteristic points

A series of "characteristic points" can be defined in a MOOP, crucial for normalizing objectives and assisting decision-makers in selecting compromise solutions from the Pareto set [116], as discussed later.

Ideal or Utopia The Utopia point ($\mathbf{u} = \{u_i\}_{i=1,\dots,m}$) represents a hypothetical scenario where all objectives attain their optimal values simultaneously. This point is determined by individually optimizing each objective function:

$$\begin{aligned} \mathbf{x}_{U,i} &= \arg\min_{\mathbf{x}\in X} f_i(\mathbf{x}) \\ u_i &= f_i(\mathbf{x}_{U,i}) \end{aligned} \qquad \forall\, i = 1,\dots,m. \tag{5.2}$$

Critical Points Critical points are defined as the solutions within the Pareto set P that maximize each objective function f_i (i.e., worst value):

$$\mathbf{x}_{\mathrm{C,i}} = \arg\max_{\mathbf{x}\in P} f_{\mathrm{i}}(\mathbf{x}) \qquad \forall i = 1,\ldots,m, \tag{5.3}$$

where P denotes the Pareto set. Identifying these points is more challenging, as it requires knowledge of the Pareto set.

Nadir The Nadir point ($\mathbf{n} = \{n_{\mathrm{i}}\}_{\mathrm{i}=1,\ldots,\mathrm{m}}$) is constructed by taking the worst (maximum) values of each objective function over the Pareto front, using the critical points:

$$n_{\mathrm{i}} = f_{\mathrm{i}}(\mathbf{x}_{\mathrm{C,i}}) \qquad \forall i = 1,\ldots,m. \tag{5.4}$$

Worst objective The worst objective point ($\mathbf{w} = \{w_{\mathrm{i}}\}_{\mathrm{i}=1,\ldots,\mathrm{m}}$) is determined by maximizing each objective function over the entire feasible set X, instead of the Pareto front:

$$\begin{aligned} \mathbf{x}_{\mathrm{W,i}} &= \arg\max\nolimits_{\mathbf{x}\in X} f_{\mathrm{i}}(\mathbf{x}) \\ w_{\mathrm{i}} &= f_{\mathrm{i}}(\mathbf{x}_{\mathrm{W,i}}) \end{aligned} \qquad \forall i = 1,\ldots,m. \tag{5.5}$$

Unlike the Nadir, this point considers the global maxima of the objectives, which may lie outside the Pareto-optimal set.

Pseudo-Nadir Given the difficulties in obtaining the Nadir point, a pseudo-Nadir point can be determined using simplified methods. One such approach is the pay-off table [117], which cross-compares the individual optimal solutions of the objectives to identify the worst value for each objective:

$$n_{\mathrm{i}}^{*} = \max_{\substack{j=1,\ldots,m \\ j\neq i}} f_{\mathrm{j}}(\mathbf{x}_{\mathrm{U,j}}) \qquad \forall i = 1,\ldots,m. \tag{5.6}$$

This method has been criticized for its inability to accurately identify the Nadir point when individual objective functions are multimodal [116]. Despite this limitation, the pay-off table method is computationally efficient.

Fig. 5.2 shows these characteristic points in a bi-objective minimization problem, highlighting how the Nadir and worst points can differ. In this particular case, the payoff table method would yield the exact Nadir, but in most cases, especially with three or more objectives, this is not the case [116]

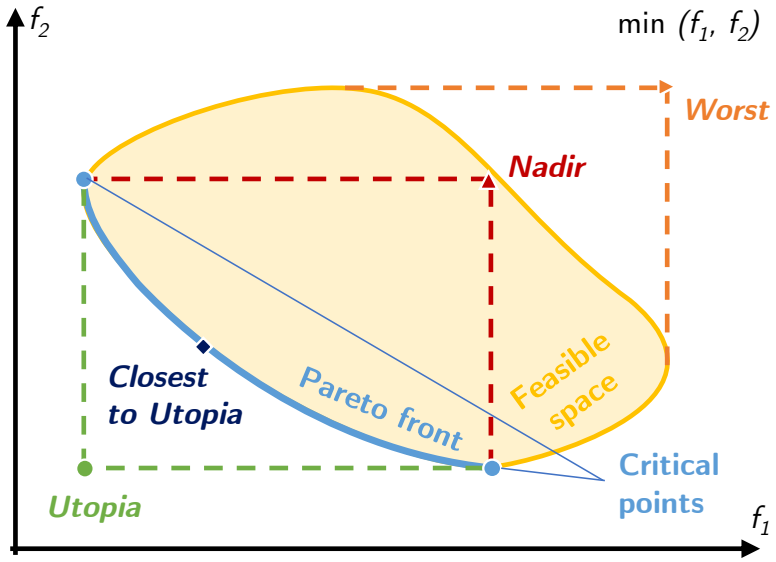

Fig. 5.2 Qualitative example of characteristic points in a bi-objective minimization problem.

As mentioned earlier, a common approach for selecting a compromise solution within the Pareto set relies on characteristic points. One example is choosing the solution that minimizes the distance from the Utopia point, as illustrated in Fig. 5.2.

5.2.2 Scalarization approaches

When MOOPs become particularly complex or computationally expensive, as in high-dimensional objective spaces, scalarization techniques can simplify the problem. Essentially, the criteria for evaluating trade-offs are applied in advance, transforming the MOOP into a single-objective optimization task easier to solve.

The simplest scalarization technique is performing a weighted sum of the objectives, as follows:

$$\begin{aligned} \underset{\mathbf{x} \in X}{\text{minimize}} \quad & \sum_{\mathrm{i}=1}^{\mathrm{m}} w_{\mathrm{i}} f_{\mathrm{i}}(\mathbf{x}) \\ \text{subject to} \quad & \ldots \end{aligned}$$

where $w_{\mathrm{i}} \in [0,1]$ is the weight assigned to the i-th objective, and $\sum_{\mathrm{i}} w_{\mathrm{i}} = 1$.

While intuitive, this method introduces subjectivity, as the choice of weights heavily influences the outcome.

Alternatively, the distance to the Utopia point can be minimized. This approach balances competing objectives by prioritizing proximity to the Utopia point, offering a more objective scalarization method. In this formulation, the MOOP is transformed into a single-objective problem, where the goal is to find the point that minimizes the Euclidean distance from the current solution to the Utopia point (x_{closest}):

$$\begin{aligned} \underset{\mathbf{x} \in X}{\text{minimize}} \quad & \left(\sum_{\mathrm{i}=1}^{\mathrm{m}} \left(f_{\mathrm{i}}(\mathbf{x}) - u_{\mathrm{i}} \right)^2 \right)^{\frac{1}{2}} \\ \text{subject to} \quad & \ldots \end{aligned} \tag{5.7}$$

A practical limitation of this method is the requirement to precompute the coordinates of the Utopia point, which involves solving m independent single-objective optimization problems.

5.2.3 Game theory approach

A game theory-inspired approach can be used to model a MOOP as a cooperative game [110]. To better understand the parallelism between games and MOOPs, a basic (and loose) nomenclature of game theory concepts is introduced [109, 118].

Game A scenario involving a set of players, the strategies they can adopt, and the utility functions determining their payoffs based on their own and other players' strategies. Games are generally classified into non-cooperative and cooperative: in non-cooperative games, each player acts independently, while in cooperative games, players can form coalitions to improve their collective outcomes.

Player and Strategy An individual or entity making decisions in a game to maximize their reward or payoff, through a set of possible actions (strategy).

Payoff and Utility Function The reward a player receives based on their strategy and the strategies of others, and the function that determines the payoffs based on the strategies.

Outcome The result or state of the game, depending on the choices made by all the players. Specific outcomes are defined depending on the type of game.

(Nash) Equilibrium The outcome of a non-cooperative game where no player can improve their payoff by changing their strategy unilaterally.

Disagreement and Agreement A situation where no cooperation occurs, and players receive suboptimal outcomes, versus a mutually beneficial outcome in a cooperative game, where players reach a consensus.

The game-theoretic adaptation of MOOP is based on a parallelism between objectives and players, specifically:

- Each objective function f_i is associated with a player, representing their utility function.
- The decision variables of the problem correspond to the players' strategies.
- A feasible solution $\mathbf{x} \in X$ represents an outcome of the game, where each player's payoff is given by the value of the associated objective function.

This formulation leads to the concept of a bargaining solution, specifically the Nash bargaining solution, which maximizes the collective utility of all players by improving their payoffs relative to the disagreement point [109].

In mathematical terms, finding the Nash-bargaining solution (x_{NB}) consists in maximizing the so-called Nash product, as follows:

$$\begin{aligned} \underset{\mathbf{x} \in X}{\text{maximize}} \quad & \prod_{\mathrm{i}=1}^{\mathrm{m}} \left(d_{\mathrm{i}} - f_{\mathrm{i}}(\mathbf{x})\right) \\ \text{subject to} \quad & f_{\mathrm{i}}(\mathbf{x}) < d_{\mathrm{i}}, \quad \forall\, i = 1, \ldots, m,, \\ & \ldots \end{aligned} \tag{5.8}$$

where d_{i} is the i-th coordinate of the disagreement point.

In game theory, the disagreement point represents a situation where players receive suboptimal payoffs due to the lack of cooperation. It reflects a scenario where no mutual agreement exists, and the players' payoffs are minimal. Thus, the disagreement point is a baseline from which cooperation (or bargaining) can improve the payoffs for all objectives involved. In the context of MOOPs, this concept directly corresponds to the Nadir point, where each objective attains its

worst possible value within the Pareto front. As mentioned, identifying the Nadir point is challenging, as it is not trivial to compute. While the pay-off table method provides a quick alternative, its accuracy is not always guaranteed.

It is important to note that the Nadir point is not always feasible in the decision space, which could weaken the parallelism between the Nadir point and a true disagreement point in game-theoretic bargaining. Given the difficulties in calculating the Nadir and its potential infeasibility, alternative methods for defining the disagreement point may be worth considering in applying game theory to MOOPs.

5.3 Collective self-consumption with sector coupling

The multi-objective ICES design is explored within a simplified context, focusing on a limited set of decision variables. Specifically, a 'collective self-consumption' (CSC) configuration is considered. This represents a specific type of REC where all participants are located within the same building. Such a configuration is particularly suitable for implementing RECs with sectors-coupling in the context of Italian residential buildings, as illustrated in Fig. 5.3.

In this setup, residents of a multifamily building can install a photovoltaic system on the rooftop to supply electricity for shared services, such as elevators and common area lighting. Furthermore, the electricity generated by the PV system can power a heat pump to meet centralized heating demands during the winter, with a gas-fired boiler serving as a backup. Excess electricity is injected into the grid and can be virtually shared among households. Flexibility in this system is further enhanced by integrating a battery electricity storage system and a heat thermal storage system.

Formally, the CSC configuration is modeled as an ICES with an active node, representing the building –where all the technologies are installed–, and a passive one, representing the aggregated electricity demand of the households in the building, exchanging electricity virtually (see Fig. 5.4).

The power balances at the active node for electricity, heat, and gas are as follows:

$$P^{\mathrm{PV}} + P^{\mathrm{BESS,out}} + P^{\mathrm{with,el}}_{\mathrm{build}} = P^{\mathrm{UE}}_{\mathrm{build}} + P^{\mathrm{BESS,in}} + P^{\mathrm{HP,in}} + P^{\mathrm{inj,el}}_{\mathrm{build}}, \tag{5.9}$$

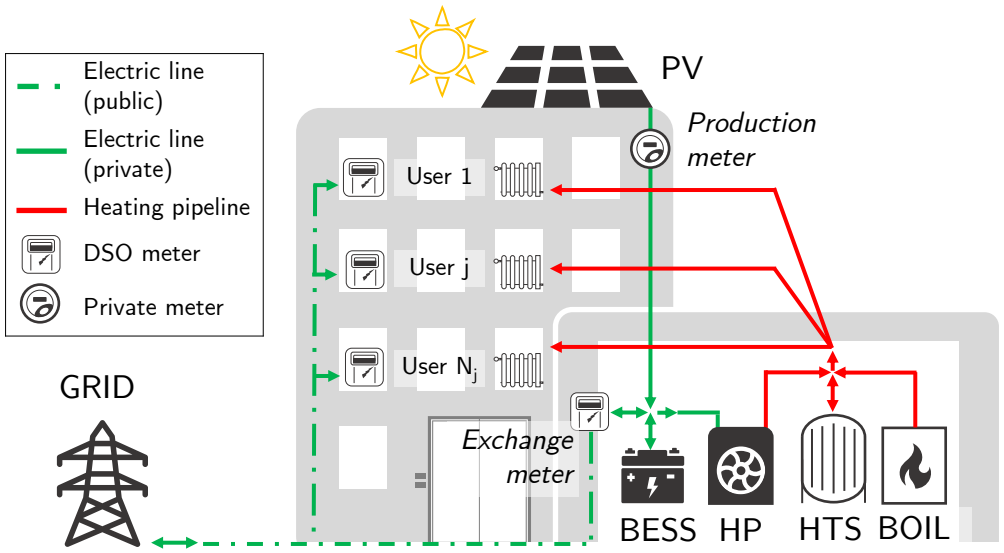

Fig. 5.3 Collective self-consumption system in a residential building. The system integrates photovoltaic generation (PV) and battery energy storage (BESS), coupled with a heat pump (HP) and heat thermal storage (HTS). (Adapted from [11]).

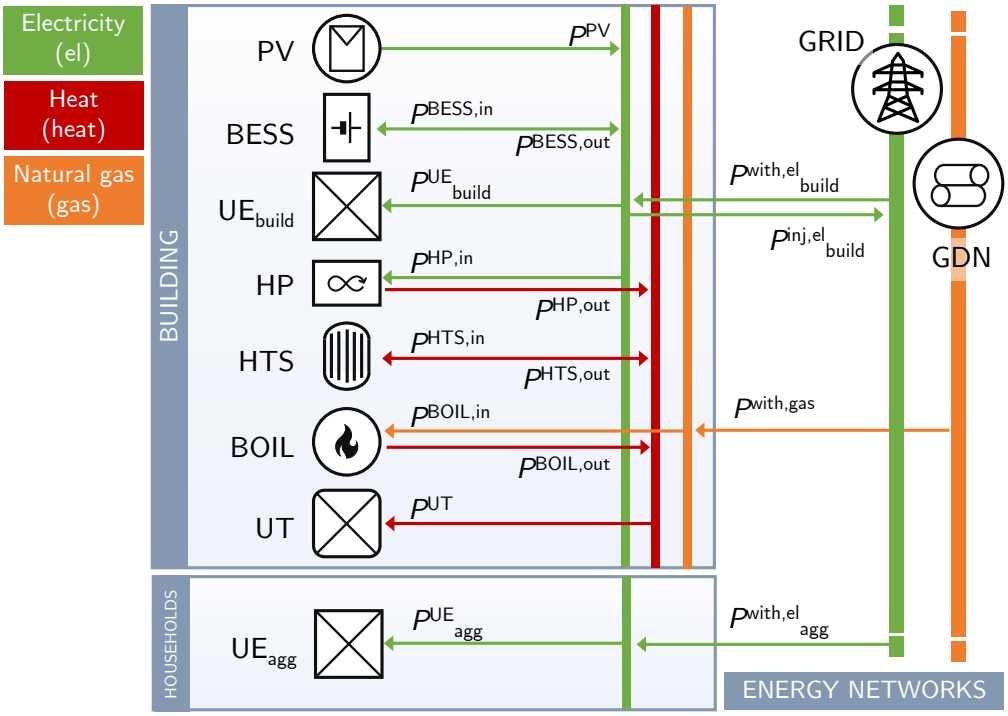

Fig. 5.4 Schematic representation of a collective self-consumption system as a two-node ICES: one active (building) and one passive (aggregated households).

$$P^{\text{HP,out}} + P^{\text{HTS,out}} + P^{\text{BOIL,out}} = P^{\text{UT}} + P^{\text{HTS,in}}, \tag{5.10}$$

$$P^{\text{with,gas}} = P^{\text{BOIL,in}}, \tag{5.11}$$

where $P^{\text{UE}}_{\text{build}}$ is the electricity demand for shared services, and P^{UT} is the centralized heating demand of the building.

The (virtual) power balance on the electricity grid for the CSC is given by:

$$P^{\text{inj,el}}_{\text{build}} + P^{\text{with,el}}_{\text{CSC}} = P^{\text{UE}}_{\text{aggr}} + P^{\text{with,el}}_{\text{build}} + P^{\text{inj,el}}_{\text{CSC}}, \tag{5.12}$$

where $P^{\text{UE}}_{\text{aggr}}$ is the aggregated electricity demand of the households in the building, and $P^{\text{inj,el}}_{\text{CSC}}$ and $P^{\text{with,el}}_{\text{CSC}}$ represent the virtual exchanges outside of the CSC configuration.

5.3.1 Design problem

The design problem consists of finding sizes for the four technologies to install in the CSC (S^{PV}, S^{HP}, S^{BESS}, S^{HTS}) –i.e., the design variables–, while considering the multiple and conflicting objectives described in the following.

The self-consumption rate of self-produced renewable energy (SC) is calculated as:

$$SC = 1 - \frac{E^{\text{inj,el}}_{\text{CSC}}}{E^{\text{PV}}}, \tag{5.13}$$

since only one renewable generator is present.

Electricity self-sufficiency rate is calculated as follows:

$$SS^{\text{el}} = 1 - \frac{E^{\text{with,el}}_{\text{CSC}}}{E^{\text{with,el}}_{\text{build}} + E^{\text{UE}}_{\text{agg}}}, \tag{5.14}$$

where the withdrawn energy ($E^{\text{with,el}}_{\text{build}}$) is used for the building rather than only electricity consumption, since the heat pump increases the electricity demand.

Heating self-sufficiency is also considered, using a slight variation from (1.15) because heating in the considered ICES is an internal energy vector with no external connections. However, since the boiler is exclusively used for heating demand and is powered by gas withdrawn from the external network, heating self-sufficiency is calculated by considering the fraction of heating demand covered

Table 5.1 Discretization of the design space for grid analysis. Each design variable is sampled uniformly within its specified range.

Design variable	Min	Max	Step	Unit
S^{PV}	10	100	15	$\mathrm{kW_p}$
S^{HP}	10	100	15	$\mathrm{kW_{th}}$
S^{BESS}	10	100	15	kWh
S^{HTS}	20	200	30	kWh

by the boiler, as follows:

$$SS^{\mathrm{heat}} = 1 - \frac{E^{\mathrm{BOIL,out}}}{E^{\mathrm{UT}}}. \tag{5.15}$$

Finally, environmental and economic KPIs are evaluated as described in Section 1.4. Specifically, CO_2 emissions reduction (ER) and total actualized cost reduction (CR) are considered, calculated as in (1.20) and (1.25), respectively.

These objectives are calculated based on a reference year and depend on the optimal energy management of the CSC, achieved by optimizing the power and energy flows within the building and among the households, using the MILP formulation described in Chapter 3.

5.3.2 Case study

The data used for specific renewable generation, energy demands, costs, and other parameters are those described in Chapter 2. The 31 households in the dataset are considered for the aggregated electricity demand. Consequently, the heating demand, initially estimated for a reference building with 40 apartments, is scaled linearly to align with the dataset. Additionally, the building's energy demand is randomly extracted from users in the dataset categorized as non-household, residential end users.

In this preliminary assessment, instead of conducting a proper optimization, the landscape of the problem is explored through a grid analysis of the design variables. The design space is discretized by sampling across the four design variables (S^{PV}, S^{HP}, S^{BESS}, S^{HTS}) within its respective range using a fixed step size as shown in Tab. 5.1, resulting in $7^4 = 2401$ combinations.

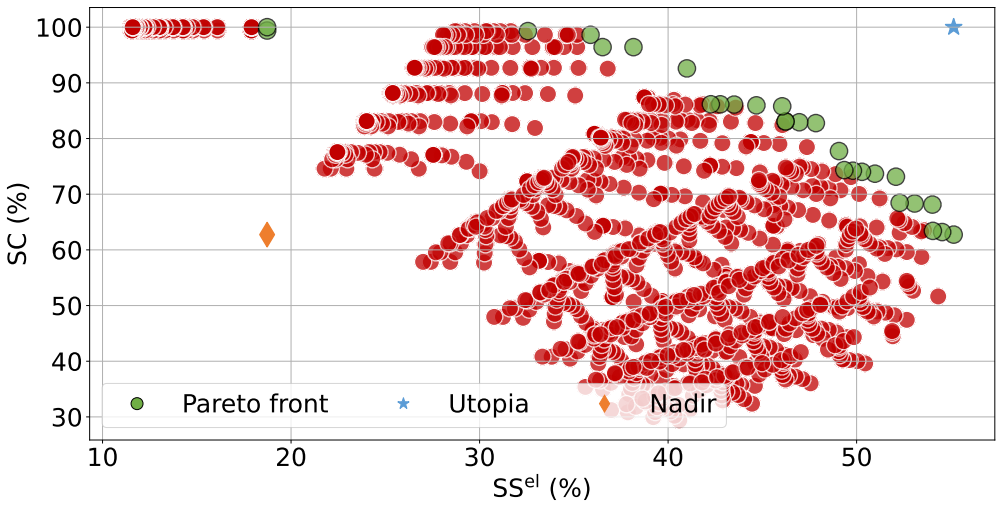

Fig. 5.5 Evaluated configurations in the self-consumption (SC) vs. electricity self-sufficiency (SS^{el}) objective space. Non-dominated solutions are highlighted in green, approximating the Pareto front of the problem. Utopia and Nadir points are also shown for reference.

5.4 Preliminary results

This section presents the findings of the preliminary analysis aimed at characterizing the MOOP under consideration. First, Pareto dominance is explored, progressively incorporating an increasing number of objectives to examine the behavior of the solution space. Subsequently, scalarization approaches, including the game theory framework, are discussed in the context of problems with many objectives.

From the 2401 configurations evaluated, 1049 resulted in a negative cost reduction and are thus excluded from further analysis. This leaves 1352 configurations, which form the basis for the subsequent exploration.

5.4.1 Two objectives

Fig. 5.5 represents the evaluated configurations in a two-objective space, with the electricity self-sufficiency rate (SS^{el}) on the x-axis and the self-consumption rate (SC) on the y-axis. Similarly, Fig. 5.6 shows configurations in a different objective space, defined by cost reduction (CR) and emission reduction (ER).

In both figures, non-dominated points (shown in green) form an approximate Pareto front. These points are located in the top-right region of the plots, as both

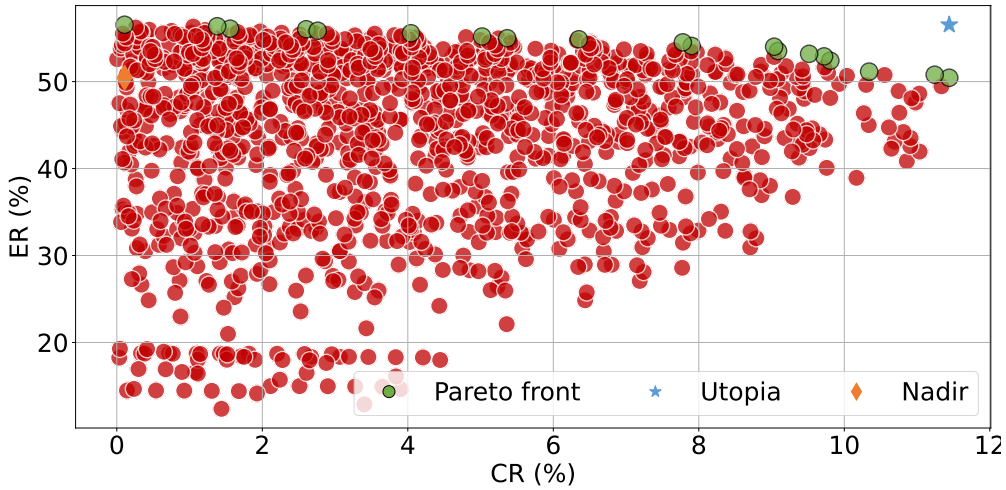

Fig. 5.6 Evaluated configurations in the emissions reduction (ER) vs. cost reduction (CR) objective space. Non-dominated solutions are highlighted in green, approximating the Pareto front of the problem. Utopia and Nadir points are also shown for reference.

objectives in each case must be maximized. The Utopia point, representing the theoretical best value for both objectives, is found at the top-right corner, while the Nadir point, indicating the worst values on the Pareto front, is located near the bottom-left corner.

It is important to note that the Nadir point does not coincide with the absolute worst values of the objectives across all configurations. This discrepancy is particularly evident in Fig. 5.6, where configurations with low ER values are largely dominated and do not contribute to the Pareto front.

In Fig. 5.5, the trade-off between SC and SS is visible, with improvements in one objective often leading to a significant reduction in the other. This conflict is less pronounced in Fig. 5.6, where the Pareto front is flatter, indicating that increases in CR have a more modest impact on ER.

5.4.2 Three objectives

To further explore the problem, a third objective, SS^{heat}, is introduced, as shown in Fig. 5.7 and Fig. 5.8. The results are visualized as 2D scatterplots, with the third objective encoded through a color gradient for the markers, helping to visualize the 3D objective space. Non-dominated points are distinguished with a black border, and the Utopia and Nadir points are displayed for reference.

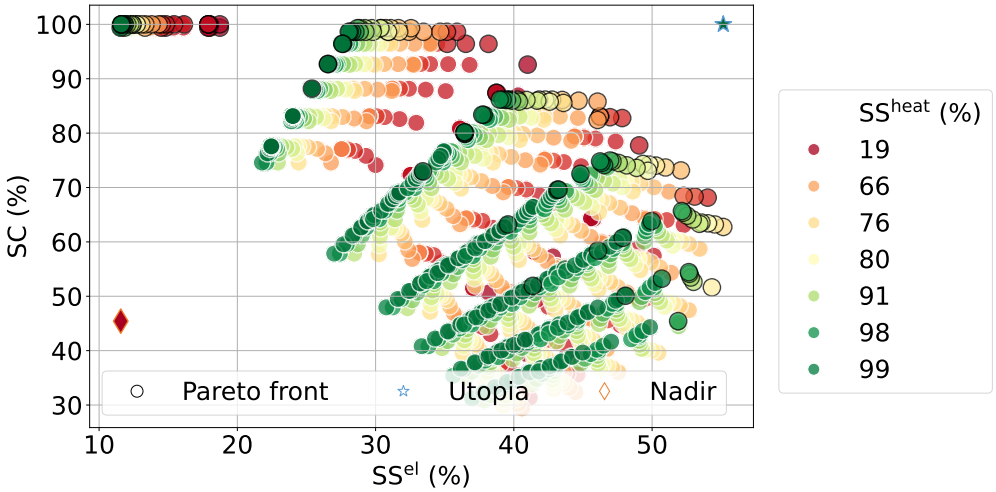

Fig. 5.7 Evaluated configurations in the self-consumption (SC) vs. electricity and heating self-sufficiency (SS^{el}, SS^{heat}) objective space. The third objective is encoded in the color of the points. Non-dominated solutions are circled in black. Utopia and Nadir points are also shown for reference.

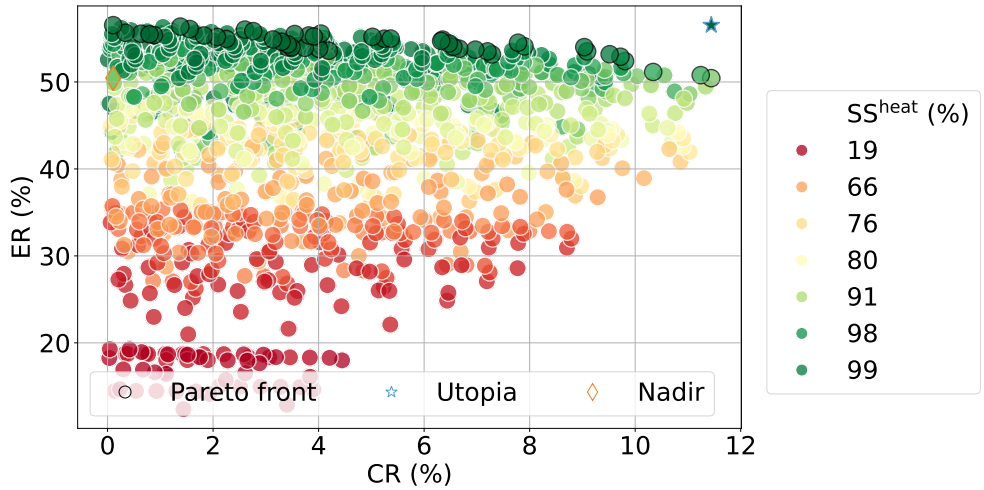

Fig. 5.8 Evaluated configurations in the emissions reduction (ER) vs. cost reduction (CR) vs. heating self-sufficiency (SS^{heat}) objective space. The third objective is encoded in the color of the points. Non-dominated solutions are circled in black. Utopia and Nadir points are also shown for reference.

Table 5.2 Number of non-dominated solutions over the number of objectives considered, among all possible combinations of the five objectives.

Objectives	Min	Median	Max
2	3	**14**	45
3	17	**129**	248
4	175	**242**	668
5		**678**	

In Fig. 5.7, the addition of SS^{heat} reveals the three-dimensional structure of the Pareto front. The number of non-dominated points increases compared to the two-objective case (Fig. 5.5), as the inclusion of a third objective introduces new trade-offs.

Conversely, the results shown in Fig. 5.8 reveal a less pronounced impact on the Pareto front when SS^{heat} is introduced. While there is still an increase in non-dominated points, the change is relatively modest compared to the first case. This behavior suggests that SS^{heat} is less in conflict with one of the two original objectives—most notably ER, as indicated by the relatively horizontal color gradients across the scatterplot.

5.4.3 Many objectives

Tab. 5.2 summarizes the minimum, median, and maximum number of non-dominated points among the evaluated configurations for all the possible combinations of objectives, ranging from 2 to 5 objectives –the latter including only one combination. The table highlights the trend of increasing non-dominated solutions as the number of objectives rises. In the case with 5 objectives, 678 out of 1352 evaluated configurations are non-dominated, representing approximately half of the dataset.

Interestingly, the combination with four objectives –which includes SS^{heat}– exhibits nearly as many non-dominated solutions as the case with five objectives. This observation aligns with the hypothesized correlation between SS^{heat} and ER, which may reduce the conflict between these objectives.

To explore this further, Fig. 5.9 illustrates the Spearman correlation coefficients among design variables and objectives in the evaluated configurations. The goal is to investigate how design variables influence objectives and the interdependencies

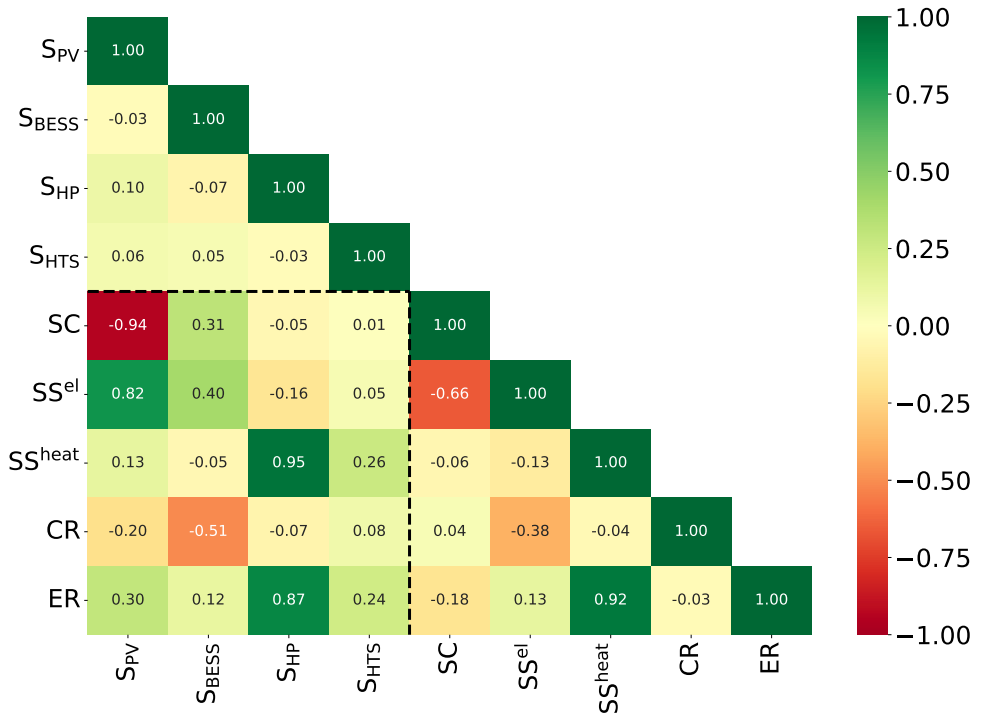

Fig. 5.9 Spearman correlation matrix among design variables and objectives in the evaluated configurations. The top-left triangle, bottom-left square, and bottom-right triangle illustrate correlations among design variables, between design variables and objectives, and among objectives, respectively.

among objectives[1]. Spearman's rank correlation is used instead of Pearson's to capture monotonic relationships rather than strict linear dependencies.

As expected (see Fig. 2.16), PV capacity (S^{PV}) exhibits a strong negative correlation with the self-consumption rate (SC) and a positive correlation with the electrical self-sufficiency rate (SS^{el}. Heat pump capacity (S^{HP}) is positively correlated with both emission reduction (ER) and heating self-sufficiency rate (SS^{heat}). Conversely, the battery energy storage system (BESS) capacity shows a negative correlation with cost reduction (CR).

Among objectives, correlations are generally negative or close to zero, highlighting their conflicting nature. The only exception is the positive correlation between ER and SS^{heat}, confirming earlier observations. Such correlations could bias the selection of compromises by favoring non-conflicting objectives. To ad-

[1]The top-left triangle shows the correlation between design variables. If all configurations were considered, these values would be zero, as the evaluated configurations are uniformly spread across the design space. However, filtering out points with negative CR may have introduced slight biases.

dress this potential bias, subsequent analyses evaluate the optimization problem in both cases.

5.4.4 Scalarization approaches

Two key scalarization approaches are analyzed and applied to the cases with four and five objectives. These are based on (5.7) and (5.8), corresponding to the metrics of closeness to the Utopia point and the Nash product, respectively.

Since these metrics combine different objectives, spanning diverse ranges, normalization prevents bias when evaluating the metrics. In particular, the values are transformed such that the Utopia point assumes value 0 and the Nadir point 1 for all objectives. Since the Nadir point does not always coincide with the absolute worst values of the objectives, normalized values can exceed 1.

The normalization for the i-th objective is defined as:

$$\hat{f}_{\mathrm{i}} = \frac{u_{\mathrm{i}} - f_{\mathrm{i}}}{u_{\mathrm{i}} - d_{\mathrm{i}}} \tag{5.16}$$

where u_{i} and d_{i} are the respective coordinates of the Utopia and Nadir points for the i-th objective.

After normalization, the closeness of each solution $\mathbf{x}$ to the Utopia point is defined as:

$$\text{closeness} = 1 - \left(\sum_{\mathrm{i}} \hat{f}_{\mathrm{i}}(\mathbf{x})^2 \right)^{\frac{1}{2}} \tag{5.17}$$

The Nash product is evaluated as follows:

$$\text{Nash product} = \begin{cases} \prod_{\mathrm{i}} \left(1 - \hat{f}_{\mathrm{i}}(\mathbf{x})\right), & \text{if } \hat{f}_{\mathrm{i}} \leq 1 \quad \forall i, \\ -\prod_{\mathrm{i}} \left|1 - \hat{f}_{\mathrm{i}}(\mathbf{x})\right|, & \text{otherwise.} \end{cases} \tag{5.18}$$

Both metrics can have a maximum value of 1 (in the Utopia point). They do not necessarily have a lower bound, but cannot go below 0 within the Pareto front.

Fig. 5.10 presents a parallel coordinates plot visualizing four normalized objectives: SC, $\mathrm{SS}^{\mathrm{el}}$, ER, and CR. This technique is particularly effective when dealing with more than three objectives, where 2D or 3D scatter plots cannot provide enough clarity [119].

The plot highlights Utopia and Nadir points as horizontal lines at 0 and 1, respectively. Non-dominated solutions are shown in gradients, with the left sub-

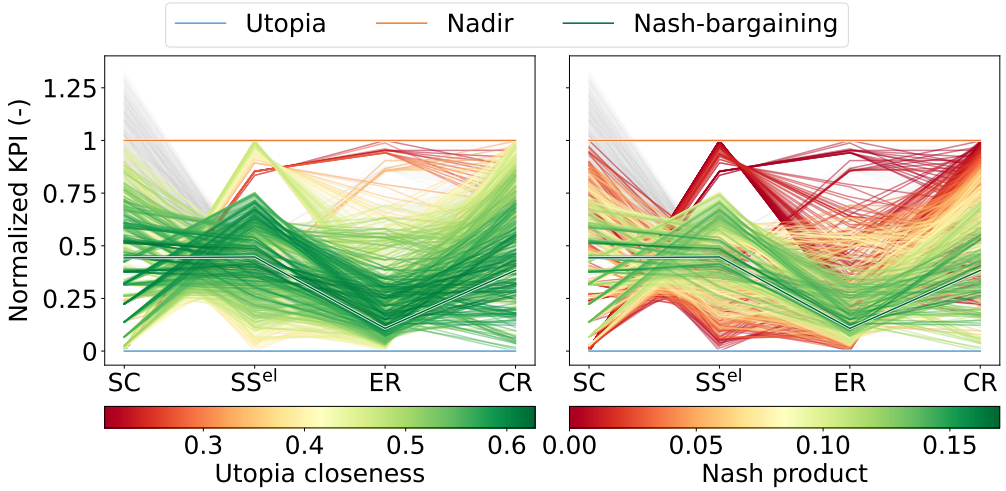

Fig. 5.10 Parallel coordinates plot of four objectives: self-consumption rate (SC), electrical self-sufficiency rate (SS^{el}), emissions reduction (ER), and cost reduction (CR). Dominated solutions are shown in gray. Non-dominated solutions are colored according to closeness to Utopia (left) and Nash product values (right). The Utopia and Nadir points are marked for reference, along with the solutions achieving the highest closeness to Utopia (left) and Nash product (right).

plot colored by closeness to Utopia and the right subplot by the Nash product. Dominated solutions are displayed in gray in the background.

Both subplots highlight how solutions near the middle of the range between Utopia and Nadir tend to exhibit higher values for both metrics, indicating balanced compromises. The Nash product, however, is more selective, as fewer solutions score highly. This is due to its sensitivity to the proximity of individual objectives to the Nadir (given by the product operator). Interestingly, the solution closest to Utopia also maximizes the Nash product, suggesting a strong correlation between these two metrics in identifying balanced compromises.

Fig. 5.11 displays the distribution of the closeness to the Utopia point and Nash product among all evaluated configurations (blue bars in the background) and non-dominated solutions (green bars). As anticipated by the color gradients in the parallel coordinates plot, the distribution of closeness to Utopia appears smooth, with values spread relatively evenly across the range. In contrast, the distribution of Nash product is heavily skewed, with most solutions clustered around lower values and fewer solutions achieving high Nash product values. These different distributions illustrate how these two metrics, although similar in identifying solutions with high values, can lead to distinct interpretations of the

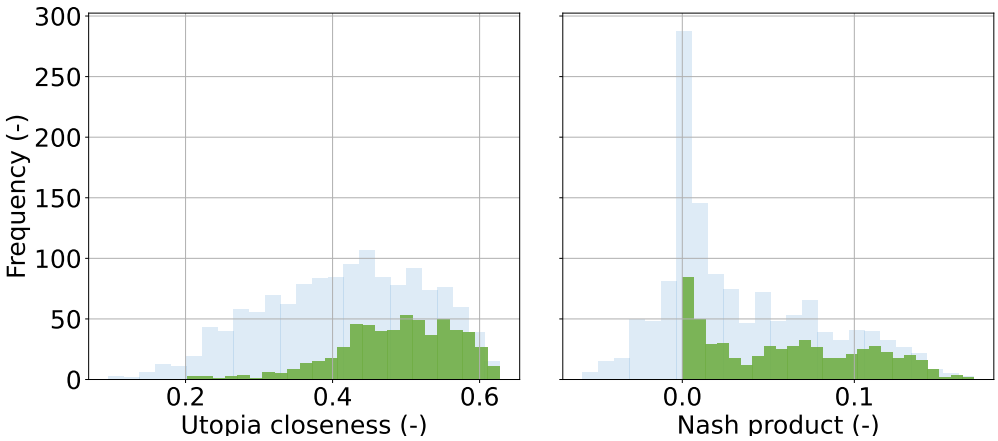

Fig. 5.11 Distribution of closeness to Utopia and Nash product among all evaluated configurations (blue, in the background) and non-dominated solutions (green).

Table 5.3 Design variables and objectives for key solutions in the four-objective case, including the Nadir, Utopia, and solutions closest to Utopia and Nash-bargaining points.

Point	$\mathbf{S}^{\mathrm{PV}}$	$\mathbf{S}^{\mathrm{BESS}}$	$\mathbf{S}^{\mathrm{HP}}$	$\mathbf{S}^{\mathrm{HTS}}$	**SC**	$\mathbf{SS}^{\mathrm{el}}$	**ER**	**CR**	$\mathbf{SS}^{\mathrm{heat}}$
		$\mathrm{kW_p}$	kWh	$\mathrm{kW_{th}}$	kWh	%	%	%	%
Nadir					47.1	11.5	12.4	0.01	
Closest to Utopia	40	55	55	170	76.6	35.6	51.8	14.1	93.5
Nash-bargaining	40	55	55	170	76.6	35.6	51.8	14.1	93.5
Utopia					100	55.1	56.5	22.9	

balance between objectives. The impact of using these metrics in optimization setups is discussed in Section 5.5.

Tab. 5.3 and Tab. 5.4 summarize the design variables and objectives for the solutions with 4 and 5 objectives, respectively.

The primary difference between the two cases lies in the Nadir values. In the 5-objective case, SC decreases slightly, and $\mathrm{SS}^{\mathrm{heat}}$ is introduced, showing a value of 19.5% at the Nadir.

Interestingly, the solution closest to Utopia and the Nash-bargaining solution remain identical between the two cases. This suggests that including $\mathrm{SS}^{\mathrm{heat}}$ does not significantly perturb the optimal solutions, even though it is correlated with emissions reduction (ER).

Table 5.4 Design variables and objectives for key solutions in the five-objective case, including the Nadir, Utopia, and solutions closest to Utopia and Nash-bargaining points.

Point	$\mathbf{S}^{\mathrm{PV}}$	$\mathbf{S}^{\mathrm{BESS}}$	$\mathbf{S}^{\mathrm{HP}}$	$\mathbf{S}^{\mathrm{HTS}}$	**SC**	$\mathbf{SS}^{\mathrm{el}}$	**ER**	**CR**	$\mathbf{SS}^{\mathrm{heat}}$
		$\mathrm{kW_p}$	kWh	$\mathrm{kW_{th}}$	kWh	%	%	%	%
Nadir					38.9	11.5	12.4	0.01	19.5
Closest to Utopia	40	55	55	170	76.6	35.6	51.8	14.1	93.5
Nash-bargaining	40	55	55	170	76.6	35.6	51.8	14.1	93.5
Utopia					100	55.1	56.5	22.9	100

5.5 Discussion

The preliminary results obtained through grid-based sampling of the design space highlight the increasing challenges of many-objective optimization, as well as the potential value of scalarization approaches in addressing these complexities.

As the number of objectives increases, the complexity of the problem grows, as evidenced by the rising number of non-dominated solutions. This increase complicates the exploration of higher-dimensional Pareto fronts and presents significant challenges for Pareto dominance-based algorithms, particularly population-based metaheuristics, which would require larger populations to approximate the front adequately. As shown in Chapter 3, accurate ICES performance assessment requires optimization problems whose complexity increases with the size of the ICES. Thus, reducing the number of optimization routine calls during the design optimization phase is crucial.

Scalarization approaches, which combine multiple objectives into a single metric, offer a practical alternative for navigating these challenges. These approaches also facilitate balancing conflicting objectives among individual energy nodes within the ICES. Metrics such as the closeness to the Utopia point and the Nash product facilitate the identification of balanced trade-offs without requiring exhaustive exploration of the Pareto front.

A comparison of these two metrics reveals notable differences in their distributions among the evaluated configurations. Closeness to the Utopia point exhibits a smoother distribution, with many solutions achieving high values, which can result in challenges such as multiple local maxima and multimodality. In contrast, the Nash product shows a skewed distribution, with many solutions concentrated around the value of 0 and only a few achieving higher values, thereby reducing the risk of local maxima.

These two metrics could be complementary in optimization applications (e.g., utilizing metaheuristic algorithms). Closeness to the Utopia point may be more suited for guiding the search toward promising regions of the design space during the early stages of optimization (exploration). Conversely, the Nash product, being more selective, can be better suited for local refinement in the later stages of optimization (exploitation).

Notably, increasing the number of objectives to include heating self-sufficiency, which correlates with emission reduction, did not significantly alter the results in this study. This consistency may be due to the discretization of the design space or the metrics' insensitivity to correlated objectives. However, further investigation is needed to validate these hypotheses and understand the implications for more complex configurations.

While the grid-based approach provides initial insights, more detailed analyses in diverse settings are required to draw definitive conclusions. Future work should test these metrics in real optimization scenarios of ICES design, where conflicting stakeholder objectives make such strategies especially relevant. Effectively addressing many-objective problems in these contexts requires robust strategies, and game-theory-based approaches, such as the Nash product, appear particularly promising for practical applications.

Conclusion

Integrated Community Energy Systems (ICES) offer a comprehensive framework for addressing community energy needs across multiple energy carriers, while Renewable Energy Communities (RECs) provide a practical way to put these principles in effect within existing regulatory and market landscapes. Therefore, these systems emerge as key solutions in shaping future energy systems, where the role of citizens and communities will be pivotal.

This thesis contributes to advancing research on ICES and RECs by providing a comprehensive framework for modeling and assessing these systems, and by formalizing and testing methodologies for their optimization. In particular, this work focused on three key areas: the optimal energy management of ICES, data-driven prediction of energy consumption profiles, and the multi-objective design optimization of energy systems. Each area addressed fundamental challenges, formalizing methodologies and exploring innovative solutions tailored to the characteristics of ICES and RECs.

The optimal energy management framework developed in Chapter 3 introduced a multi-node, multi-energy model leveraging Mixed-Integer Linear Programming (MILP). Testing this framework demonstrated that:

- Collective optimization strategies and detailed multi-node modeling are necessary to properly assess economic, energy, and environmental performance.
- Consolidated MILP optimization solvers can handle complex multi-node and multi-energy systems. However, scalability issues arise with increasing ICES size (e.g., number of active nodes), necessitating trade-offs between model accuracy and computational complexity.

The observed correlations between collective and individual optimization results suggest opportunities for future research to integrate data-driven approximations, enhancing scalability and computational efficiency.

Operational optimization often relies on high-resolution data, which may not always be available, particularly for energy consumption diverse and numerous end users. To address this limitation, Chapter 4 proposed a data-driven methodology using k-nearest neighbors (k-NN) regression to predict energy consumption profiles from minimal input data, such as time-of-use energy bills.

- This method demonstrated superior accuracy compared to traditional benchmarks, particularly for non-residential end users.
- The practicality of these predictions was validated in applications to ICES assessment and optimization.

Future research should refine this methodology by exploring category-specific models, incorporating seasonal variability, and assessing the impact of individual-level errors on final outcomes.

The thesis addressed the design optimization of ICES as a many-objective problem in Chapter 5, through preliminary work that explored the optimization problem by sampling the design space and analyzing the optimization landscape with an increasing number of objectives. Pareto-dominance-based assessments revealed how non-dominated solutions increase with additional objectives, complicating optimization tasks. To navigate this complexity, scalarization approaches combining objectives into a single metric were analyzed. The traditional closeness to the Utopia point was evaluated alongside a game-theory-inspired approach based on the Nash product.

- The analyses highlighted both metrics' capacity to identify balanced compromises, with the Nash product being more selective than closeness to the Utopia point.
- These insights suggest that the two metrics could be complementary, with each serving distinct stages of optimization, such as exploration and exploitation.

However, these findings remain preliminary, as the optimization itself was not performed, and further studies are necessary to validate their applicability in real-world scenarios.

Despite its contributions, the field of ICES modeling and optimization still requires significant attention in areas not covered by this thesis. Apart from specific improvements to the proposed methods, advancements are needed in addressing uncertainties in energy generation and consumption data. The thesis focused on deterministic assessments, while real-world scenarios often involve variability. Sensitivity analysis can help propagate the uncertainties on the model inputs (energy data and prices) to the output of the optimization runs. Moreover, robust optimization methods could provide solutions that account for these uncertainties, but they further complicate the problem and emphasize the need for computationally efficient techniques. In this context, leveraging data-driven and machine-learning methods to approximate optimal solutions appears crucial.

Real-time operation of ICES also presents significant challenges, as highlighted in Chapter 3. The findings demonstrated that ICES performance is highly sensitive to the optimal management of available resources. For instance, collective optimization greatly improves economic outcomes, but achieving such coordination in practical settings remains difficult. Future research should explore methods to enable real-time collective optimization, bridging the gap between theoretical frameworks and operational feasibility.

The thesis also offered insights on how game theory concepts, commonly deployed in community energy systems to design business models, can be integrated into system design problems to find compromise solutions among many conflicting objectives. However, only a simplified case was considered. In real-world settings, more complex scenarios typically arise, where, beyond ICES-level performance objectives, individual stakeholder objectives also play a critical role. Future work should therefore test these methods in more complex contexts.

References

[1] European Parliament & Council of the European Union, "Directive (EU) 2018/2001 on the promotion of the use of energy from renewable sources," 2018. [Online]. Available: https://eur-lex.europa.eu/eli/dir/2018/2001/oj

[2] A. Caramizaru and A. Uihlein, "Energy communities: an overview of energy and social innovation," https://publications.jrc.ec.europa.eu/repository/handle/JRC119433, 2020.

[3] European Commission: Directorate-General for Energy, "Clean Energy for all Europeans," 2019. [Online]. Available: https://energy.ec.europa.eu/topics/energy-strategy/clean-energy-all-europeans-package_en

[4] A. Cielo, P. Lazzeroni, P. Margiaria, I. Mariuzzo, and M. Repetto, "Renewable Energy Communities business models under the 2020 Italian regulation," *Journal of Cleaner Production*, vol. 316, p. 128217, 2021, doi:10.1016/j.jclepro.2021.128217.

[5] V. Z. Gjorgievski, S. Cundeva, and G. E. Georghiou, "Social arrangements, technical designs and impacts of energy communities: A review," *Renewable Energy*, vol. 169, pp. 1138–1156, 2021.

[6] E. Giarmanà, "Managing renewable electricity within collective self-consumption schemes: A systematic private law approach," *Renewable and Sustainable Energy Reviews*, vol. 188, p. 113896, 2023, doi:10.1016/j.rser.2023.113896.

[7] D. de São José, P. Faria, and Z. Vale, "Smart energy community: A systematic review with metanalysis," *Energy Strategy Reviews*, vol. 36, p. 100678, 2021, doi:10.1016/j.esr.2021.100678.

[8] B. P. Koirala, E. Koliou, J. Friege, R. A. Hakvoort, and P. M. Herder, "Energetic communities for community energy: A review of key issues and trends shaping integrated community energy systems," *Renewable and Sustainable Energy Reviews*, vol. 56, pp. 722–744, 2016, doi:10.1016/j.rser.2015.11.080.

[9] M. Fodstad, P. Crespo del Granado, L. Hellemo, B. R. Knudsen, P. Pisciella, A. Silvast, C. Bordin, S. Schmidt, and J. Straus, "Next frontiers in energy system modelling: A review on challenges and the state of the art," *Renewable and Sustainable Energy Reviews*, vol. 160, p. 112246, 2022, doi:10.1016/j.rser.2022.112246.

[10] I. F.G. Reis, I. Gonçalves, M. A.R. Lopes, and C. Henggeler Antunes, "Business models for energy communities: A review of key issues and trends," *Renewable and Sustainable Energy Reviews*, vol. 144, p. 111013, 2021.

[11] A. Canova, P. Lazzeroni, G. Lorenti, F. Moraglio, A. Porcelli, and M. Repetto, "Decarbonizing residential energy consumption under the Italian collective self-consumption regulation," *Sustainable Cities and Society*, vol. 87, p. 104196, 2022, doi:10.1016/j.scs.2022.104196.

[12] J. M. Schwidtal, P. Piccini, M. Troncia, R. Chitchyan, M. Montakhabi, C. Francis, A. Gorbatcheva, T. Capper, M. A. Mustafa, M. Andoni, V. Robu, M. Bahloul, I. J. Scott, T. Mbavarira, J. M. España, and L. Kiesling, "Emerging business models in local energy markets: A systematic review of peer-to-peer, community self-consumption, and transactive energy models," *Renewable and Sustainable Energy Reviews*, vol. 179, p. 113273, 2023, doi:10.1016/j.rser.2023.113273.

[13] G. Lorenti, P. Lazzeroni, and M. Repetto, "A Data-Driven Approach to Predict Hourly Load Profiles From Time-of-Use Electricity Bills," *IEEE Access*, vol. 11, pp. 60 501–60 515, 2023, doi:10.1109/ACCESS.2023.3286020.

[14] F. Gullì, P. Lazzeroni, G. Lorenti, I. Mariuzzo, F. Moraglio, and M. Repetto, "Recoupled: A simulation tool for renewable energy communities coupling electric and thermal energies," *ECONOMICS AND POLICY OF ENERGY AND THE ENVIRONMENT*, vol. 2/2022, pp. 49–60, 2022, doi:10.3280/EFE2022-002003.

[15] G. Lorenti, P. Lazzeroni, and M. Repetto, "A Game Theory Approach to the Multi-Objective Design of Renewable Energy Communities," in *2024 International Conference on Smart Energy Systems and Technologies (SEST)*, 2024, pp. 1–6.

[16] P. Lazzeroni, G. Lorenti, F. Moraglio, and M. Repetto, "Modeling of Renewable Energy Communities: the RECoupled approach," in *2022 IEEE 46th Annual Computers, Software, and Applications Conference (COMPSAC)*, 2022, pp. 1349–1354, doi:10.1109/COMPSAC54236.2022.00213.

[17] ——, "A MILP Approach for Demand Management in Renewable Energy Communities with Residential End-Users," in *36th International Conference on Efficiency, Cost, Optimization, Simulation and Environmental Impact of Energy Systems (ECOS 2023)*, 2023, doi:10.52202/069564-0229.

[18] G. Lorenti, C. S. Ragusa, M. Repetto, and L. Solimene, "Data-driven constraint handling in multi-objective inductor design," *Electronics*, vol. 12, no. 4, 2023, doi:10.3390/electronics12040781.

[19] G. Lorenti, I. Mariuzzo, F. Moraglio, and M. Repetto, "Heuristic optimization applied to ANN training for predicting renewable energy sources production," *COMPEL The International Journal for Computation and Mathematics*

in Electrical and Electronic Engineering, 2022, doi:10.1108/COMPEL-11-2021-0420.

[20] M. Repetto, F. Moraglio, and G. Lorenti, "Understanding reinforcement learning control in cyber-physical energy systems," in *2022 10th Workshop on Modelling and Simulation of Cyber-Physical Energy Systems (MSCPES)*, 2022, pp. 1–6, doi:10.1109/MSCPES55116.2022.9770172.

[21] L. Solimene, S. Ferrari, C. Anerdi, F. Freschi, L. Giaccone, G. Lorenti, F. Lucchini, R. Torchio, P. Alotto, G. Pellegrino, and M. Repetto, "Data-Driven Approaches for Electromagnetic Analysis of Traction Electrical Motors: A Proposal for a Benchmark Problem," in *2024 International Conference on Electrical Machines (ICEM)*, 2024, pp. 1–7, doi:10.1109/ICEM60801.2024.10700274.

[22] G. Lorenti, C. S. Ragusa, M. Repetto, and L. Solimene, "Support vector classifier for constraints handling in the design of inductors for dc-dc converters," in *2023 24th International Conference on the Computation of Electromagnetic Fields (COMPUMAG)*, 2023, pp. 1–4, doi:10.1109/COMPUMAG56388.2023.10411814.

[23] M. Farrokhabadi, C. A. Cañizares, J. W. Simpson-Porco, E. Nasr, L. Fan, P. A. Mendoza-Araya, R. Tonkoski, U. Tamrakar, N. Hatziargyriou, D. Lagos, R. W. Wies, M. Paolone, M. Liserre, L. Meegahapola, M. Kabalan, A. H. Hajimiragha, D. Peralta, M. A. Elizondo, K. P. Schneider, F. K. Tuffner, and J. Reilly, "Microgrid stability definitions, analysis, and examples," *IEEE Transactions on Power Systems*, vol. 35, no. 1, pp. 13–29, 2020, doi:10.1109/TPWRS.2019.2925703.

[24] K. Schaber, F. Steinke, and T. Hamacher, "Managing Temporary Oversupply from Renewables Efficiently: Electricity Storage Versus Energy Sector Coupling in Germany," in *International Energy Workshop 2013*, 2013. [Online]. Available: https://www.internationalenergyworkshop.org/docs/IEW%202013_4E3paperSchaber.pdf

[25] T. van der Schoor and B. Scholtens, "Power to the people: Local community initiatives and the transition to sustainable energy," *Renewable and Sustainable Energy Reviews*, vol. 43, pp. 666–675, 2015, doi:10.1016/j.rser.2014.10.089.

[26] Governo della Repubblica Italiana, "Testo del decreto-legge 30 dicembre 2019, n. 162, coordinato con la legge di conversione 28 febbraio 2020, n. 8 [Text of the Decree-Law of 30 December 2019, no. 162, coordinated with the conversion law of 28 February 2020, no. 8]," 2020, in Italian. [Online]. Available: https://www.gazzettaufficiale.it/eli/id/2020/02/29/20A01353/sg

[27] ARERA, "Delibera 318/2020/R/EEL 4 agosto 2020: Regolazione delle partite economiche relative all'energia elettrica condivisa da un gruppo di autoconsumatori di energia rinnovabile che agiscono collettivamente

in edifici e condomini oppure condivisa in una comunità di energia rinnovabile [Resolution 318/2020/R/EEL August 4, 2020: Regulation of economic matches related to electricity shared by a group of self-consumers of renewable energy acting collectively in buildings and condominiums or shared in a renewable energy community]," 2020, in Italian. [Online]. Available: https://www.arera.it/atti-e-provvedimenti/dettaglio/20/318-20

[28] Ministero dello Sviluppo Economico, "Decreto Ministeriale 16 settembre 2020 - Individuazione della tariffa incentivante per la remunerazione degli impianti a fonti rinnovabili inseriti nelle configurazioni sperimentali di autoconsumo collettivo e comunità energetiche rinnovabili [Ministerial Decree September 16, 2020 - Identification of the incentive tariff for the remuneration of renewable energy plants included in the experimental configurations of collective self-consumption and renewable energy communities]," 2020, in Italian. [Online]. Available: https://www.gazzettaufficiale.it/eli/id/2020/11/16/20A06224/sg

[29] GSE, "Regole tecniche per l'accesso al servizio di valorizzazione e incentivazione dell'energia elettrica condivisa [Technical rules for access to the shared power enhancement and incentive service]," 2020, in Italian. [Online]. Available: https://tinyurl.com/GSE-Regole-tecniche-CER

[30] Governo della Repubblica Italiana, "Testo del decreto legislativo 8 novembre 2021, n. 199: Attuazione della direttiva (UE) 2018/2001 del Parlamento europeo e del Consiglio, dell'11 dicembre 2018, sulla promozione dell'uso dell'energia da fonti rinnovabili [Text of Legislative Decree of 8 November 2021, no. 199: Implementation of Directive (EU) 2018/2001 of the European Parliament and of the Council of 11 December 2018, on the promotion of the use of energy from renewable sources]," 2021, in Italian. [Online]. Available: https://www.gazzettaufficiale.it/eli/id/2021/11/30/21G00214/sg

[31] ARERA, "Delibera 727/2022/R/eel 27 dicembre 2022: Definizione, ai sensi del decreto legislativo 199/21 e del decreto legislativo 210/21, della regolazione dell'autoconsumo diffuso. Approvazione del Testo Integrato Autoconsumo Diffuso (TIAD) [Resolution 727/2022/R/eel December 27, 2022: Definition, pursuant to Legislative Decree 199/21 and Legislative Decree 210/21, of the regulation of diffuse self-consumption. Approval of the Integrated Text for Diffuse Self-Consumption (TIAD)]," 2022, in Italian. [Online]. Available: https://www.arera.it/fileadmin/allegati/docs/22/727-22TIAD.pdf

[32] Ministero dello'Ambiente e della SIcurezza Energetica, "Decreto Ministeriale 7 dicembre 2023, n. 414 - Individuazione di una tariffa incentivante per impianti a fonti rinnovabili inseriti in comunita' energetiche rinnovabili e nelle configurazioni di autoconsumo singolo a distanza e collettivo [Ministerial Decree No. 414 of December 7, 2023 - Identification of an incentive tariff for renewable energy systems included in renewable energy communities and in remote and collective single

self-consumption configurations],” 2024, in Italian. [Online]. Available: https://www.mase.gov.it/sites/default/files/Decreto%20CER.pdf

[33] GSE, “Decreto CACER e TIAD – Regole operative per l’accesso al servizio per l’autoconsumo diffuso e al contributo PNRR [CACER and TIAD Decree - Operational rules for accessing the service for widespread self-consumption and the PNRR grant],” 2024, in Italian. [Online]. Available: https://www.gse.it/servizi-per-te/news/cacer-aggiornate-le-regole-operative-e-pubblicato-il-decreto-corrispettivi

[34] GME, “Mercato elettrico [Eletricity market],” 2024, in Italian. [Online]. Available: https://www.mercatoelettrico.org/

[35] ARERA, “Elettricità: prezzi e tariffe [Electricity: prices and tariffs],” 2024. [Online]. Available: https://www.arera.it/dati-e-statistiche?ambito=55&keyword=&settore=4&orderby=

[36] Enedis, “Collective Self-Consumption overview in France,” 2021. [Online]. Available: https://flux50.com/media/5757/05%20Enedis.pdf

[37] H. Radet, “Integrated design methods for distributed multi-energy systems under uncertainties,” Ph.D. dissertation, Ecole doctorale Génie électrique, électronique, télécommunications et santé : du système au nanosystème (Toulouse), 2022. [Online]. Available: https://theses.fr/2022INPT0023

[38] J. Coignard, “Local Energy community: sharing energy resources connected to the distribution grid,” Ph.D. dissertation, Université Grenoble Alpes, Grenoble, France, 2022. [Online]. Available: https://theses.hal.science/tel-03957669

[39] NREL, “Life Cycle Greenhouse Gas Emissions from Solar Photovoltaics,” 2012. [Online]. Available: https://www.nrel.gov/docs/fy13osti/56487.pdf

[40] C. Boennec, L. Albuquerque, B. Sareni, F. Lacressonnière, and S. U. Ngueveu, “Comparison of Battery Models Integrating Energy Efficiency and Aging for the Design of Microgrids,” *Smart Grids and Energy*, vol. 9, pp. 1–20, 2024, doi:10.1007/s40866-023-00174-1.

[41] D. Fioriti, A. Frangioni, and D. Poli, “Optimal Sizing of Energy Communities with Fair Revenue Sharing and Exit Clauses: Value, Role and Business Model of Aggregators and Users,” *Applied Energy*, vol. 299, p. 117328, 2021, doi:10.1016/j.apenergy.2021.117328.

[42] ODYSSEE-MURE, “Electricity consumption per dwelling,” 2024. [Online]. Available: https://www.odyssee-mure.eu/publications/efficiency-by-sector/households/electricity-consumption-dwelling.html

[43] Joint Research Center, “Photovoltaic Geographical Information System (PVGIS),” 2018. [Online]. Available: https://joint-research-centre.ec.europa.eu/photovoltaic-geographical-information-system-pvgis_en

[44] Valentin Software, "PV*SOL premium: The design and simulation software for photovoltaic systems," 2024. [Online]. Available: https://valentin-software.com/en/products/pvsol-premium/

[45] CEN, "EN 12831-1:2017 – Energy performance of buildings - Method for calculation of the design heat load - Part 1: Space heating load," 2017.

[46] V. Corrado, I. Ballarini, and S. P. Corgnati, "Building Typology Brochure - Ialy," 2014. [Online]. Available: https://episcope.eu/fileadmin/tabula/public/docs/brochure/IT_TABULA_TypologyBrochure_POLITO.pdf

[47] JRC, "Typical Meteorological Year generator," 2021. [Online]. Available: https://ec.europa.eu/jrc/en/PVGIS/tools/tmy

[48] TERNA, "Electricity market," 2024. [Online]. Available: https://www.terna.it/en/electric-system/electricity-market

[49] ARERA, "Dati e statistiche [data and statistics]," 2024, in Italian. [Online]. Available: https://www.arera.it/dati-e-statistiche

[50] ISPRA, "Fattori di emissione per la produzione ed il consumo di energia elettrica in Italia [Emissions factors for electricity production and consumption in Italy]," 2024, in Italian. [Online]. Available: https://emissioni.sina.isprambiente.it/wp-content/uploads/2024/02/FE_energia_elettrica_2023-V1.xlsx

[51] ——, "Italian Greenhouse Gas Inventory, 1990-2020, National Inventory Report," 2022. [Online]. Available: https://www.isprambiente.gov.it/files2022/pubblicazioni/rapporti/nir2022_italy_r360.pdf

[52] C. Klemm and P. Vennemann, "Modeling and optimization of multi-energy systems in mixed-use districts: A review of existing methods and approaches," *Renewable and Sustainable Energy Reviews*, vol. 135, p. 110206, 2021, doi:10.1016/j.rser.2020.110206.

[53] E. Widl, D. Cronbach, P. Sorknæs, J. Fitó, D. Muschick, M. Repetto, J. Ramousse, and A. Ianakiev, "Expert survey and classification of tools for modeling and simulating hybrid energy networks," *Sustainable Energy, Grids and Networks*, vol. 32, 2022, 10.1016/j.segan.2022.100913.

[54] S. Rech, "Smart Energy Systems: Guidelines for Modelling and Optimizing a Fleet of Units of Different Configurations," *Energies*, vol. 12, no. 7, p. 1320, 2019, doi:10.3390/en12071320.

[55] G. Chicco and A. Mazza, "Metaheuristic optimization of power and energy systems: Underlying principles and main issues of the 'rush to heuristics'," *Energies*, vol. 13, no. 19, 2020, doi:10.3390/en13195097.

[56] E. Barabino, D. Fioriti, E. Guerrazzi, I. Mariuzzo, D. Poli, M. Raugi, E. Razaei, E. Schito, and D. Thomopulos, "Energy Communities: A review on trends, energy system modelling, business models, and optimisation objectives," *Sustainable Energy, Grids and Networks*, vol. 36, p. 101187, 2023.

[57] G. Coletta and L. Pellegrino, "Optimal Design of Energy Communities in the Italian Regulatory Framework," in *2021 AEIT International Annual Conference (AEIT)*, 2021, pp. 1–6, doi:10.23919/AEIT53387.2021.9626852.

[58] A. Cosic, M. Stadler, M. Mansoor, and M. Zellinger, "Mixed-integer linear programming based optimization strategies for renewable energy communities," *Energy*, vol. 237, p. 121559, 2021, doi:10.1016/j.energy.2021.121559.

[59] M. Zatti, M. Moncecchi, M. Gabba, A. Chiesa, F. Bovera, and M. Merlo, "Energy Communities Design Optimization in the Italian Framework," *Applied Sciences*, vol. 11, no. 11, 2021, doi:10.3390/app11115218.

[60] A. Bartolini, F. Carducci, C. B. Muñoz, and G. Comodi, "Energy storage and multi energy systems in local energy communities with high renewable energy penetration," *Renewable Energy*, vol. 159, pp. 595–609, 2020, doi:10.1016/j.renene.2020.05.131.

[61] I. Mariuzzo, D. Fioriti, E. Guerrazzi, D. Thomopulos, and M. Raugi, "Multi-objective planning method for renewable energy communities with economic, environmental and social goals," *International Journal of Electrical Power & Energy Systems*, vol. 153, p. 109331, 2023, doi:10.1016/j.ijepes.2023.109331.

[62] R. J. De Souza, M. Reini, L. M. Serra, M. A. Lozano, E. Nadalon, and M. Casisi, "Multi-Objective Optimization of an Energy Community Powered by a Distributed Polygeneration System," *Energies*, vol. 17, no. 13, 2024, 10.3390/en17133085.

[63] E. Dal Cin, G. Carraro, G. Volpato, A. Lazzaretto, and P. Danieli, "A multi-criteria approach to optimize the design-operation of Energy Communities considering economic-environmental objectives and demand side management," *Energy Conversion and Management*, vol. 263, p. 115677, 2022, doi:10.1016/j.enconman.2022.115677.

[64] CADEMA, "RECOpt - Renewable Energy Communities Optimization," 2021. [Online]. Available: https://github.com/cadema-PoliTO/RECOpt

[65] GSE - Gestore dei Servizi Energetici, "Regole tecniche per l'attuazione delle disposizioni relative all'integrazione di sistemi di accumulo di energia elettrica nel sistema elettrico Nazionale [Technical rules for the implementation of provisions for the integration of electricity storage systems into the National Electricity System]." 2021. [Online]. Available: https://tinyurl.com/GSE-Regole-tecniche-accumulo

[66] R. A. Horn, *Topics in Matrix Analysis*. Cambridge University Press, 1991, ch. The Hadamard product, doi:10.1017/CBO9780511840371.

[67] S. P. Bradley, A. C. Hax, and T. L. Magnanti, *Applied Mathematical Programming*. Addison-Wesley, 1977. [Online]. Available: https://web.mit.edu/15.053/www/AMP.htm

[68] X. Kang, J. An, and D. Yan, "A systematic review of building electricity use profile models," *Energy and Buildings*, vol. 281, p. 112753, 2023, doi:10.1016/j.enbuild.2022.112753.

[69] E. Proedrou, "A comprehensive review of residential electricity load profile models," *IEEE Access*, vol. 9, pp. 12 114–12 133, 2021, doi:10.1109/ACCESS.2021.3050074.

[70] T. Räsänen, D. Voukantsis, H. Niska, K. Karatzas, and M. Kolehmainen, "Data-based method for creating electricity use load profiles using large amount of customer-specific hourly measured electricity use data," *Applied Energy*, vol. 87, no. 11, pp. 3538–3545, 2010, doi:10.1016/j.apenergy.2010.05.015.

[71] A. Rajabi, M. Eskandari, M. J. Ghadi, L. Li, J. Zhang, and P. Siano, "A comparative study of clustering techniques for electrical load pattern segmentation," *Renewable and Sustainable Energy Reviews*, vol. 120, p. 109628, 2020, doi:10.1016/j.rser.2019.109628.

[72] GSE - Gestore dei Servizi Energetici, "Modalità di profilazione dei dati di misura e relative modalità di utilizzo [Modes for measured data profiling and their usage]." 2022. [Online]. Available: https://tinyurl.com/GSE-Profilazione

[73] S. Köhler, R. Rongstock, M. Hein, and U. Eicker, "Similarity measures and comparison methods for residential electricity load profiles," *Energy and Buildings*, vol. 271, p. 112327, 2022, doi:10.1016/j.enbuild.2022.112327.

[74] G. Chicco, "Overview and performance assessment of the clustering methods for electrical load pattern grouping," *Energy*, vol. 42, no. 1, pp. 68–80, 2012, doi:10.1016/j.energy.2011.12.031.

[75] Y. Wang, Q. Chen, T. Hong, and C. Kang, "Review of Smart Meter Data Analytics: Applications, Methodologies, and Challenges," *IEEE Transactions on Smart Grid*, vol. 10, no. 3, pp. 3125–3148, 2019, doi:10.1109/TSG.2018.2818167.

[76] Y. Zhao, C. Zhang, Y. Zhang, Z. Wang, and J. Li, "A review of data mining technologies in building energy systems: Load prediction, pattern identification, fault detection and diagnosis," *Energy and Built Environment*, vol. 1, no. 2, pp. 149–164, 2020, doi:10.1016/j.enbenv.2019.11.003.

[77] T. Fu, "A review on time series data mining," *Engineering Applications of Artificial Intelligence*, vol. 24, no. 1, pp. 164–181, 2011, doi:10.1016/j.engappai.2010.09.007.

[78] T. Hong, P. Pinson, Y. Wang, R. Weron, D. Yang, and H. Zareipour, "Energy Forecasting: A Review and Outlook," *IEEE Open Access Journal of Power and Energy*, vol. 7, pp. 376–388, 2020, doi:10.1109/OAJPE.2020.3029979.

[79] X. Luo, T. Hong, Y. Chen, and M. A. Piette, "Electric load shape benchmarking for small- and medium-sized commercial buildings," *Applied Energy*, vol. 204, pp. 715–725, 2017, doi:10.1016/j.apenergy.2017.07.108.

[80] S. Eiraudo, L. Barbierato, R. Giannantonio, A. Porta, A. Lanzini, R. Borchiellini, E. Macii, E. Patti, and L. Bottaccioli, "A Machine Learning Based Methodology for Load Profiles Clustering and Non-Residential Buildings Benchmarking," *IEEE Transactions on Industry Applications*, vol. 59, no. 3, pp. 2963–2973, 2023, doi:10.1109/TIA.2023.3240669.

[81] F. D. Minuto, P. Lazzeroni, R. Borchiellini, S. Olivero, L. Bottaccioli, and A. Lanzini, "Modeling technology retrofit scenarios for the conversion of condominium into an energy community: An Italian case study," *Journal of Cleaner Production*, vol. 282, p. 124536, 2021, doi:10.1016/j.jclepro.2020.124536.

[82] D. Vercamer, B. Steurtewagen, D. Van den Poel, and F. Vermeulen, "Predicting Consumer Load Profiles Using Commercial and Open Data," *IEEE Transactions on Power Systems*, vol. 31, no. 5, pp. 3693–3701, 2016, doi:10.1109/TPWRS.2015.2493083.

[83] J. L. Viegas, S. M. Vieira, R. Melício, V. M. F. Mendes, and J. M. Sousa, "Classification of new electricity customers based on surveys and smart metering data," *Energy*, vol. 107, pp. 804–817, 2016, doi:10.1016/j.energy.2016.04.065.

[84] M. S. Piscitelli, S. Brandi, and A. Capozzoli, "Recognition and classification of typical load profiles in buildings with non-intrusive learning approach," *Applied Energy*, vol. 255, p. 113727, 2019, doi:10.1016/j.apenergy.2019.113727.

[85] J. Y. Park, X. Yang, C. Miller, P. Arjunan, and Z. Nagy, "Apples or oranges? Identification of fundamental load shape profiles for benchmarking buildings using a large and diverse dataset," *Applied Energy*, vol. 236, pp. 1280–1295, 2019, doi:10.1016/j.apenergy.2018.12.025.

[86] A. Mutanen, M. Ruska, S. Repo, and P. Jarventausta, "Customer Classification and Load Profiling Method for Distribution Systems," *IEEE Transactions on Power Delivery*, vol. 26, no. 3, pp. 1755–1763, 2011, doi:10.1109/TPWRD.2011.2142198.

[87] S. Zhan, Z. Liu, A. Chong, and D. Yan, "Building categorization revisited: A clustering-based approach to using smart meter data for building energy benchmarking," *Applied Energy*, vol. 269, p. 114920, 2020, doi:10.1016/j.apenergy.2020.114920.

[88] C. M. Bishop, *Pattern Recognition and Machine Learning (Information Science and Statistics)*. Berlin, Heidelberg: Springer-Verlag, 2006.

[89] K. le Zhou, S. lin Yang, and C. Shen, "A review of electric load classification in smart grid environment," *Renewable and Sustainable Energy Reviews*, vol. 24, pp. 103–110, 2013, doi:10.1016/j.rser.2013.03.023.

[90] R. Granell, C. J. Axon, M. Kolokotroni, and D. C. Wallom, "A data-driven approach for electricity load profile prediction of new supermarkets," *Energy Procedia*, vol. 161, pp. 242–250, 2019, doi:10.1016/j.egypro.2019.02.087.

[91] ARERA, "Proposte in materia di definizione delle fasce orarie per l'anno 2007 e successivi [Proposals for the definition of the time-of-use time slots starting from year 2007.]," 2006. [Online]. Available: https://www.arera.it/it/docs/06/181-06.htm

[92] N. S. Altman, "An Introduction to Kernel and Nearest-Neighbor Nonparametric Regression," *The American Statistician*, vol. 46, no. 3, pp. 175–185, 1992, doi:10.1080/00031305.1992.10475879.

[93] S. A. Dudani, "The Distance-Weighted k-Nearest-Neighbor Rule," *IEEE Transactions on Systems, Man, and Cybernetics*, vol. SMC-6, no. 4, pp. 325–327, 1976, doi:10.1109/TSMC.1976.5408784.

[94] T.-T. Wong, "Performance evaluation of classification algorithms by k-fold and leave-one-out cross validation," *Pattern Recognition*, vol. 48, no. 9, pp. 2839–2846, 2015, doi:10.1016/j.patcog.2015.03.009.

[95] "Scikit-learn: Machine Learning in Python," 2024. [Online]. Available: https://scikit-learn.org/

[96] F. Pedregosa, G. Varoquaux, A. Gramfort, V. Michel, B. Thirion, O. Grisel, M. Blondel, P. Prettenhofer, R. Weiss, V. Dubourg, J. Vanderplas, A. Passos, D. Cournapeau, M. Brucher, M. Perrot, and E. Duchesnay, "Scikit-learn: Machine learning in python," *Journal of Machine Learning Research*, vol. 12, no. 85, pp. 2825–2830, 2011. [Online]. Available: https://jmlr.csail.mit.edu/papers/v12/pedregosa11a.html

[97] A. Manso-Burgos, D. Ribó-Pérez, T. Gómez-Navarro, and M. Alcázar-Ortega, "Local energy communities modelling and optimisation considering storage, demand configuration and sharing strategies: A case study in Valencia (Spain)," *Energy Reports*, vol. 8, pp. 10 395–10 408, 2022, doi:10.1016/j.egyr.2022.08.181.

[98] E. Bakhtavar, T. Prabatha, H. Karunathilake, R. Sadiq, and K. Hewage, "Assessment of renewable energy-based strategies for net-zero energy communities: A planning model using multi-objective goal programming," *Journal of Cleaner Production*, vol. 272, p. 122886, 2020, doi:10.1016/j.jclepro.2020.122886.

[99] S.-H. Park, Y.-S. Jang, and E.-J. Ki, "Multi-objective optimization for sizing multi-source renewable energy systems in the community center of a residential apartment complex," *Energy Conversion and Management*, vol. 244, p. 114446, 2021, doi:10.1016/j.enconman.2021.114446.

[100] K. Yang, Y. Ding, N. Zhu, F. Yang, and Q. Wang, "Multi-criteria integrated evaluation of distributed energy system for community energy planning based on improved grey incidence approach: A case study in Tianjin," *Applied Energy*, vol. 229, pp. 352—-363, 2018, doi:10.1016/j.apenergy.2018.08.016.

[101] R. Evins, "A review of computational optimisation methods applied to sustainable building design," *Renewable and Sustainable Energy Reviews*, vol. 22, pp. 230–245, 2013, doi:10.1016/j.rser.2013.02.004.

[102] I. Rahman, P. M. Vasant, B. S. M. Singh, M. Abdullah-Al-Wadud, and N. Adnan, "Review of recent trends in optimization techniques for plug-in hybrid, and electric vehicle charging infrastructures," *Renewable and Sustainable Energy Reviews*, vol. 58, pp. 1039–1047, 2016, doi:10.1016/j.rser.2015.12.353.

[103] G. Mavrotas, "Effective implementation of the ε-constraint method in Multi-Objective Mathematical Programming problems," *Applied Mathematics and Computation*, vol. 213, no. 2, pp. 455–465, 2009, doi:10.1016/j.amc.2009.03.037.

[104] K. Deb, A. Pratap, S. Agarwal, and T. Meyarivan, "A fast and elitist multiobjective genetic algorithm: NSGA-II," *IEEE Transactions on Evolutionary Computation*, vol. 6, no. 2, pp. 182–197, 2022, doi.org/10.1109/4235.996017.

[105] C. A. Coello Coello, "Recent Research Topics in Evolutionary Multiobjective Optimization: A Personal Perspective," in *Computational Intelligence*, J. Garibaldi, C. Wagner, T. Bäck, H.-K. Lam, M. Cottrell, K. Madani, and K. Warwick, Eds. Springer International Publishing, 2023, pp. 90–120, doi:10.1007/978-3-031-46221-4_5.

[106] C.-L. Hwang, Y.-J. Lai, and T.-Y. Liu, "A new approach for multiple objective decision making," *Computers & Operations Research*, vol. 20, pp. 889–899, 1993, doi:10.1016/0305-0548(93)90109-V.

[107] K. Deb and J. Sundar, "Reference point based multi-objective optimization using evolutionary algorithms," in *Proceedings of the 8th Annual Conference on Genetic and Evolutionary Computation*. New York, NY, USA: Association for Computing Machinery, 2006, pp. 635—-642, doi:10.1145/1143997.1144112.

[108] J.-H. Cho, Y. Wang, I.-R. Chen, K. S. Chan, and A. Swami, "A Survey on Modeling and Optimizing Multi-Objective Systems," *IEEE Communications Surveys & Tutorials*, vol. 19, no. 3, pp. 1867–1901, 2017, doi:10.1109/COMST.2017.2698366.

[109] J. F. Nash, "The bargaining problem," *Econometrica*, vol. 18, no. 2, pp. 155–162, 1950.

[110] K. K. Annamdas and S. S. Rao, "Multi-objective optimization of engineering systems using game theory and particle swarm optimization," *Engineering Optimization*, vol. 41, no. 8, pp. 737–752, 2009, doi:10.1080/03052150902822141.

[111] W. Gan, M. Yan, W. Yao, and J. Wen, "Peer to peer transactive energy for multiple energy hub with the penetration of high-level renewable energy," *Applied Energy*, vol. 295, p. 117027, 2021, doi:10.1016/j.apenergy.2021.117027.

[112] S. Rao, "Game theory approach for multiobjective structural optimization," *Computers & Structures*, vol. 25, no. 1, pp. 119–127, 1987, doi:10.1016/0045-7949(87)90223-9.

[113] K. Deb and H. Jain, "An Evolutionary Many-Objective Optimization Algorithm Using Reference-Point-Based Nondominated Sorting Approach, Part I: Solving Problems With Box Constraints," *IEEE Transactions on Evolutionary Computation*, vol. 18, no. 4, pp. 577–601, 2014, doi:10.1109/TEVC.2013.2281535.

[114] A. Konak, W. D. Coit, and A. E. Smith, "Multi-objective optimization using genetic algorithms: A tutorial," *Reliability Engineering and System Safety*, vol. 91, pp. 992–1007, 2006, doi:10.1016/j.ress.2005.11.018.

[115] H. Ma, Y. Zhang, S. Sun, T. Liu, and Y. Shan, "A comprehensive survey on NSGA-II for multi-objective optimization and applications," *Artificial Intelligence Review*, vol. 56, 2023, doi:10.1007/s10462-023-10526-z.

[116] K. Deb, K. Miettinen, and S. Chaudhuri, "Toward an estimation of nadir objective vector using a hybrid of evolutionary and local search approaches," *IEEE Transactions on Evolutionary Computation*, vol. 14, no. 6, pp. 821–841, 2010, 10.1109/TEVC.2010.2041667.

[117] R. Benayoun, J. de Montgolfier, J. Tergny, and O. Laritchev, "Linear programming with multiple objective functions: Step method (stem)," *Mathematical Programming*, vol. 1, 1971, doi:10.1007/BF01584098.

[118] M. J. Osborne, *An Introduction to Game Theory*. Oxford University Press, 2009.

[119] T. Tušar and B. Filipič, "Visualization of Pareto Front Approximations in Evolutionary Multiobjective Optimization: A Critical Review and the Prosection Method," *IEEE Transactions on Evolutionary Computation*, vol. 19, no. 2, pp. 225–245, 2015, 10.1109/TEVC.2014.2313407.